The Dissertation Committee for Sungkyun Lim Certifies that this is the approved version of the following dissertation:

Analysis and Design of Electrically Small Antennas for Non-Line-of-Sight Communications

Committee:

Hao Ling, Supervisor

Dean P. Neikirk

Mircea Driga

Edward J. Powers Jr.

Robert L. Rogers

Analysis and Design of Electrically Small Antennas for Non-Line-of-Sight Communications

by

Sungkyun Lim, B.S.; M.S.

Dissertation

Presented to the Faculty of the Graduate School of

The University of Texas at Austin

in Partial Fulfillment

of the Requirements

for the Degree of

Doctor of Philosophy

The University of Texas at Austin

May 2007

Acknowledgements

I was fortunate to have the opportunity to work with my supervisor, Professor Hao Ling, for 5 years at the University of Texas at Austin. I am deeply grateful for his excellent advice and counsel, which he always offered with enthusiasm and good spirits. His deep insights and professional knowledge were invaluable in making me aware of innumerable interesting new ideas related to my topic. Occasionally, he could be stern like a father. At other times he could be considerate and patient like a mother. Without his help, I could never have produced meaningful results from my Ph.D. research.

There are many other to whom I owe my gratitude. I especially appreciate the advice of Dr. Robert Rogers, who proved to be an indispensable source of information about electrically small antennas for HF/VHF wave propagation over non-line-of-sight forested environments. In addition, I would like to extend my deepest thanks to Professor Dean Neikirk, who served as the chair of my committee. My sincere thanks also go to Professor Mircea Driga for his thoughtful review of my work. I am profoundly obliged to Professor Edward Powers for his timely suggestions and scholarly guidance. To all my former group members—Dr. Hosung Choo, Dr. Yong Zhou, Dr. Yaoqing Yang, and Dr. Adrian Lin—I will forever be thankful for their encouragement as I pursued my research. Their help took many forms, both direct and indirect. Finally, I would like to thank my present group members, Mr. Youngwook Kim, Ms. Ann Raynal, Ms. Shobha Ram, and Mr. Yang Li, for their invaluable assistance as I carried out my work.

Analysis and Design of Electrically Small Antennas for Non-Line-of-Sight Communications

Publication No._____

Sungkyun Lim, Ph.D.

The University of Texas at Austin, 2007

Supervisor: Hao Ling

As the demand for compact, portable communication electronics increases, the technology of miniaturization has made great progress. A beneficiary of that progress has been research into new concepts for the antenna, one of the essential components in wireless communications. As the size of an antenna becomes smaller, however, the antenna suffers from high Q and low radiation resistance. The results are narrow bandwidth, poor matching, low efficiency, and, more generally, poor performance throughout the communication system.

First, the design of a small antenna for HF/VHF communications is described. As the operating frequency of an antenna decreases, for example, into the HF and low VHF regions, the physical size of the antenna becomes a critical issue. It is desirable to design a truly electrically small antenna by reducing the ground plane size. Moreover, when the antenna size is very small, the bandwidth of the antenna is extremely narrow, which is critical to various deployment variances and propagation effects such as multi-path fading. The new design, which is an inductively coupled, top-loaded, monopole structure

optimized by a genetic algorithm (GA), maximizes transmission of HF/VHF waves. Electrically small, spiral ground planes for the monopole and the electrically small antenna are designed for HF ground-wave transmission. In addition, a tunable small antenna is investigated that overcomes the narrow-bandwidth limitation of electrically small antennas.

Second, new design methodologies for electrically small antennas are discussed. Use of an inductively coupled feed is one of the well-known methods for boosting input resistance. As the antenna size becomes smaller, however, it is found that the efficiency of an antenna using an inductively coupled feed is lower than an antenna using multiple folds. After a comparison of the two methods, the design of a thin, multiply folded, electrically small antenna is proposed for achieving high efficiency in a physically compact size. The GA is used to assess the effect of geometry on the performance (in terms of efficiency and bandwidth) of the electrically small antennas, including the folded conical helix and folded spherical helix.

Finally, the prospects of using the new Yagi antennas to achieve small size are explored. Yagi antennas are used widely to obtain high gain in a simple structures. The antenna is composed of the driven element and the parasitic elements, which include a reflector and one or more directors. Typically, sufficient spacing on the order of 0.15λ to 0.4λ between the driven element and the parasitic elements is needed for the Yagi antenna to operate well. For some applications, however, it is desirable to reduce the spacing and the length of the elements to achieve a physically more compact size. In this dissertation, closely spaced, folded Yagi antennas in both three dimensions and two dimensions are investigated, and a design for an electrically small Yagi antenna is suggested.

Table of Contents

List of Tables

List of Figures

Chapter 1

Introduction

1.1 DEMAND FOR THE MINIATURIZATION OF ANTENNAS IN WIRELESS COMMUNICATIONS

Antenna is one of the most essential components in wireless communications. With the demand of compact size and portability, miniaturization of communication electronics has seen much progress. As a result, the antenna is becoming the last remaining bottleneck in the miniaturization process. In addition, multiple antennas having different functionalities often have to be incorporated into a limited volume on such platforms as cell phones, ships and aircraft. Having small antennas that can fit into small form factors is therefore a very desirable design goal. Antenna size reduction is also required for camouflage in military applications.

The physical size of antennas in the lower operating ranges of the radio frequency (RF) spectrum such as LF (Low Frequency: 30~300KHz), MF (Medium Frequency: 300~3000KHz), and HF (High Frequency: 3MHz ~30MHz) ranges is particularly problematic. It is well known that the antenna size must be a significant portion of the operating wavelength for the antenna to work well. Since the wavelengths at these frequency ranges are typically large, so are the antennas. For example, a quarter-wavelength monopole at 300KHz is 250m long. Consequently, antennas in these lower frequencies are quite large to be easily manageable by humans and quite costly to erect. As early as 1959, Belrose *et al.* tried to reduce the height of a low frequency broadcast antenna by using a 250-foot umbrella-type top-loaded antenna [1].

1.2 DEFINITION AND BASIC CHARACTERISTICS OF SMALL ANTENNAS

An "electrically small antenna", or simply a small antenna, is an antenna that can be physically enclosed by a radian sphere having a radius less than or equal to $1/2\pi$ wavelength [2, 3]. Typically it is more customary to represent the size of the antenna by kr, where k is the wave number ($2\pi/\lambda$) and r is the radius of the enclosing radian sphere as shown in Figure 1.1(a). The electrical size of a $\lambda/2$ dipole, kr, is equal to 1.6 (Figure 1.1(b)). For an electrically small dipole, the radius enclosing sphere is much less than the wavelength and the size of kr is less than 1 by the definition of Wheeler [2].

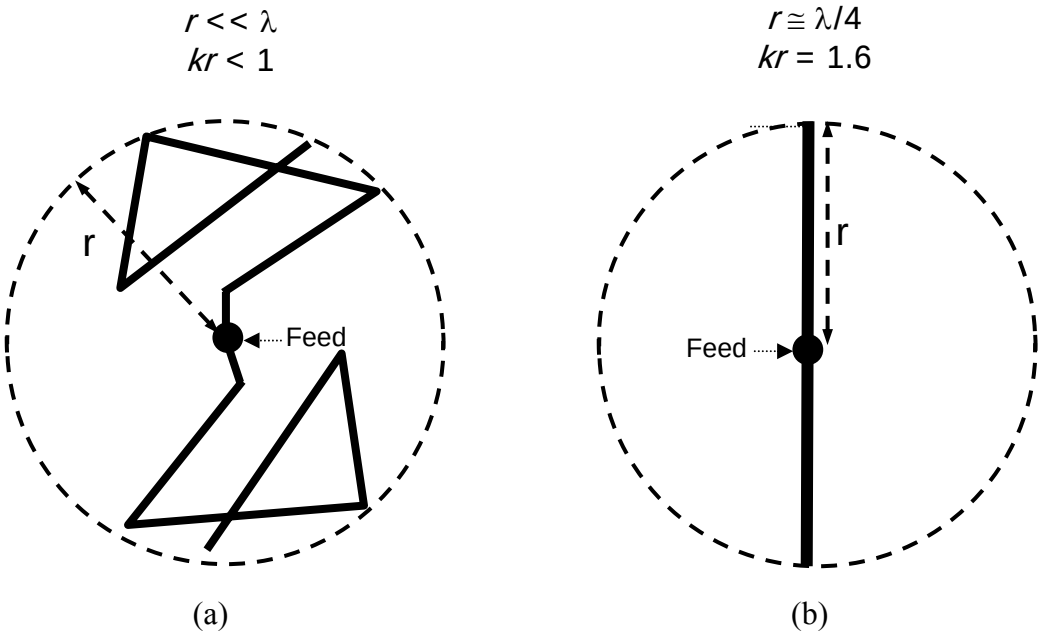

Figure 1. 1: Antenna size in terms of kr
(a) Electrically small dipole
(b) $\lambda/2$ dipole

There are three important factors to consider when discussing the performance of a small antenna: matching, radiation efficiency, and half-power impedance bandwidth. The antenna matching factor is defined as:

$$\text{Antenna matching} = 1 - |\Gamma|^2 \qquad \text{Eq. 1.1}$$

where Γ is the refection coefficient from the antenna feed. One way to address the poor matching problem is to use a matching network. However, it is costly and incurs additional system losses. Therefore, 'self resonance' is preferred for small antennas. 'Self resonance' means that the input reactance is zero without the introduction of any L/C tuning networks.

Radiation efficiency can be defined by considering two different resistive components in the antenna, the radiation resistance and the loss resistance. The efficiency of an antenna (η_a) is defined as

$$\eta_a = \frac{R_{rad}}{R_{rad} + R_{loss}} \qquad \text{Eq. 1.2}$$

where R_{rad} is the radiation resistance and R_{loss} is the loss resistance. To achieve good radiation efficiency, the radiation resistance should be much larger than the loss resistance, which represents the material losses in the antenna structure.

The half-power (3dB) impedance bandwidth of an antenna is defined as,

$$\textit{Half-power impedance bandwidth} = \frac{f_{upper} - f_{lower}}{f_{center}} \qquad \text{Eq. 1.3}$$

where f_{upper} and f_{lower} are the highest and lowest frequencies where the return loss of the antenna is less than -3dB. f_{center} is the average between f_{upper} and f_{lower}. Although the 10dB point is sometimes used, the 3dB bandwidth is the more commonly used quantity when

discussing small antennas. From this point forward, the term bandwidth refers to the half-power impedance bandwidth.

For a narrow band antenna, the Q (quality factor) of the antenna is simply related to the bandwidth as [5, 61]:

$$Q = \frac{1}{bandwidth} \qquad \text{Eq. 1.4}$$

The Q will be discussed in more detail in Sec. 1.3.

As the size of an antenna gets smaller, the antenna suffers from high Q and low radiation resistance. These effects in turn cause the antenna to have narrow bandwidth, poor matching and low efficiency. This in turn leads to poor system performance of the communication link.

1.3 PREVIOUS RESEARCH AND FUNDAMENTAL PROPERTIES OF SMALL ANTENNAS

As the earliest work to quantify small antennas, Wheeler in 1947 [2] introduced the concept of the small antenna by using an equivalent lumped element circuit to model an electromagnetic radiator. In 1948, Chu analyzed in detail the fields surrounding an arbitrarily shaped radiator [6]. He introduced the concept of the minimum Q, and showed that the minimum Q of a small radiator is intrinsically limited by its size. The smaller the radiator, the higher the Q. However, his analysis did not include losses in the antenna. In 1960, Harrington extended Chu's analysis to include the loss effect on the Q factor for an idealized lossy metal sphere [7]. Hansen in 1981 [5] reported that the efficiency-bandwidth product of a small antenna is limited by its Q. He also gave an approximate analytical solution for the Q including higher modes as a function of the antenna size *kr* assuming 100% efficiency:

$$Q = \frac{1 + 3k^2r^2}{k^3r^3(1 + k^2r^2)} \qquad \text{Eq. 1.5}$$

Mclean in 1996 [9] found that the Hansen's analytical solution (Eq. 1.5) was incorrect. He obtained an expression which is now well-accepted:

$$Q = \frac{1 + 2k^2r^2}{k^3r^3(1 + k^2r^2)} \qquad \text{Eq. 1.6}$$

He also gave an exact calculation of the minimum radiation Q of a general antenna with the lowest spherical TM_{01} mode or the TE_{01} mode. The Q is given by:

$$Q = \frac{1}{k^3r^3} + \frac{1}{kr} \qquad \text{Eq. 1.7}$$

For small *kr*, Q can be approximated as

$$Q \approx \frac{1}{k^3r^3} \qquad \text{Eq. 1.8}$$

Based on Eq. 1.7, the fundamental limit between the fractional bandwidth and the size (*kr*) is plotted by assuming 100% efficiency in Figure 1.2 as the solid curve. Also shown in the figure are five different antenna examples, which will be introduced specifically in Section 1.4. In the graph, it is observed that the fundamental limit drops precipitously as *kr* gets smaller. Moreover, the bandwidths of all the small antenna examples fall below the fundamental limit, regardless the antenna size.

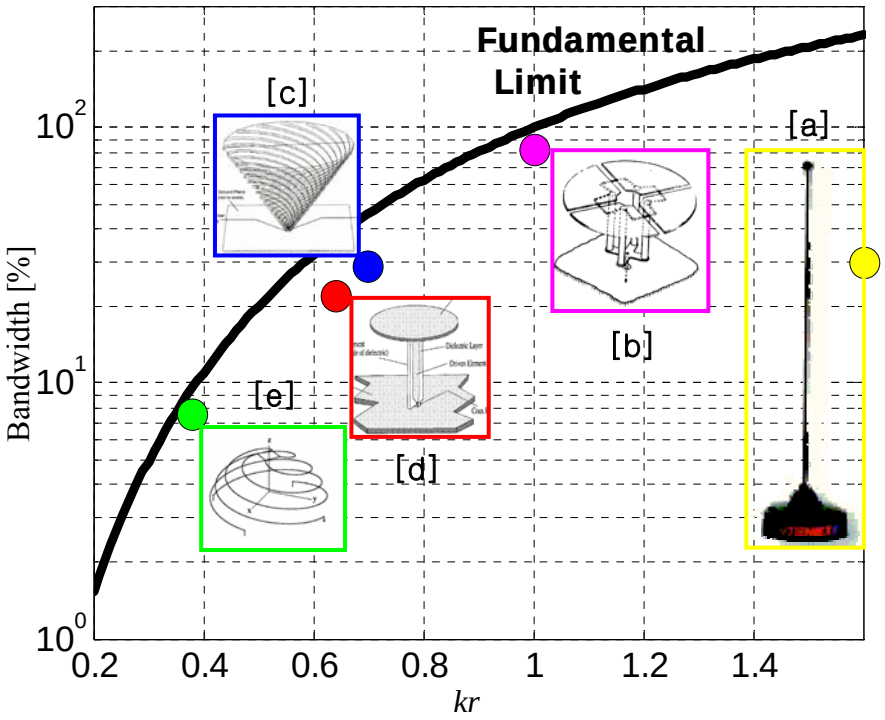

[a] Quarter-wave length monopole.
[b] Goubau Antenna (1976) [10]
[c] Disk loaded monopole (Foltz & McLean, 1998) [11]
[d] Folded conical helix antenna (Dobbins & Rogers, 2001) [12]
[e] Folded spherical helix antenna (Best, 2002) [13]

Figure 1.2: Fundamental limit of antenna Q

1.4 DESIGN METHODOLOGIES AND SOME EXAMPLES OF SMALL ANTENNAS

While the theory discussed in the last section provides a fundamental limit on small antenna bandwidth, it does not provide any details about how to actually design a small antenna to approach the fundamental performance bound. Therefore, it is worthwhile to review some basic design methods for small antennas. In Section 1.4.1, two well known methodologies to increase the radiation resistance, namely top loading and folding, are introduced. In Section 1.4.2, some examples of small antennas that use

the top loading and/or folding techniques are illustrated. In Section 1.4.3, an inductively coupled feed is introduced as a different methodology to increase the radiation resistance.

1.4.1 Top loading and folding

Top loading an antenna is one of the standard ways to achieve miniaturization. One way to interpret the effect of top loading an antenna is that the current no longer has to vanish at the top of the antenna. Therefore, the current distribution tends to become more uniform along its length, and this increases the radiation resistance. A good example of a top-loaded antenna is the capacitor plate antenna as shown in Fig. 1.3. Most of the charges are located at the top-disk. The radiation resistance this antenna is $160\pi^2(h/\lambda)^2$ [8].

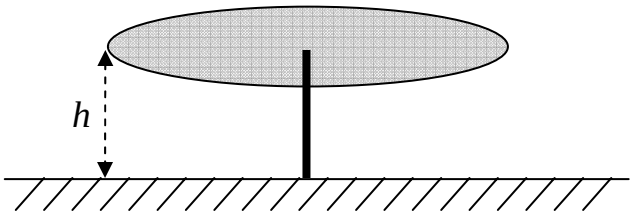

Figure 1.3: Top-loaded (capacitor-plate) antenna

The folding technique is another well known methodology in antenna miniaturization. Consider a singly-folded dipole as shown in Figure 1.4(a), where R_d is the radiation resistance of a simple dipole and R_{rad} is the radiation resistance of the folded antenna. A folded dipole works principally as an unbalanced transmission line, and the current can be divided into a transmission line mode and an antenna mode [19]. At half-wave resonance, the antenna mode dominates and the radiation resistance is increased by a factor 4, as the current is doubled and the radiated power is quadrupled. When N

multiple arms are folded as shown in Figure 1.4(b) the radiation resistance scales approximately as N^2.

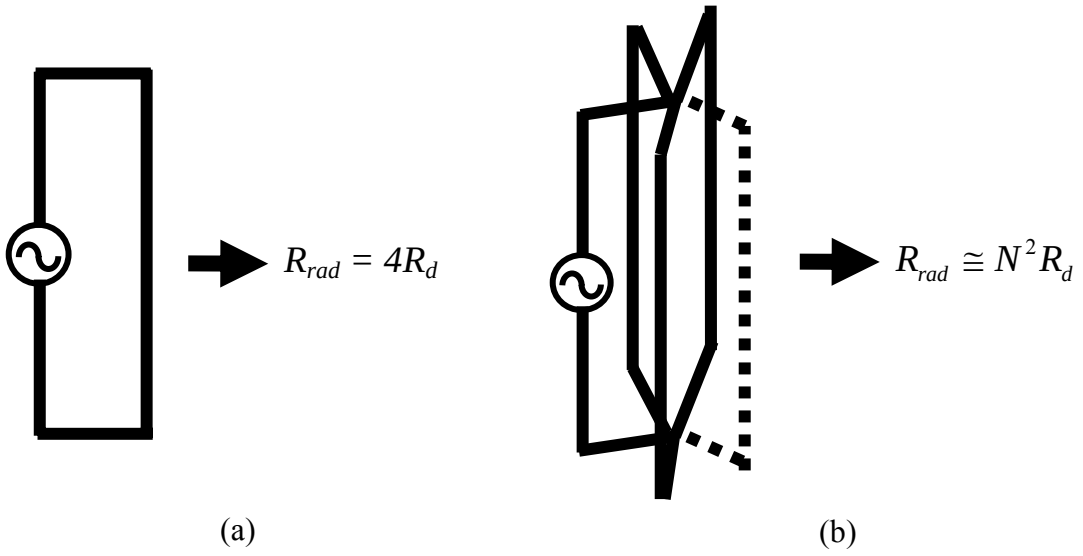

Figure 1.4: Folded dipoles and equivalent impedance
(a) Single folds (b) Multi folds

The multiple-arm folding effect can also be produced by making the wire radius of the additional folding arm thicker. When the wire radius of a singly-folded dipole antenna is increased as shown in the inset of Figure 1.5, a larger impedance step-up occurs. The step-up impedance ratio has been calculated in [17] and is reproduced in Figure 1.5. The step-up ratio is given by

$$\text{Step-up ratio} = (1+a)^2 \qquad \text{Eq. 1.9}$$

$$a = \frac{\cosh^{-1}\dfrac{v^2 - \mu^2 + 1}{2v}}{\cosh^{-1}\dfrac{v^2 + \mu^2 - 1}{2v\mu}} \qquad \text{Eq. 1.10}$$

$$\mu = \rho_2/\rho_1 \qquad \text{Eq. 1.11}$$

$$\nu = d//\rho_1 \qquad \text{Eq. 1.12}$$

where ρ_2, ρ_1 are the wire radii of the wire segments 1, 2 shown in the inset of Figure 1.5, and d is the spacing between the segments 1 and 2.

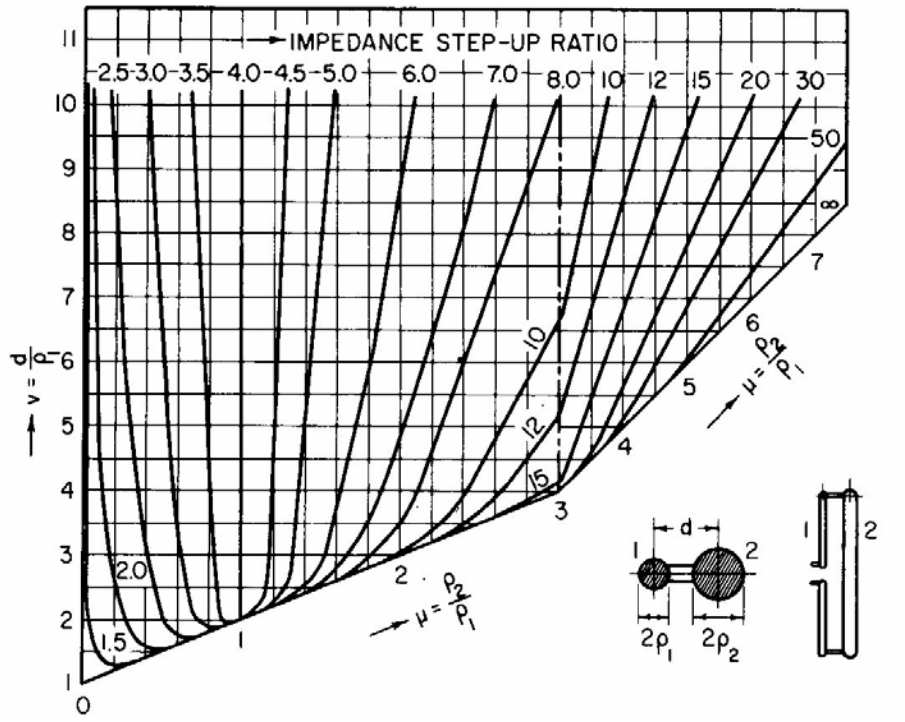

Figure 1.5: Step-up transformation chart for a folded dipole [17]

1.4.2 Some examples of small antennas using top loading and/or folding

The inverted L antenna (Figure: 1.6(a)) can be considered as one of the simplest, top-loaded antennas. The input impedances of the top loaded structures including inverted-L, T, and four-element shapes are investigated by Simpson [15]. However, top loading alone cannot yield sufficient radiation resistance step-up and these antennas usually have low radiation resistance. Therefore, impedance matching networks or internal step up designs are needed.

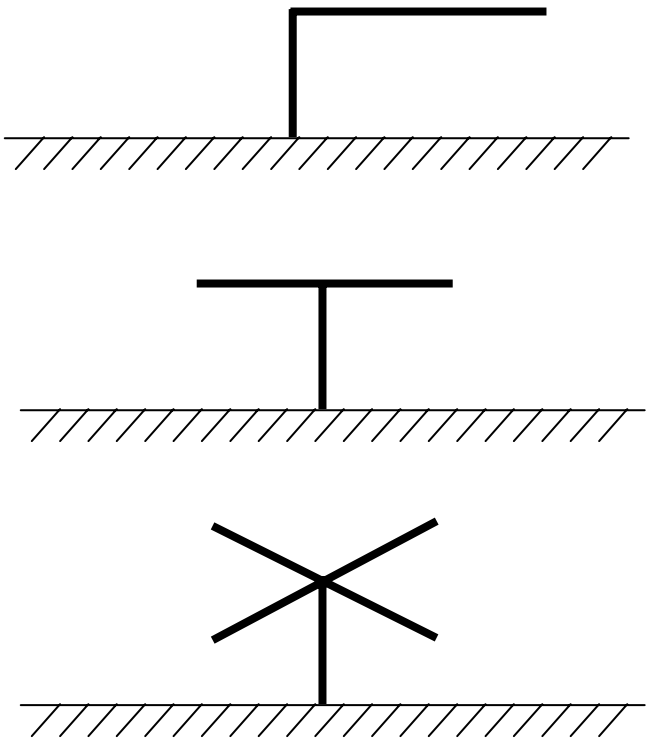

Figure 1.6: Inverted L, T, and four-element top-loaded antenna [15]

A spiral top-loaded monopole is another simple top-loaded antenna. Since additional inductance is generated by the spiral on top, it is easy to be self-resonant unless

the antenna is extremely small. Bhojwani and Zelby in 1973 [16] presented the design and characteristics of the spiral top-loaded monopole for the VLF/LF band. Typically, this antenna shows good characteristics including electrically small size and no tuning inductors.

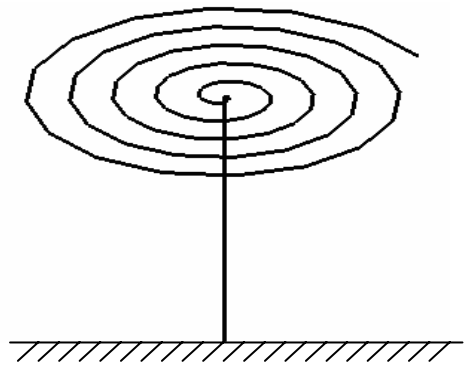

Figure 1.7: Spiral top-loaded monopole [16]

The Goubau antenna [10] is a classic electrically small antenna. It is composed of four disks on top of the antenna. Each disk is connected to each other on the top and to four different small monopoles. The radiation resistance is increased by folding the structure. The antenna gives broad bandwidth. The electrical size, *kr*, of the antenna is around 1.

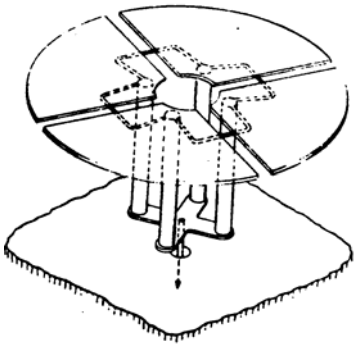

Figure 1.8: Goubau antenna [10]

The disk-loaded monopole with parallel strip elements was introduced by Foltz *et al* [11]. The antenna is composed of (i) top loading with a capacitive disk, which allows the antenna to be resonant with a reduced height, and (ii) folding of the vertical element, which allows transformation of the input impedance to compensate for the radiation resistance reduction that occurs when the size is decreased. The presence of the dielectric and the flat strip geometry permits control of the resonance frequency, the susceptance slope, and the impedance step-up ratio. The published antenna sizes have *kr* in the range of 0.62 ~ 0.73.

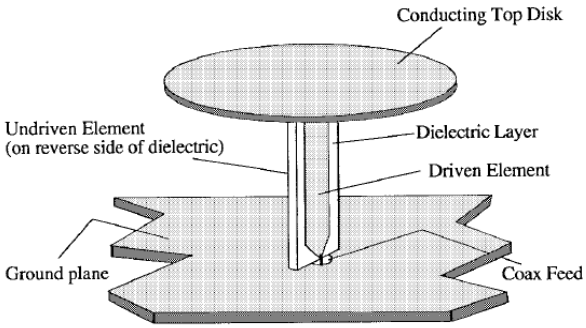

Figure 1.9: Disk-loaded monopoles with parallel strip elements [11]

The Folded Conical Helix (FLEX) antenna was presented by Dobbins and Rogers [12]. The antenna is shown in Figure 1.10 and is composed of spiral wires with 16 single-folded arms. Each arm is folded once. The antenna was built to operate in the HF to VHF frequency bands. The achievable antenna size has a *kr* of 0.6. Even smaller size FLEX antennas have been achieved by using wire radius step-up in a single folded structure [35].

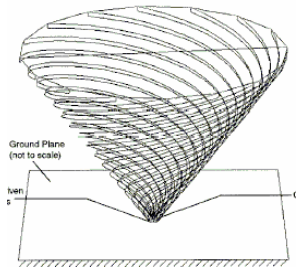

Figure 1.10: Folded Conical Helix (FLEX) antenna [12]

Best introduced an electrically small, folded spherical helix antenna with excellent performance [13]. In Figure 1.11, four arms are wound helically along the enclosing sphere and the arms are connected at the top. The reported size of *kr* is 0.38. The folded spherical helix antenna yields low Q (32) and high efficiency (98.6%) despite its small size. This antenna uses multiple folds to step up the radiation resistance.

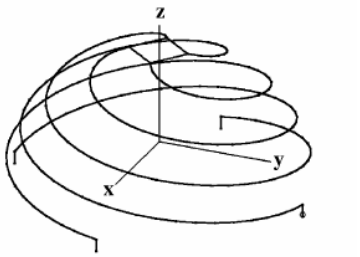

Figure 1.11: Folded spherical helix antenna [13]

1.4.3. An inductively coupled feed

A different concept from top loading and folding, the inductively coupled feed, was introduced by Choo and Ling [20] recently. The inductively coupled feed is shown in Figure. 1.12 and is used to boost up the input resistance. The inductively coupled feed is composed of two parts, the primary arm and the secondary arm. Together they act as a

transformer. The primary arm is the bottom loop and the secondary arm is the bottom part of the upper spiral. Mutual coupling occurs between the two parts, and the stepped-up input impedance is given as

$$Z_{in} = Z_1 + \frac{\omega^2 M^2}{Z_2} \qquad \text{Eq. 1.13}$$

where Z_1, Z_2 are the self impedances of the primary part and the secondary part, respectively. M is the mutual inductance. Antennas based on the structure in Figure. 1.12 with kr in the range of 0.2~0.6 have been built and tested.

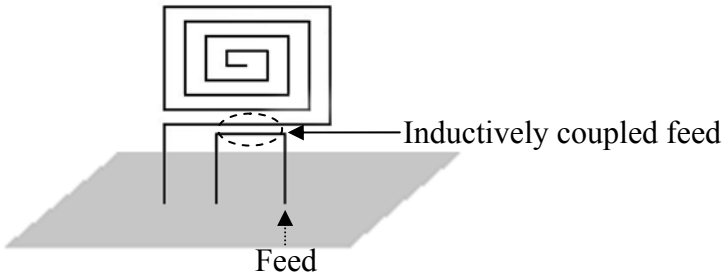

Figure 1.12: Inductively coupled feed antenna [20]

1.5 OBJECTIVES OF THE DISSERTATION

The objectives of this dissertation are as follows. The first objective is to explore and develop new design methodologies for electrically small antennas. The second objective is to use the developed methodologies to design and implement electrically small antenna for HF/VHF communication. The third objective is to incorporate additional design features associated with electrically small antennas including miniaturized ground plane and frequency tunability. The final objective is to utilize electrically small antennas as the basis for building high gain arrays that are electrically small.

1.6 THE ORGANIZATION OF THE DISSERTATION

In this dissertation, the designs and analysis of several classes of small antennas are researched for wireless communications. The dissertation is organized as follows.

Chapter 2 introduces an electrically small antenna for maximizing transmission into HF ground waves [21]. HF ground wave is useful for extended-range, non-line-of-sight communications. One of the main challenges is how to design a small antenna that can efficiently couple to the ground wave at HF frequencies. Two concepts are incorporated. One is the inductively coupled feed structure to step up the input resistance. The other is a spiral shaped top loading to achieve small size and self resonance. An HF antenna with a kr of 0.2 is designed and tested at 30 MHz. .

Chapter 3 describes the design of an electrically small ground plane to couple to the electrically small antenna in Chapter 2 [22]. Since a small monopole antenna still requires a sizable ground plane to operate well, it is desirable to design a truly electrically small antenna by also reducing the ground plane size. First, a small ground plane with a full-size monopole is investigated to gain insights into the design issues. Next, a small ground plane is designed for the inductively coupled, top-loaded monopole antenna.

In Chapter 4, the frequency tunability of the inductively coupled, top-loaded monopole antenna is developed [23]. Since the bandwidth of an electrically small antenna is fundamentally limited, achieve frequency tuning capability is the next best thing. The resonant frequency of the inductively coupled electrically small antenna is tuned by the introduction of a tunable lumped-element component. It is shown that the developed frequency agility can be used to overcome various deployment variances and propagation effects.

In Chapter 5, the comparison between two design methodologies, namely the inductively coupled feed and the multiple folds are compared. It is found that the

inductively coupled feed steps up the radiation resistance and the loss resistance by the same ratio and does not improve the efficiency of the antenna. On the other hand, when N multiple folded arms are used, the radiation resistance scales approximately as N^2 while the loss resistance scales approximately as N. This results in an increase of the radiation efficiency. Based on this study, a thin, efficient, electrically small antenna using multiple folds is designed and tested [24]. This antenna is shown to have higher efficiency than a comparable inductively coupled design.

In Chapter 6, two very successful small antenna designs, the folded conical helix and the spherical helix antenna, are compared [25]. These two antennas are similar, with the major difference being their space-filling geometry. A genetic algorithm is used as a search tool to determine the optimal geometry for maximizing bandwidth and/or efficiency. Results and conclusions are drawn to assess the role of wire geometry in the performance of small antennas.

Chapter 7 deals with design of a Yagi antenna with very close spacing between the elements [27]. When the spacing between the elements is reduced, the antenna suffers from small radiation resistance, very similar to the behavior of small antennas. The folding concept is therefore used to boost up the radiation resistance to achieve high efficiency and good matching. The resulting closely spaced, folded Yagi is then evaluated for HF sky wave transmission.

In Chapter 8, the work in Chapter 7 is extended to realize a printable Yagi antenna with closely spaced elements [28]. Two planar Yagi antenna structures with close element spacing including a driver-plus-reflector case and a driver-plus-director case are investigated. The resulting planar antenna can be useful for such applications as RFID.

In Chapter 9, a two-element, electrically small Yagi antenna is presented to achieve high gain [29]. By using the small antenna design presented in Chapter 5 and the

closely spaced Yagi concept developed in Chapters 7 and 8, an electrically small Yagi antenna with good gain is realized. This work opens up the possibility of achieving very high gain arrays, the so-called supergain arrays, in an electrically small size.

In Chapter 10, conclusions are drawn and future research directions are discussed.

Chapter 2

An Electrically Small Antenna for Maximizing Transmission into HF Ground Waves

2.1 INTRODUCTION

It is well known that an HF ground wave is useful for non-line-of-sight communication over extended ranges. A key challenge is the design of small antennas that can couple efficiently to HF ground waves. Previously, the design of electrically small, arbitrarily shaped wire antennas was investigated using genetic algorithms (GA) [30, 31]. Subsequently, a class of planar, inductively coupled antennas was proposed in [20]. Whereas those antennas were optimized for bandwidth and efficiency using GA, the test results at HF frequencies showed high transmission losses for ground-wave links. It is believed those losses were due to low directivity to the horizon. Therefore, it is important to take ground-wave coupling into consideration in the design for such applications.

In this chapter, the design of an arbitrary wire antenna using GA is discussed. Next, the design of a new GA antenna optimized for ground wave coupling is presented, followed by a discussion of an electrically small antenna design that maximizes transmission into HF ground waves. The antenna structure entails three design concepts: (i) a vertical antenna body to maximize coupling to ground waves, (ii) top loading to achieve self-resonance in a small size, and (iii) an inductively coupled feed to step up the input resistance and broaden the bandwidth. The design parameters are chosen by using a genetic algorithm in conjunction with the Numerical Electromagnetics Code (NEC). Two prototype antennas with a kr of 0.2 are built and measured at 30 MHz to confirm design performance.

2.2 ANTENNA DESIGN

To find the general shape of the antenna to maximize ground-wave coupling, an arbitrary wire antenna design is investigated first. An arbitrary wire antenna design in a hemisphere of radius *r* is shown in Figure 1.1(a).

The GA is used to optimize the arbitrary wire design by maximizing directivity to the horizon while the 50-ohm input resistance is ignored. It is costly to compute the Sommerfeld integral on a lossy half-space in the NEC, and because GA optimization needs several thousand NEC runs, this approach is not practical. Numerical testing, however, indicates that the coupling with ground waves is closely correlated with the antenna directivity along the horizon, given an infinite conducting ground. In GA optimization, therefore, the Sommerfeld calculation is replaced with a simulation of the antenna on an infinite conducting ground.

In Figure 2.1, note the common features of the antennas selected by the GA: top loading to achieve resonance, and the vertical antenna body to maximize coupling to the vertically polarized ground wave mode.

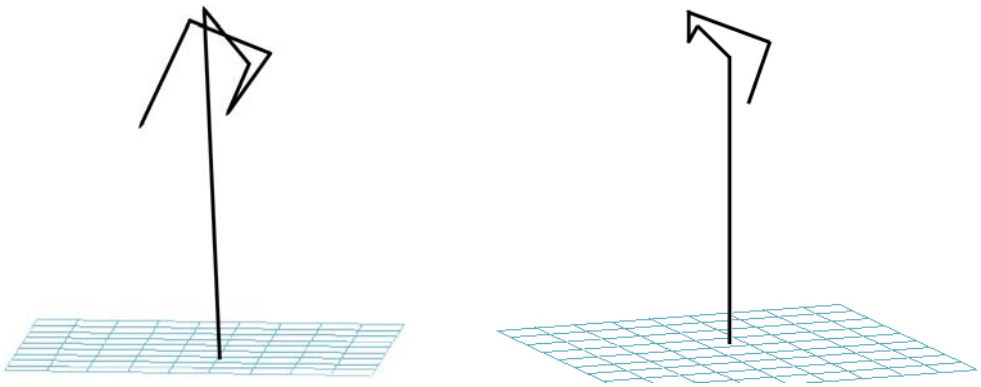

(a) (b)

Figure 2.1: Converged samples of the arbitrary wire design by GA.

From an initial application of the GA exploration process, several new antenna designs are derived. Figure 2.2 illustrates an attempt to identify canonical designs that maximize the coupling to the vertically polarized ground waves. Based on this attempt, it is found that three things are required for the ground wave maximization.

First, a vertical antenna body is necessary to maximize coupling to the ground-wave mode, because it is this main part of the antenna that radiates with vertical polarization.

Second**,** top loading is necessary to achieve self-resonance. In this case, multi-arm winding achieves the top-loading effect. A spherical helix top-loaded design shows the best performance among the tested top-loaded structures. The multi-arm spherical-helix top-loading is attached to the vertical antenna body at its top end. There are two reasons for this superiority. First, the vertical antenna body can be extended straight to the top of the given volume to maximize coupling to ground-wave excitation with vertical polarization. Second, the vertical current cancellation between the top loading, which has mostly horizontal current, and the vertical antenna body is small. Similar spherical helix designs are reported in [32] (a simple hemispherical helix structure) and in [13] (a folded monopole structure).

Finally, the third essential feature is an inductively coupled feed to step up the input resistance and increase the bandwidth. The size of the antenna in Figure 2.1 is a *kr* of 0.88. If the *kr* is reduced from 0.88 to 0.2, the result is a low input resistance. Thus, the purpose of the inductively coupled feed concept is to increase the input resistance. However, with the inductively coupled feed design of the planar antenna [20], it is difficult to produce enough coupling in a *kr* of 0.2, because the coupling is produced by two variables. One is the distance between the loop and the coiled bottom wire of the antenna body part, and the other is the area of the loop. If a planar antenna achieves a *kr*

of 0.2 and we wish to have desirable coupling, then the distance between the loop and bottom wire must be extremely small, and the area of the loop must be larger than a given volume. The three-dimensional coil overcomes this coupling insufficiency of the planar inductively coupled feed.

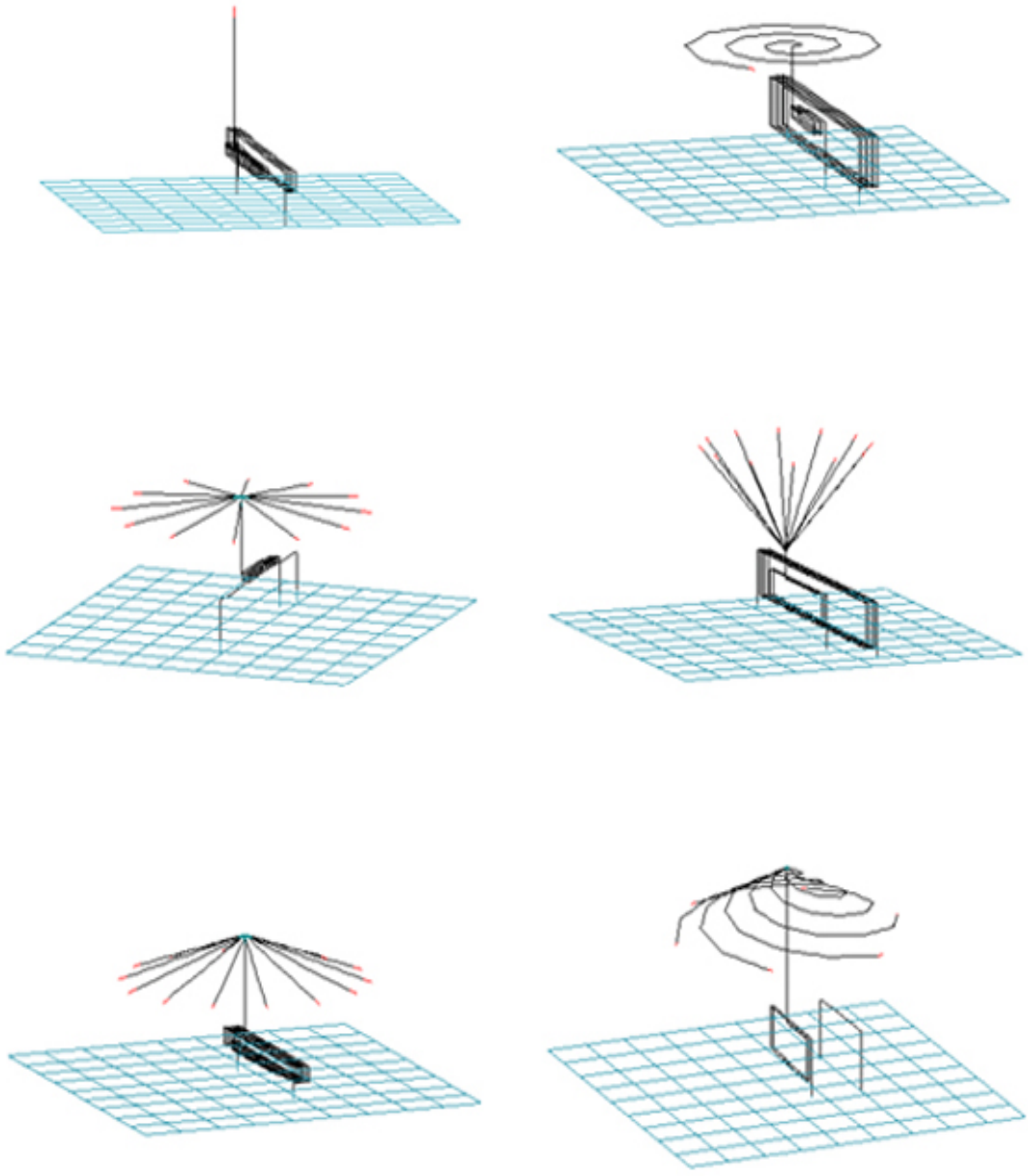

Figure 2.2: Several new antenna designs.

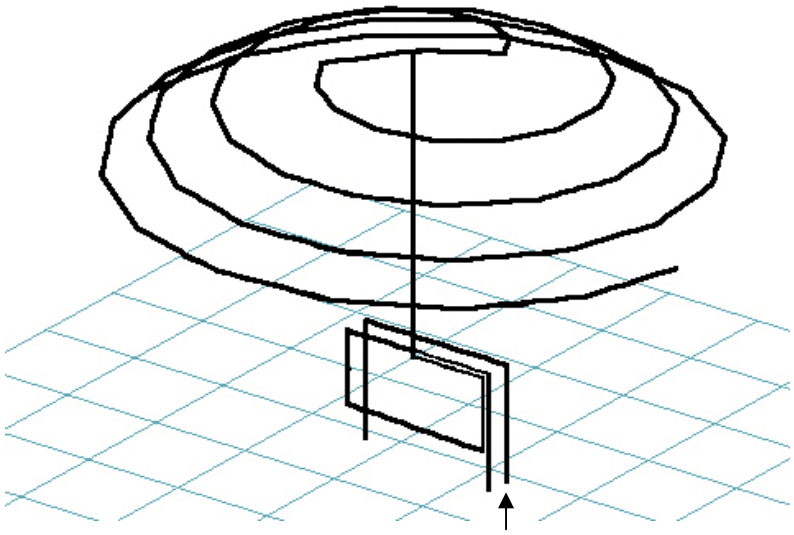

(a)

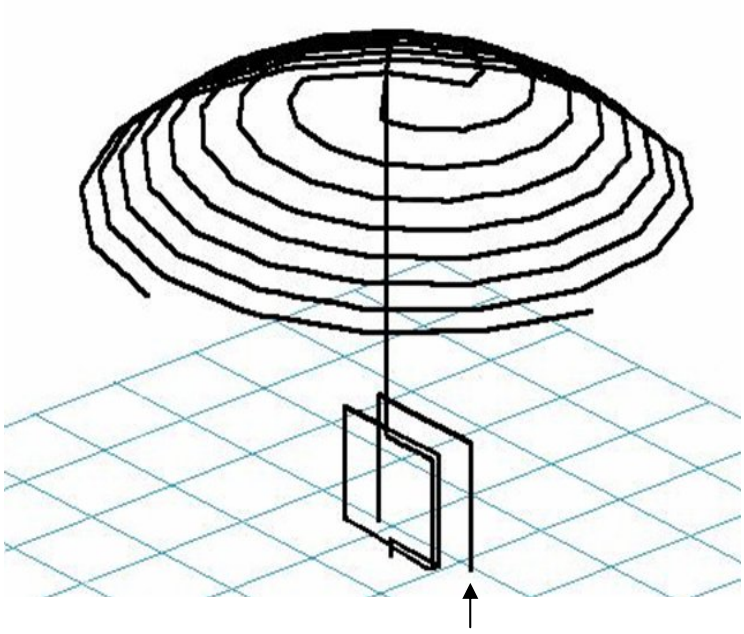

(b)

Figure 2.3: New antenna designs, top-loaded GA antenna. (a) The two-arm top-loaded GA antenna. (b) The four-arm top-loaded GA antenna.

Figure 2.3 shows the new antenna design. It consists of an inductively coupled feed structure at the bottom. The primary loop is fed by a coaxial line at one end and shorted to ground at the other. The secondary loop is located at the base of the antenna body. It starts from the ground and goes through multiple turns before connecting to the vertical antenna segment. This inductively coupled feed serves to step up the input resistance of the small antenna, which is much less than 50 ohms. The step-up ratio is controlled by the areas, the number of turns, and the distance between the primary and secondary loops. In contrast to the planar design presented in [20], the present design can achieve a much tighter inductive coupling, thus providing a larger step-up that is necessary for very small antennas. The vertical antenna body is extended straight up to the topmost point of the antenna to maximize coupling to the HF ground wave, which is vertically polarized. The top of the antenna is top loaded by a multi-arm spherical helix structure to achieve self-resonance while at the same time maximizing any reduction in the ground wave coupling.

GA is used in conjunction with NEC to optimize the antenna design parameters. The realized gain in the horizon is used as the cost function. The design parameters are the dimensions of the feed and the length and pitch of the spherical helix. A simple binary GA is implemented, and the result typically converges after 50 generations with a population of 100 chromosomes. Because the NEC calculation takes too much time to carry out on the lossy ground based on the Sommerfeld integral, the calculation is also carried out on the infinite conducting ground plane as the arbitrary wire design.

Figure 2.3(a) is the two-arm, top-loaded design optimized by the GA. The antenna dimensions, which include a *kr* of 0.2, are the following. The distance between the loop and the secondary coil is 2cm. The height and the width of the loop are 8.9cm and 12cm, respectively. The secondary coil also has the same height and width as the loop except for

the 3.3cm gap between the ground and the bottom of the secondary coil. This secondary coil has one and a quarter turns. The length of the vertical segment is 23.1cm. Two turns of the spherical helix are used for the top loading, and the distance between the ground and one end of the top-load arm is 25.9cm.

It is found that, as the number of arms increases, the directivity of the antenna along the horizon improves, and the resonance frequency decreases. For that reason, a four-arm, top-loaded design is optimized by the GA as shown in Figure 2.3(b). The vertical antenna body rises to the top and splits into four arms. This design also operates at 30MHz with the same *kr* of 0.2. The improvement quickly diminishes, however, as the number of arms increases beyond four.

The dimensions of the four-arm GA antenna shown in Figure 2.3(b) are as follows. The distance between the loop and the secondary coil is 3cm. The height and the width of the loop are 8.3cm and 10cm, respectively. The secondary coil also has the same height and width as the loop, except for the 1cm gap between the ground and the bottom of the secondary coil. The secondary loop has one and a half turns. For structural support of the antenna, the ground point of the secondary coil is centralized directly beneath the vertical antenna body. The length of the starting segment that connects to the ground of the secondary coil is 1cm. The length of the vertical segment is 23.7cm. Two turns of the spherical helix are used for the top loading, and the distance between the ground and one end of the arm of the top loading is 23.4cm.

2.3 SIMULATED AND MEASURED RESULTS

A two-arm and a four-arm GA antenna were simulated, built, and measured. The prototypes of the two-arm and four-arm GA antennas (Figure 2.4(a) and (b)) were built with a radius of 0.5mm (18AWG) wire for the antenna and Styrofoam for structural

support. For testing and measuring the prototypes, a 120cm-by-120cm-square ground plane is used.

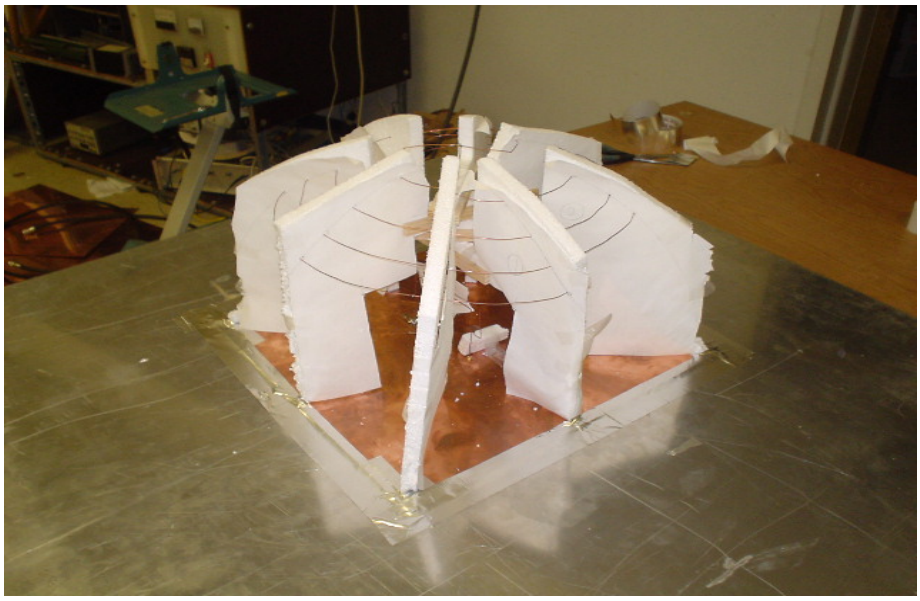

(a)

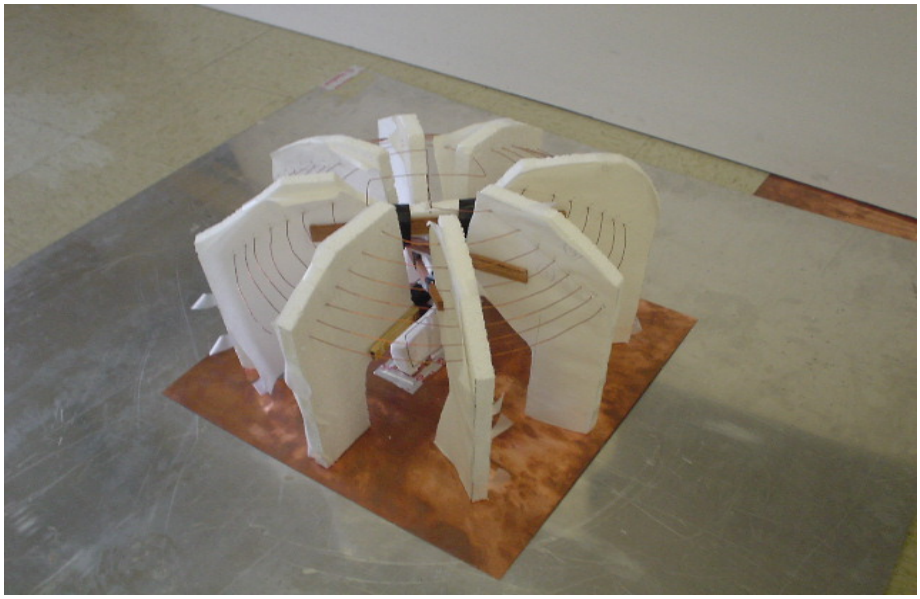

(b)

Figure 2.4:
(a) Prototype of the two arm GA antenna.
(b) Prototype of the four arm GA antenna.

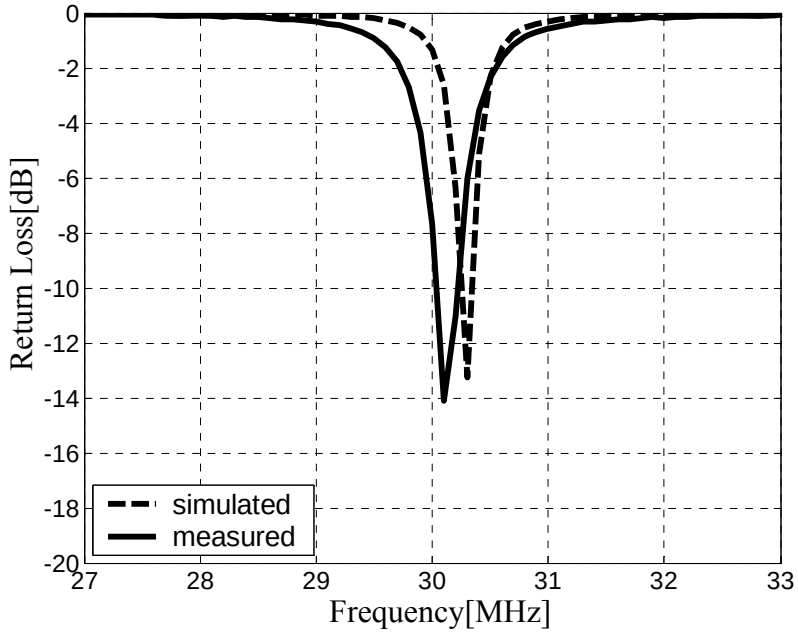

(a)

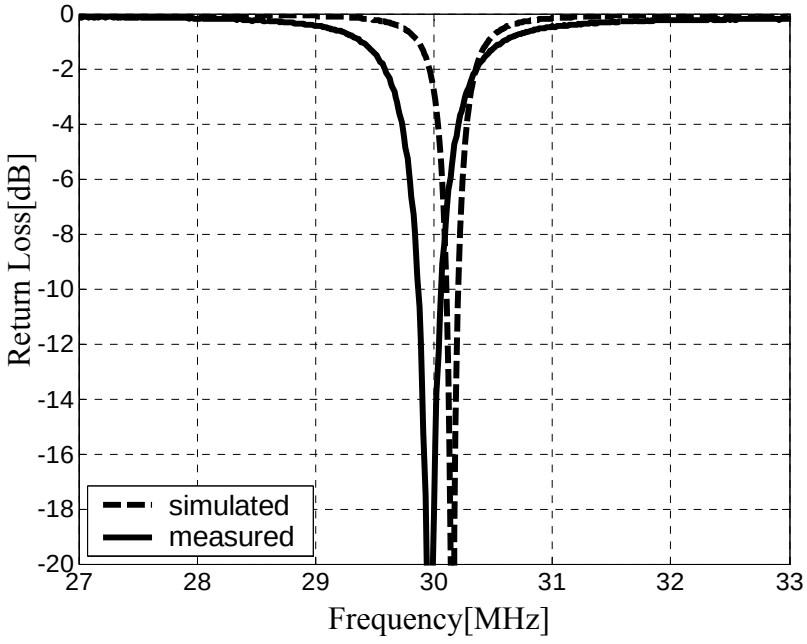

(b)

Figure 2.5:
(a) Return loss of the two-arm GA antenna.
(b) Return loss of the four-arm GA antenna.

Figs. 2.5(a) and (b) are graphs of the return loss versus frequency for the two-arm and the four-arm GA-derived antennas, respectively. The simulated 3dB bandwidth of the two-arm antenna is 1.2%, and that of the four-arm antenna is 1.0%. Those numbers are to be compared to the measured bandwidth of the two-arm antenna, which is 2%, and of the four-arm antenna, which is 1.9%. The discrepancy between the simulation and measurement is likely due to the electrically small size of the ground plane used in the measurement, which measures 1.2m by 1.2m.

The efficiency of the antennas is measured by using the Wheeler cap method. Two input impedance measurements are needed to obtain the efficiency of the antenna [4, 33]. One measurement is the input impedance before covering the antenna with a conducting cap, and the other measurement is the input impedance after putting the cap over the antenna.

The measured efficiency is calculated by

$$\eta_{measured} = \frac{R_{nocap} - R_{cap}}{R_{nocap}} = \frac{R_{rad}}{R_{rad} + R_{loss}} \qquad \text{Eq. 2.1}$$

where R_{cap} is with the cap and R_{nocap} is without the cap. Contrary to the case without cap, which gives the total resistance of the antenna ($R_{rad} + R_{loss}$), the presence of the metal cap prevents any radiation, which gives the measured loss resistance.

In this measurement, a box with thin aluminum plates is used for the cap. The size of the box is 51cm by 54cm by 54cm. The efficiency is calculated based on the standard formula for the Wheeler cap measurement using Eq. 2.1. Figure 2.6 shows efficiency versus frequency for the four-arm GA antenna. The dotted line is the simulation results from NEC, and the solid line is the extracted efficiency using the formula from the Wheeler cap measurement. Clearly, the two results do not agree well. In fact, a dip occurs

near the resonant frequency in the measured efficiency. This lack of agreement is easy to understand since Eq. 2.1 is true only if the antenna can be modeled as a simple RLC circuit. The fact is, however, that the antenna contains an inductively coupled feed and therefore cannot be represented by a simple RLC circuit. To obtain the efficiency of the antenna from the input impedance measurements is not a straightforward computation.

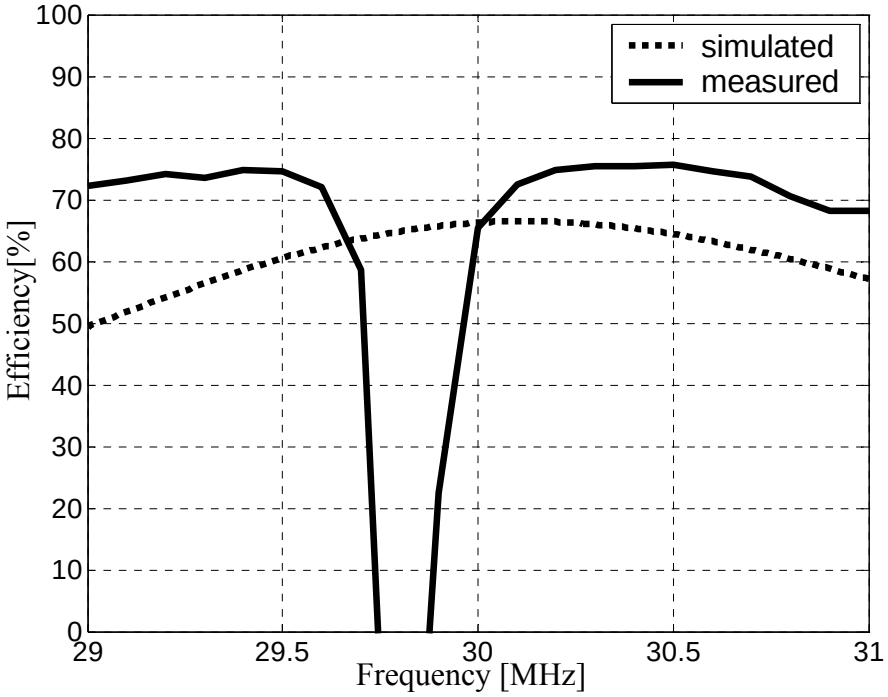

Figure 2.6: The efficiency based on the standard formula from the Wheeler cap measurement.

To remove the dip near the resonant frequency, a better equivalent circuit model is required for the antenna, as shown in Figure 2.7. In this circuit, a transformer is used to represent the mutual coupling in the inductively coupled feed. Furthermore, the resistance

R is assumed to be frequency dependent in order to model the combination of the radiation resistance and the loss resistance in the wire. This resistance resides in the body of the GA antenna. The resistance at the primary coil is omitted since the resistance in the feed loop is negligible compared to the resistance in the antenna body.

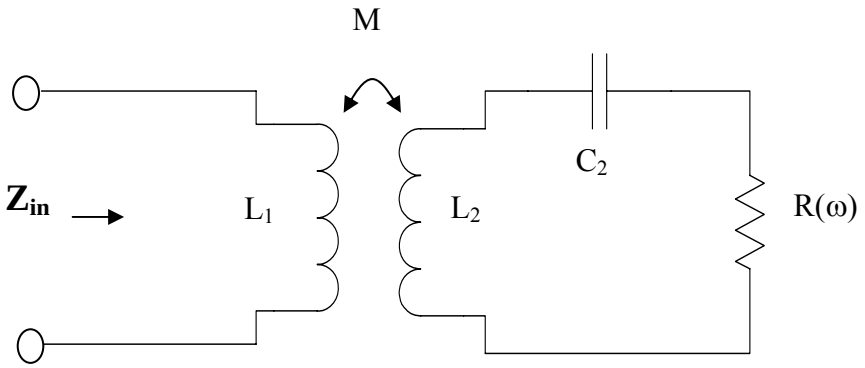

Figure 2.7: Equivalent circuit model.

The input impedance of the antenna before cap and after cap can be derived based on the circuit model as follows:

$$Z_{in_{before}}(\omega) = j\omega L_1 + \frac{\omega^2 M^2}{j\omega L_2 + R_{before}(\omega) + \frac{1}{j\omega C_{2_{before}}}} \qquad \text{Eq. 2.2}$$

$$Z_{in_{after}}(\omega) = j\omega L_1 + \frac{\omega^2 M^2}{j\omega L_2 + R_{after}(\omega) + \frac{1}{j\omega C_{2_{after}}}} \qquad \text{Eq. 2.3}$$

Eq. 2.2 and Eq. 2.3 are fitted to the measured input impedance data before cap and after cap. When the equivalent circuit model in Figure 2.7 is used, the value of resistance before and after the cap can be known, where resistance before cap is assumed to be a second-order polynomial. A nonlinear fitting method with an optimizer is used to minimize the sum of two root-mean-square values to extract all the lumped element values R, L, C, and M from the measurement data about the resonant frequency for both the with-cap and without-cap cases. Regardless of the cap, R_1, L_1, M, and L_2 are assumed to have the same values since the cap does not change the values. The optimizer combines a GA-based global search with a subsequent local search using the simplex search method described in [34]. After the parameter extraction, the input impedance of the circuit model agrees well with the input impedance from the measurement for both the with-cap and without-cap cases for the four-arm GA antenna, as shown in Figure 2.8.

Efficiency can then be calculated from the resistance R(ω) before and after the cap. Figure 2.9 shows the efficiency from the improved equivalent circuit model for the four-arm GA antenna. The dip in the measured efficiency has been removed, and the measurement and the simulation now match much better.

At 30MHz, the simulated efficiency is 67%, and the measured efficiency is 73%. The results of simulation and measured data show good correlation, and both exceed 65%. Even higher efficiency can be expected if thicker wires are used.

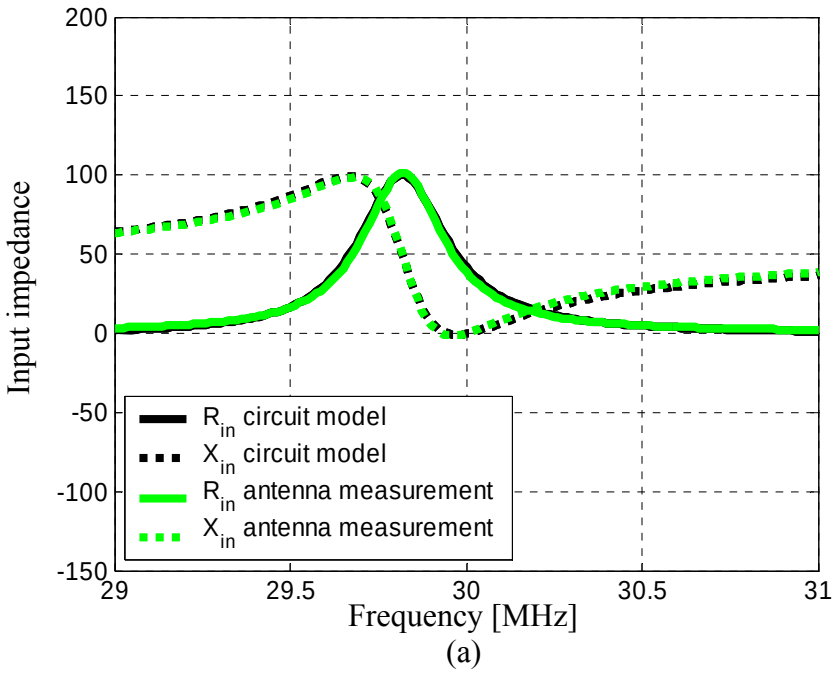

(a)

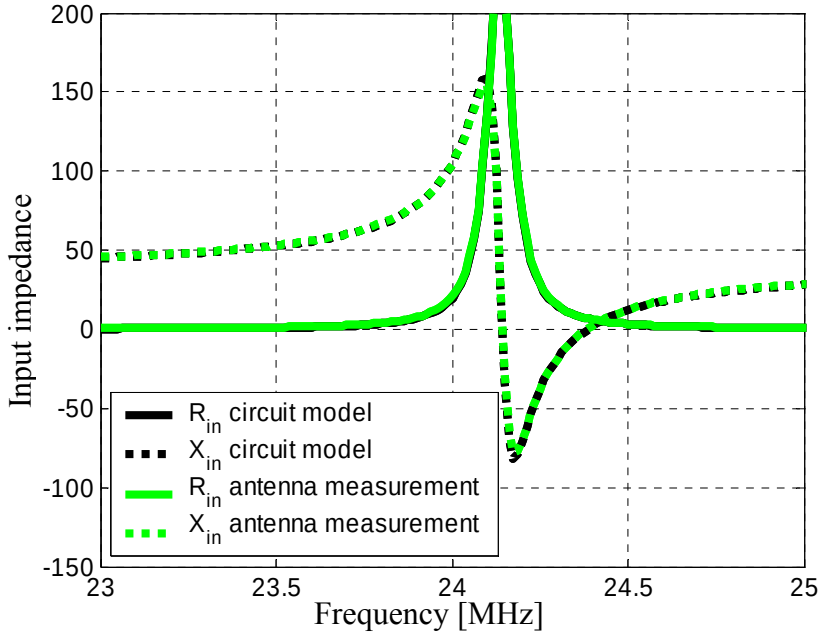

(b)

Figure 2.8: Input impedance of the four-arm GA antenna.
(a) Before the cap.
(b) After the cap.

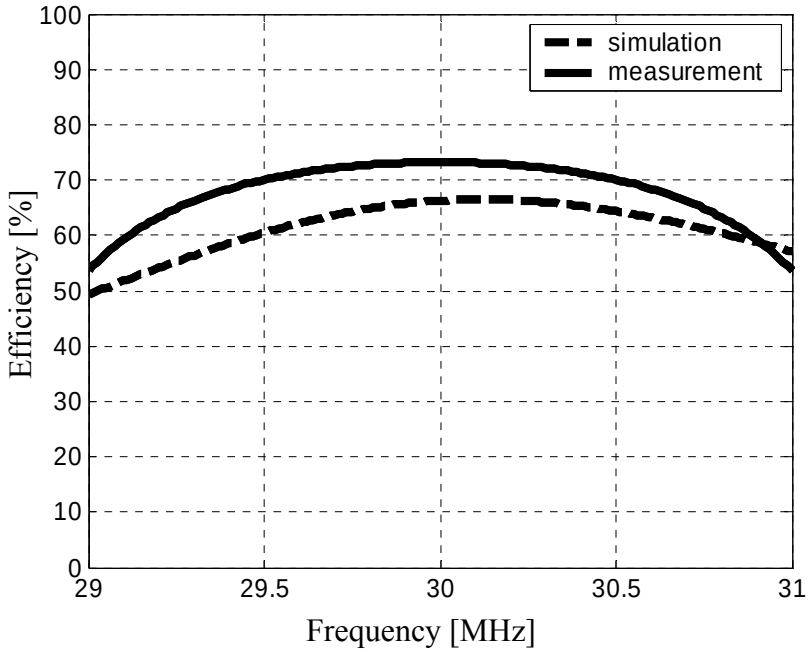

Figure 2.9: The efficiency from the improved equivalent circuit model for the four-arm GA antenna.

The antennas were also tested outdoors on flat grassy ground to characterize the transmission loss. Four different transmitting antennas were tested: a commercial whip (from GLA Systems), a planar GA antenna based on the design in [20], the two-arm GA antenna, and the four-arm GA antenna. Another commercial whip was used for the receiving antenna in all cases. The distance between the transmitter and the receiver was 15 m. Figure 2.10 shows the measured transmission loss taken using a network analyzer for the four different transmitting antennas. The figure shows that the planar GA antenna design was about 5 dB worse than the commercial whip. On the other hand, the transmission losses of the two-arm and the four-arm GA antennas are both within 1dB of the commercial whip. The transmission loss difference between the two-arm and the four-arm GA antennas is negligible. The NEC transmission loss simulation based on the

exact Sommerfeld integral with dry soil (ε_r=3, σ=0.0001S/m) shows that the four-arm and the two-arm GA antennas are better than the planar GA antenna by 3.3dB and 3.1dB, respectively. These numbers are comparable to the measurement result of 3.7dB and 3.5dB.

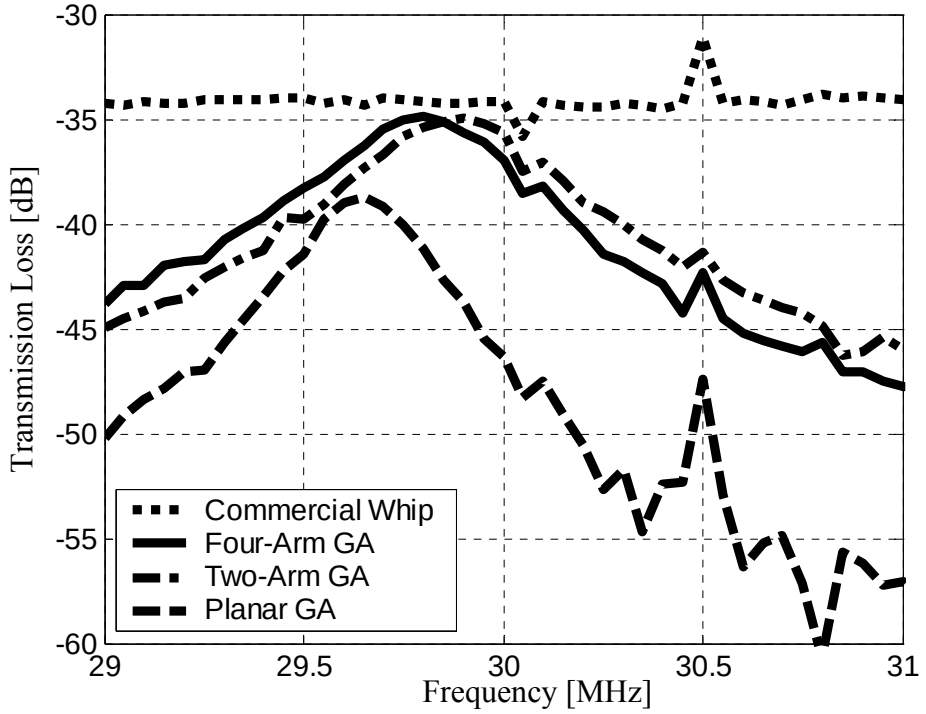

Figure. 2.10: The efficiency from the improved equivalent circuit model for the four-arm GA antenna.

Figure 2.11 shows the NEC-simulated directivities of the four-arm, two-arm, and planar antennas at the horizon on an infinite conducting ground. As we can see, the directivities of the new GA antennas are greater than that of the planar antenna. In addition, the new GA antennas are isotropic in azimuth, whereas the planar GA antenna is not.

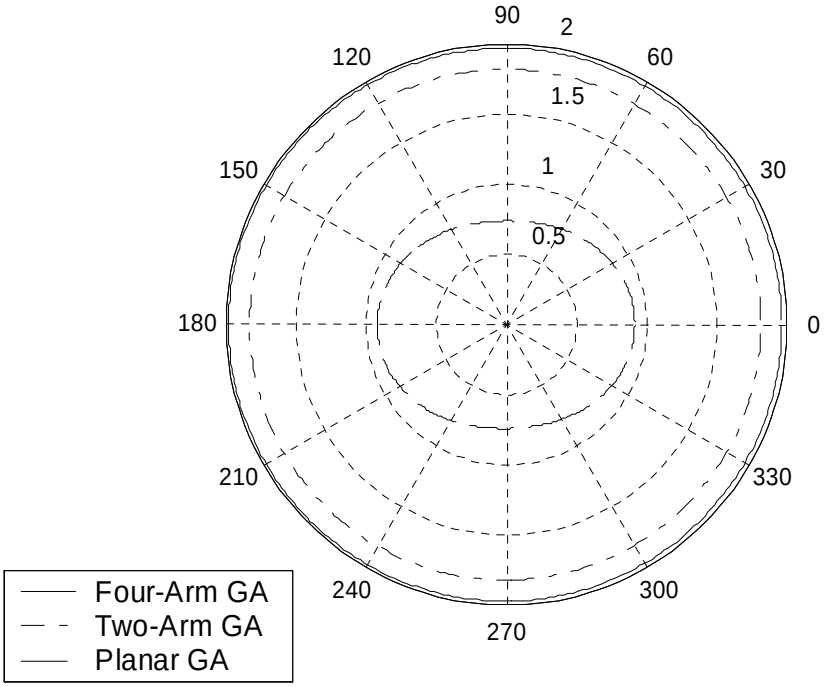

Figure 2.11: The simulated directivities of the three different antennas at the horizon on an infinite conducting ground.

The figure of merit for small antennas, Ψ, which was introduced by Rogers *et al.* [35] to evaluate small-antenna performance, is as follows:

$$\psi = \frac{eb}{2}\left(\frac{1}{kr} + \frac{1}{(kr)^3}\right) \qquad \text{Eq. 2.4}$$

where e is the fractional efficiency and b is the fractional bandwidth. The figure of merit is basically the efficiency-bandwidth product normalized by the antenna size to the third power. Table 2.1 shows that the figure of merit of the planar antenna is 0.22, only about

half of the figures of merit for the two new antennas. The figures of merit for the new antennas are superior even though those antennas, unlike the planar antenna, are not optimized for bandwidth and efficiency, but for realized gain instead. The likely reason for the improvement is that the planar antenna design is confined to two dimensions, whereas the designs of the two new antennas are three dimensional.

Antennas	Size (kr)	Bandwidth	Efficiency	Ψ
Planar GA	0.2	0.70%	49%	0.22
two-arm GA	0.2	1.20%	61%	0.48
Four-arm GA	0.2	1.00%	67%	0.44

Table 2.1: Figure of merit.

2.4 SUMMARY

This chapter has described a class of electrically small antennas that maximize HF ground-wave transmission. The antennas have been designed, constructed, and tested at 30MHz. Design concepts incorporated into the antennas include an inductively coupled feed structure and an antenna body with a vertical section plus multi-arm top-loading. The design parameters were chosen by using a GA in conjunction with NEC. Two prototype antennas, each with a kr of 0.2, were built and measured at 30MHz to determine design performance. The efficiency of the antennas was measured by using the Wheeler cap method. Because the conventional Wheeler cap method is valid only if the antenna can be modeled as a simple RLC circuit, an improved but equivalent circuit model was used for the efficiency measurement. This measured efficiency agrees well

with that of NEC simulation. An outdoor transmission test showed that the transmission loss of the new antenna design is within 1dB of the loss from a commercial whip.

Chapter 3

Design of Electrically Small Ground Planes for HF Ground Wave Transmission

3.1 INTRODUCTION

Monopole antennas are usually used with a ground plane to efficiently couple energy to the vertically polarized ground wave mode. It is commonly accepted that, for a quarter-wavelength monopole, the radius of the ground plane should be approximately $\lambda/4$, where λ is the wavelength [36]. If the diameter of the ground plane falls below $\lambda/10$, the transmission loss deteriorates rapidly. Therefore, it is desirable to develop reduced-size ground planes without the associated performance degradation. Some research has been reported on methods to reduce the ground plane size to improve the performance of antennas in the PCS band [37, 38].

This chapter presents the design of reduced-size ground planes that do not incur drastic transmission losses of HF ground waves. The proposed ground plane shapes are based on the spiral. The concept is first demonstrated on a quarter-wave monopole. It is shown by simulation and measurement that the performance of a reduced-size (0.043λ) spiral ground plane is on a par with a ground plane that is three times larger. Next, the spiral ground plane idea is adapted for the top-loaded, inductively coupled small antenna described in Chapter 2. Although that antenna is electrically small (0.032λ in height), it requires a sizable ground plane to operate well. It is shown that by using a modified spiral ground plane of size 0.05λ, the measured transmission loss of the small antenna is 7dB better than the same size solid ground.

3.2. EFFECT OF GROUND PLANE SIZE ON TRANSMISSION LOSS

A monopole antenna is used to illustrate the effect of a reduced-size ground plane on transmission loss. Figure 3.1 shows the effect of ground-plane size on transmission loss. For the testing antennas, quarter-wavelength monopoles of 30MHz and 100MHz are used. Dry soil ($\varepsilon_r = 3$, $\sigma = 0.0001$S/m) is assumed in the Sommerfeld calculation. A radial ground plane composed of 20 arms is used in Figure 3.1(a), and a rectangular ground plane is used in Figure 3.1(b). In both cases, the transmitter and the receiver are identical.

As Figure 3.1(a) shows, the curve for transmission loss drops drastically for ground-plane diameters less than $\lambda/10$. A similar observation can be made for the rectangular ground plane in Figure 3.1(b). Instead of a rectangular solid ground plane, a rectangular grid ground plane is used in this investigation because NEC cannot simulate a solid surface.

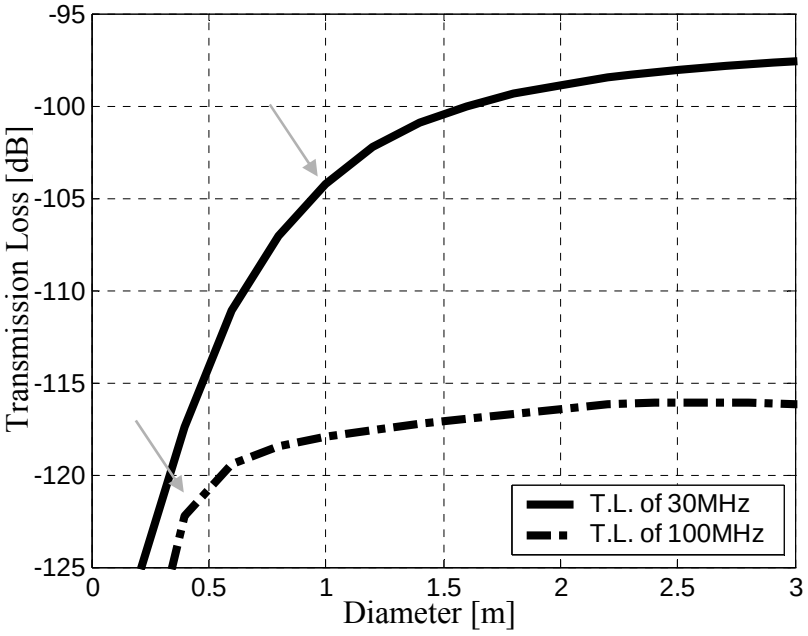

(a)

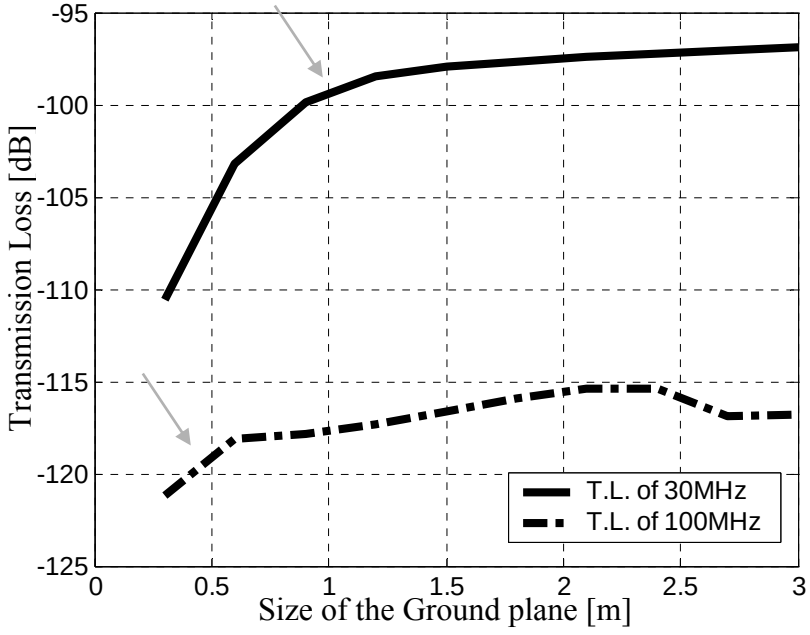

(b)

Figure 3.1: Ground plane size effect to the transmission loss.
(a) Radial ground plane (20 arms).
(b) Rectangular ground plane.

To determine the cause of the rapid transmission loss in ground planes of decreasingly small sizes, the resonant frequency of the 30MHz monopole is investigated with two different sizes of eight-arm radial ground planes. One of these ground planes (Figure 3.2(a)) has a diameter of 4.8m, which is about λ/2 diameter, and the other (Figure 3.2(b)) is 0.4m, which is less than λ/10 diameter. A dry soil is assumed for the soil characteristic. Figure 3.2(c) shows the simulated VSWR of a quarter-wavelength 30MHz monopole with the two different sizes of eight-arm radial ground planes.

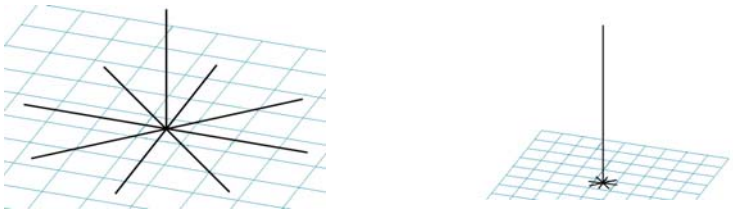

(a) (b)

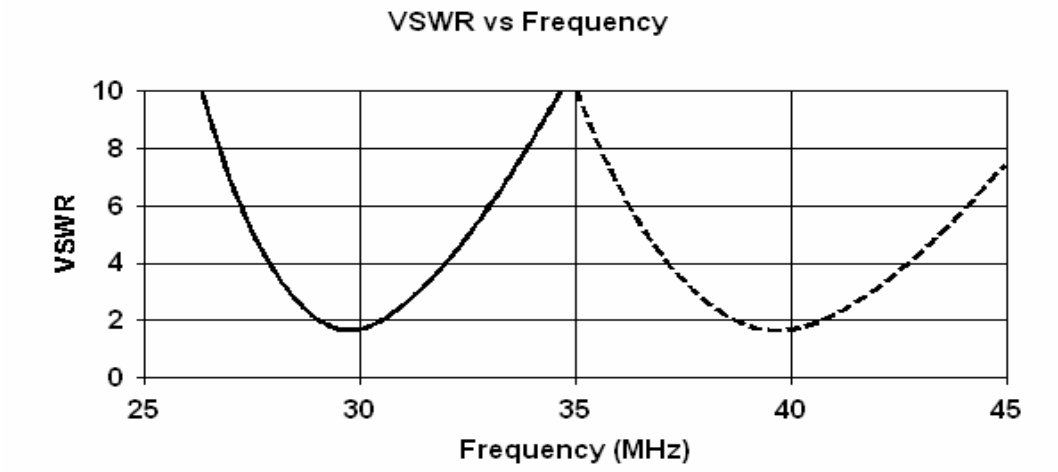

(c)

Figure 3.2: VSWR of the 30 MHz monopole with two different ground planes.
(a) Diameter = 4.8m.
(b) Diameter = 0.4m.
(c) (**—**)**:** VSWR of (a), (----): VSWR of (b).

As we can see in Figure 3.2, the resonant frequency shifts up about 10MHz as the diameter of the ground plane decreases from 4.8m to 0.4m. A similar shift can be observed for a 20-arm radial ground plane. As the ground plane size decreases from infinity to zero, the monopole antenna eventually becomes an end-fed dipole without a ground plane. The resonant frequency increases from 30MHz to approximately 60MHz, that is, from the resonant frequency of a monopole to that of a dipole. Interestingly, at the same time, the directivity changes from 3.2 to 1.6 [39], that is, from the directivity of a monopole to that of a dipole. Therefore, a small ground plane results in a mismatching loss, and if the mismatching loss is removed, the drastic drop in the transmission-loss curve due to the small size of the ground plane disappears.

The transmission-loss curve in Figure 3.1 can be regenerated to reflect the removal of the mismatching loss. This new curve is shown in Figure 3.3, where the solid lines represent transmission loss before mismatching-loss removal, and the dotted lines represent transmission loss after the removal of mismatching loss. Figure 3.3(a) represents the curve for the 30MHz quarter-wavelength monopole, and Figure 3.3(b) represents the curve for the 100MHz quarter-wavelength monopole. In both cases, 20 arms are used for the radial ground plane.

As Figure 3.3 shows, the drastic drop in the transmission-loss curve disappears when the mismatching loss is removed. We can see that, by reducing the resonant frequency, which otherwise increases as the size of the ground plane grows smaller, we can remove much of the transmission loss, which also normally increases as the ground plane grows smaller. The process of tuning the new antennas, moreover, reveals that inductance decreases the resonant frequency and capacitance increases it.

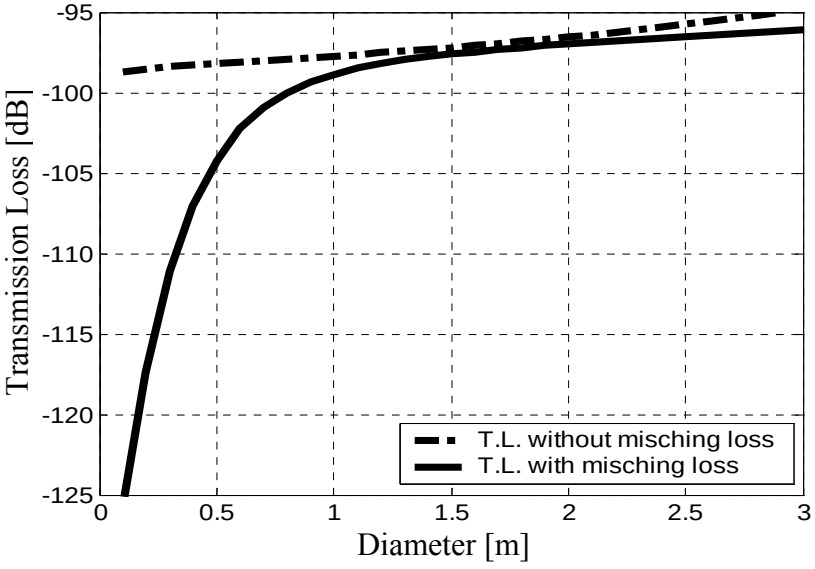

(a)

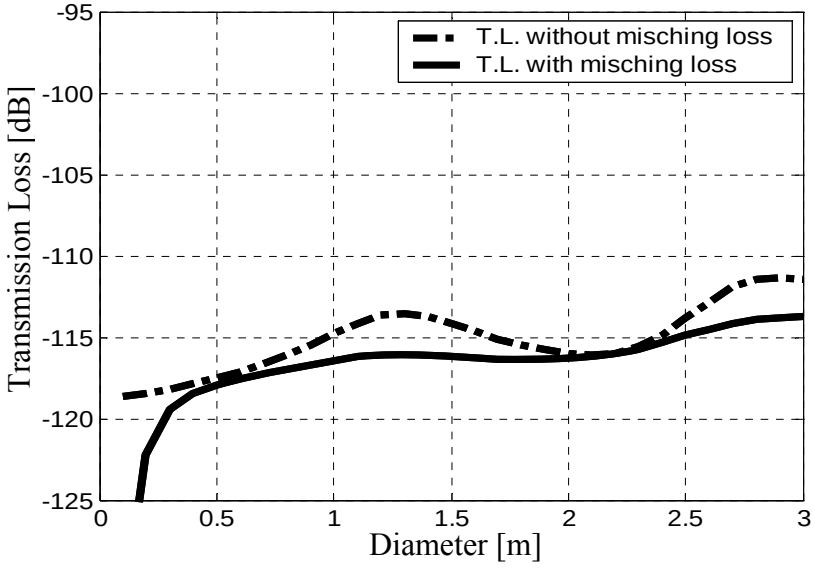

(b)

Figure 3.3: Removal of the drastic TL drop.
(a) 30MHz quarter wavelength monopole.
(b) 100MHz quarter wavelength monopole.

Both the inductively loaded ground plane and the capacitively loaded ground plane can be simulated using the 30MHz monopole for antennas. Again, a dry soil is assumed. The simulation shows that inductive loading on the ground plane helps shift the resonant frequency down, and capacitance loading does not.

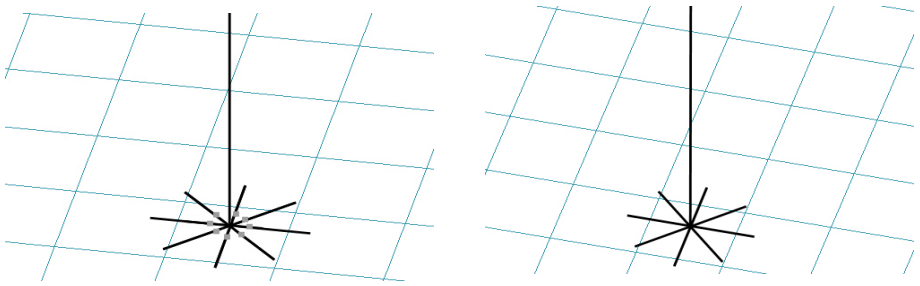

(a) (b)

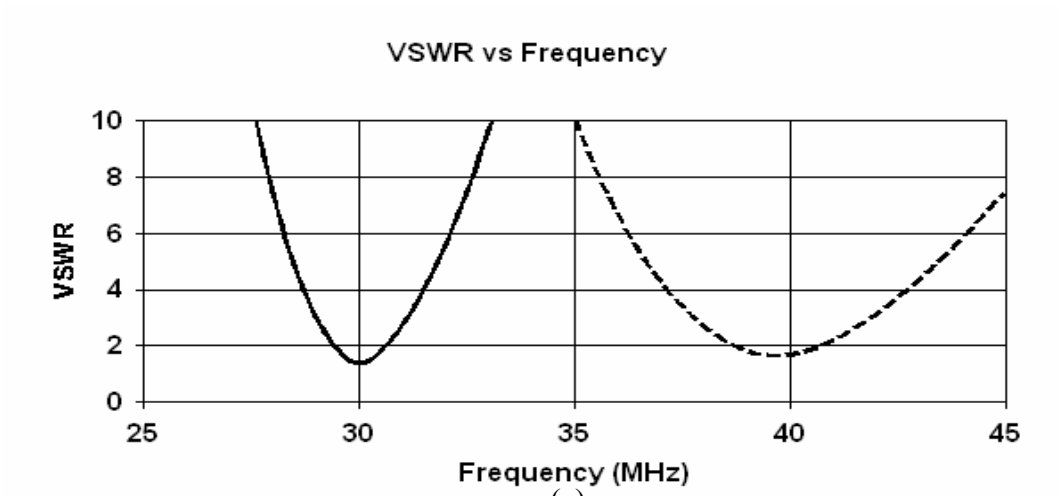

(c)

Figure 3.4: VSWR of the 30MHz monopole with and without ground-plane loadings.
(a) Diameter = 0.4m, with the inductance loaded.
(b) Diameter = 0.4m, without the inductance.
(c) **(—):** VSWR of (a), (----): VSWR of (b).

Figure 3.4 illustrates the results of the two different ground-plane loadings. Eight-arm radial ground planes with 0.4m diameters are used in both cases. Figure 3.4(a) is the inductively loaded ground plane, and Figure 3.4(b) is the regular radial ground plane. For the inductively loaded ground plane, each arm has an inductance value, and 21uH of the

inductance value is used. Figure 3.4(c), which gives the VSWR of the ground plane both with and without inductive loading, shows that the resonant frequency of the inductively loaded ground plane returns to 30MHz.

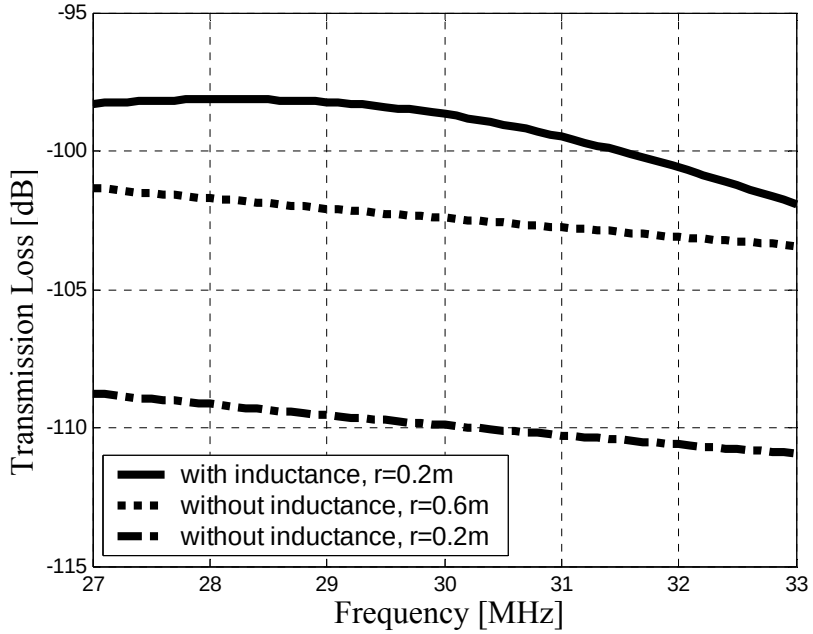

Figure. 3.5: Transmission loss with three kinds of ground plane.

Figure 3.5 shows the transmission losses of three kinds of ground planes with the same 30MHz quarter-wavelength monopole: one has an inductance-loaded ground plane with a 0.4m diameter; one has a regular radial ground plane with a 1.2m diameter; and the third has a regular radial ground plane with a 0.4m diameter. The number of arms in each of the three radial ground planes is eight. The soil characteristic is again dry. For the inductance-loaded ground plane, each arm has its own inductance value, and 21uH of the inductance value is installed on each arm, as in the case illustrated in Figure 3.4.

3.3 SPIRAL GROUND PLANE FOR A QUARTER-WAVE MONOPOLE

In order to remove the mismatch loss, a spiral ground plane is proposed. The spiral ground plane generates a large inductance that helps shift the resonant frequency downwards. A genetic algorithm is used to optimize the dimensions of the spiral ground plane. A top view of a spiral ground plane that can generate a large inductance value is presented in Figure 3.6. A 30MHz quarter-wavelength monopole is used as the antenna. The spiral ground plane is composed of eight arms, and each arm has three turns. The diameter of the spiral is 0.53m.

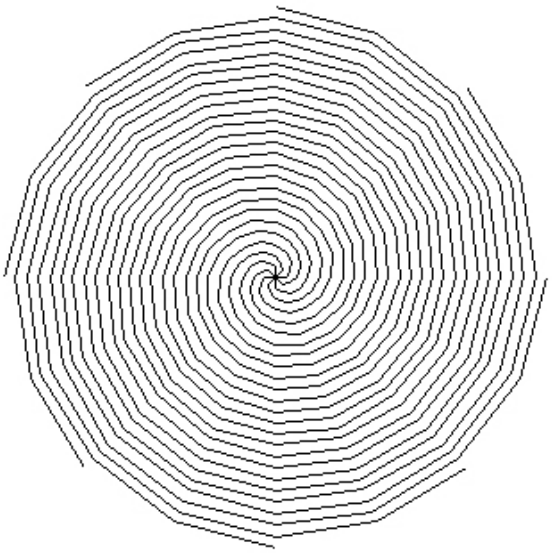

Figure 3.6: Top view of the spiral ground plane.

The principle underlying the use of a spiral ground plane to control resonant frequency is as following: Given a fixed diameter of ground plane, the resonant frequency decreases if we increase the number of turns in the spiral. On the other hand,

given a fixed number of turns in the spiral, the resonant frequency also decreases if we increase the ground-plane diameter.

As shown in Figure 3.7, the resonant frequency of the spiral ground plane is almost the same as that of the 21uH inductively loaded ground plane, whereas the resonant frequency of the regular radial ground plane is still 40MHz. Dry soil is used for the soil property.

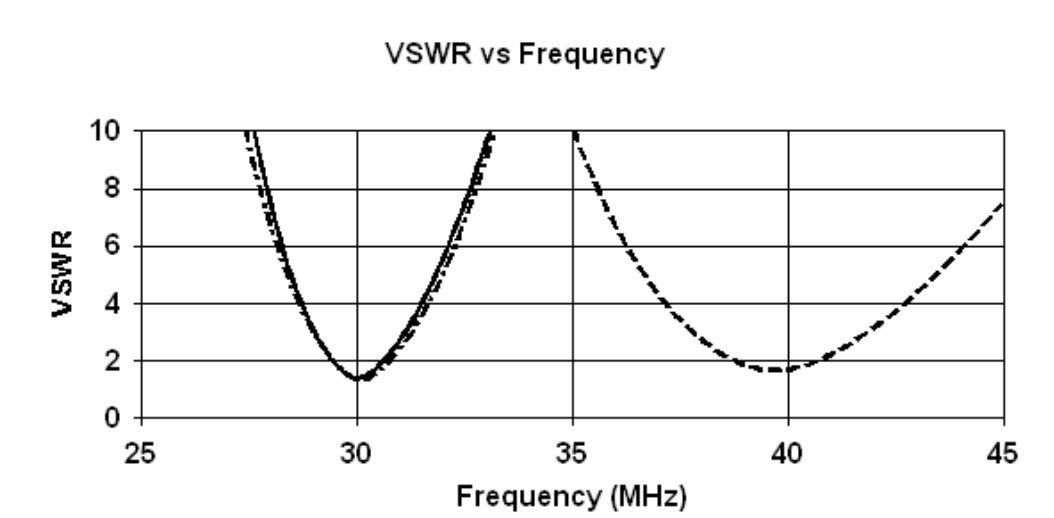

Figure 3.7: VSWR of three kinds of ground plane.
(**—):** VSWR of the spiral ground plane (diameter=0.53m).
(-.-.): VSWR of the inductance (21μH) loaded ground plane (diameter=0.4m).
(----): VSWR of the regular radial ground plane (diameter=0.4m).

Figure 3.8(a) presents the simulated VSWR of the eight-arm, spiral ground plane. In simulation, an intermediate soil is used for the simulation, and a 30MHz quarter-wavelength monopole is the antenna. The spiral ground plane has a 0.5m diameter, and the simulated resonant frequency is 29MHz.

The solid line of Figure 3.8(b) indicates the measured VSWR of the spiral ground plane. To suppress this outside surface current, a balun ("balanced-to-unbalanced

transformer") is used. Compared to the simulated value, the measured resonant frequency is shifted down about 1.5MHz. Tuning, therefore, is the process of adjusting the length of each arm of the spiral ground plane. The results of tuning are shown by the dotted line in Figure 3.8(b). Note that the resonant frequency now becomes 30MHz.

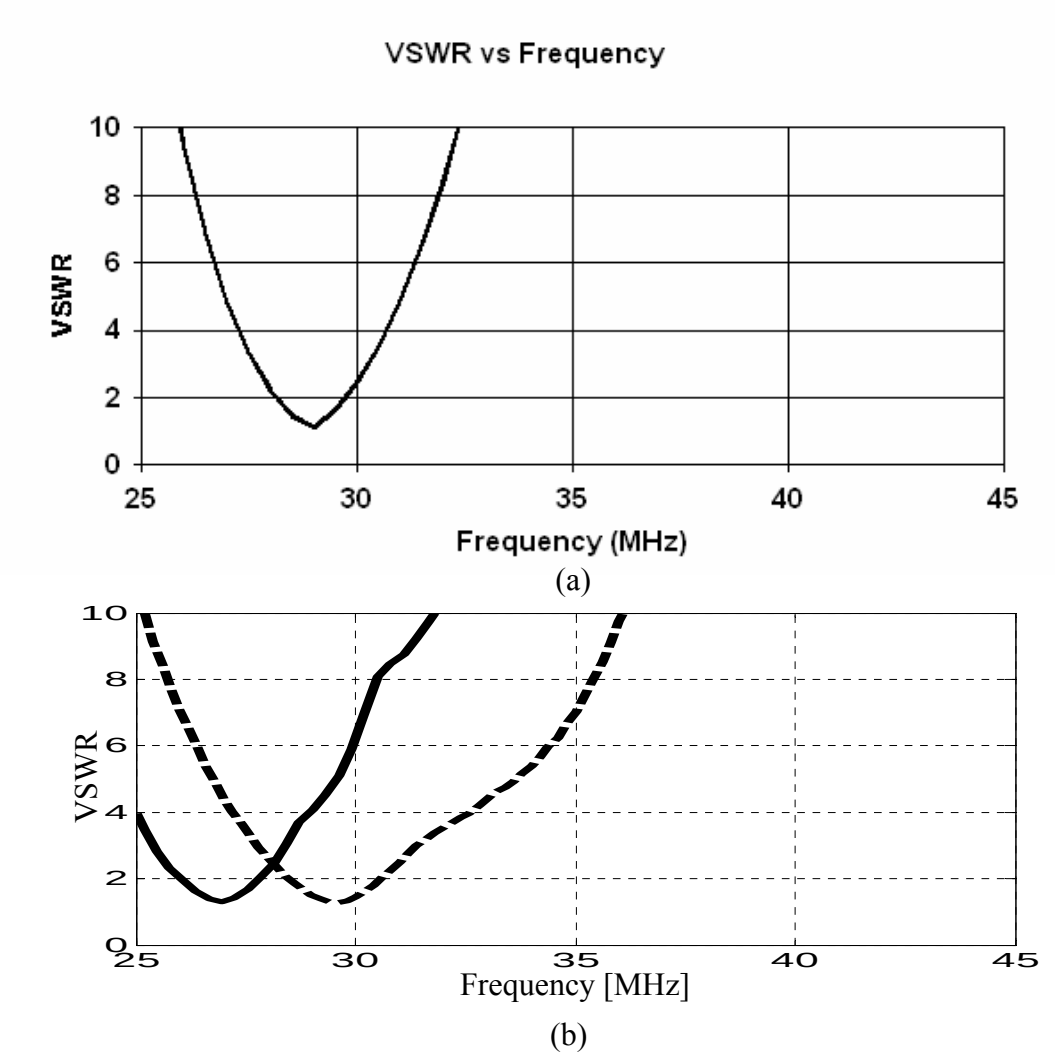

Figure 3.8: Simulated and measured VSWR of the 30MHz monopole with the spiral ground plane.
(a) Simulated VSWR: diameter = 0.5m.
(b) Measured VSWR: (**—):** diameter = 0.5m, (----): diameter = 0.43m.

Figure 3.9 depicts a prototype of the tuned spiral ground plane constructed of 18 gauge copper wire.

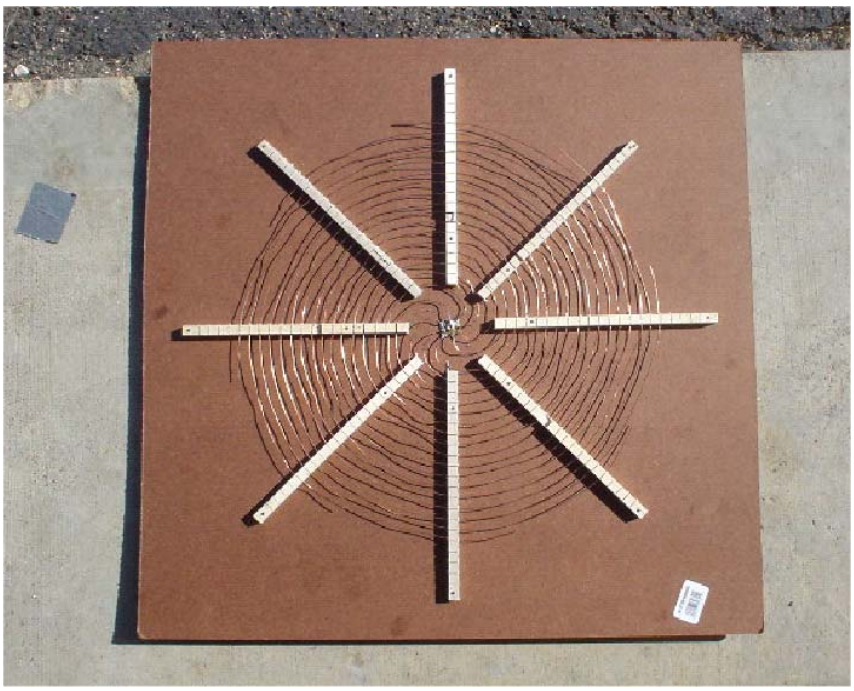

Figure 3.9: Prototype of the spiral ground plane.

Next, Figure 3.10 shows the results of outdoor transmission tests carried out with four different ground planes. The 30MHz quarter-wavelength monopoles are used at the transmitter and receiver, which are 15m apart. Each ground plane is tested on grassy ground. A network analyzer is used to measure the transmission loss. For the receiver, a fixed 50cm x 50cm rectangular ground plane is used. For the transmitter, four ground planes are used: a spiral ground plane with a diameter of 0.43m, an eight-arm radial ground plane with a diameter of 0.5m, an eight-arm radial ground plane with a diameter of 1.2m, and a 120cm x 120cm rectangular ground plane.

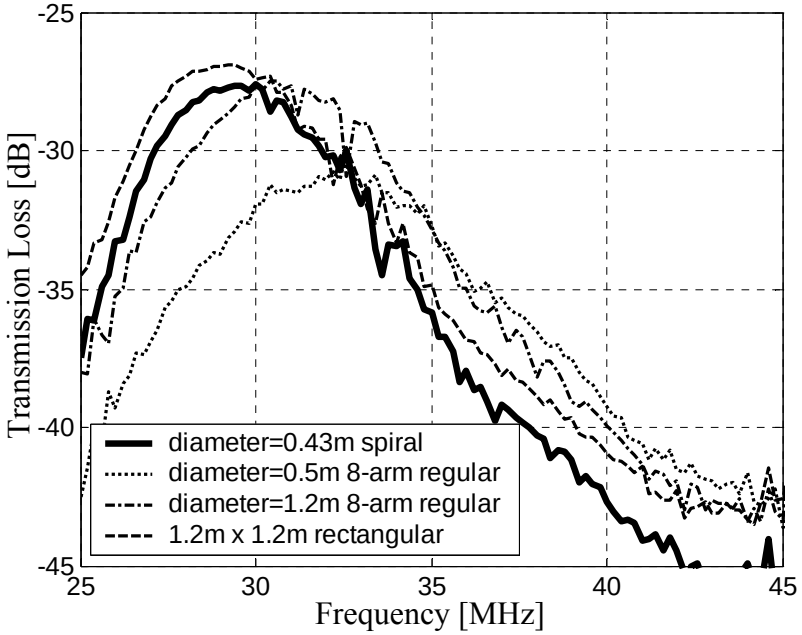

Figure 3.10: Transmission losses of four different ground planes.

As shown in Figure 3.10, the transmission loss of the 0.43m-diameter spiral ground plane is almost the same as that of the 1.2m-diameter eight-arm radial ground plane and that of the 120cm × 120cm rectangular ground plane. Despite the very small size of the spiral ground plane, its transmission loss is 4dB better than that of the 0.5m-diameter radial ground plane. These results show that the spiral ground radial is a good structure for achieving a miniaturized ground plane.

3.4 SMALL GROUND PLANE FOR AN ELECTRICALLY SMALL ANTENNA

Next, the concept is adapted for the electrically small GA antenna described in Chapter 2. After much struggle, it is found that the key in the design is not to perturb the image current beneath the antenna. The monopole image is represented by a single point, and thus the image is not a design issue. The image for a GA antenna, however, takes up some surface area, which has to be addressed by the combination of the solid ground

plane and the spiral ground plane. This requirement was confirmed by an investigation of the complex image current on the ground plane, as shown in Figure 3.11.

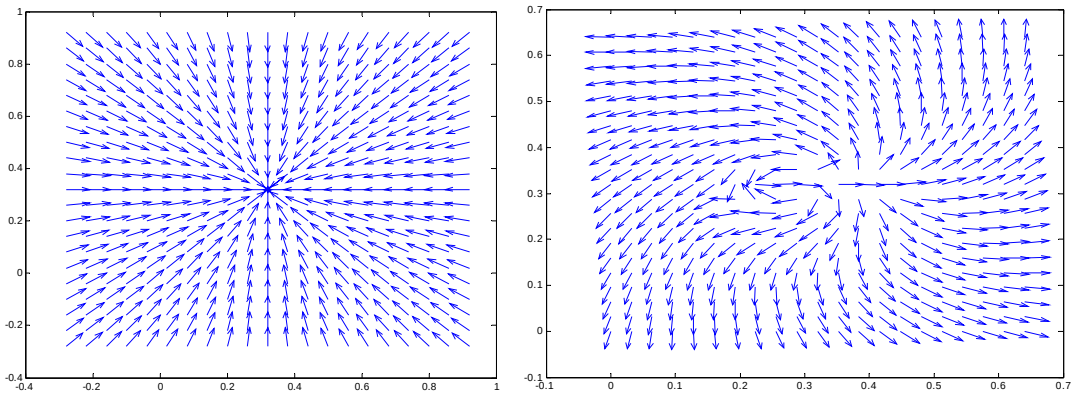

(a) (b)

Figure 3.11: Current distribution on infinite PEC ground planes.
(a) A quarter-wave monopole.
(b) The electrically small GA antenna.

Figure 3.12 shows the combination of a spiral ground plane and a GA antenna. An essential requirement is a minimum solid surface, which is used to support the image current from the top-loading. In the design, the solid surface is in the form of an octagon. Eight spiral arms are connected to the edge of the solid surface and wind along the edge. Note that the spirals are folded upwards to keep the overall form factor small. The size of the solid surface is 50cm, or 0.05λ at 30MHz. The spiral dimensions are optimized by a genetic algorithm. Each arm of the spiral contains $1^1/_8$ turns. The space between the wires is 0.86cm, and the total height of the ground spirals is 8.6cm above the ground. The measured VSWR of the small antenna on the small ground plane is 1.43 at 30MHz.

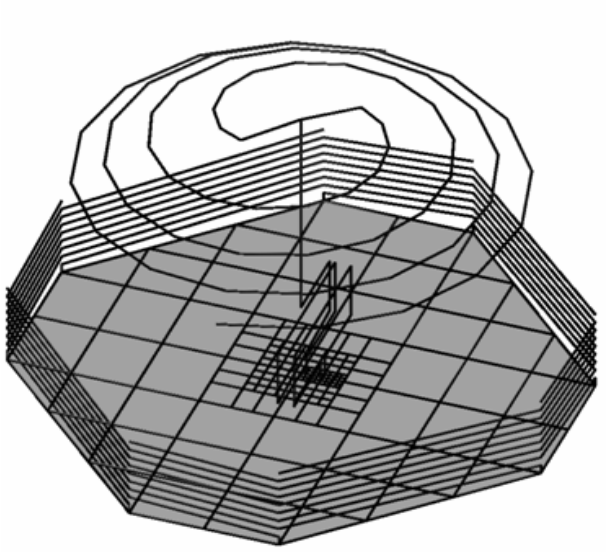

(a)

(b)

Figure 3.12: The combination of the spiral ground plane and the GA antenna.
(a) Design of a Ground plane.
(b) A prototype.

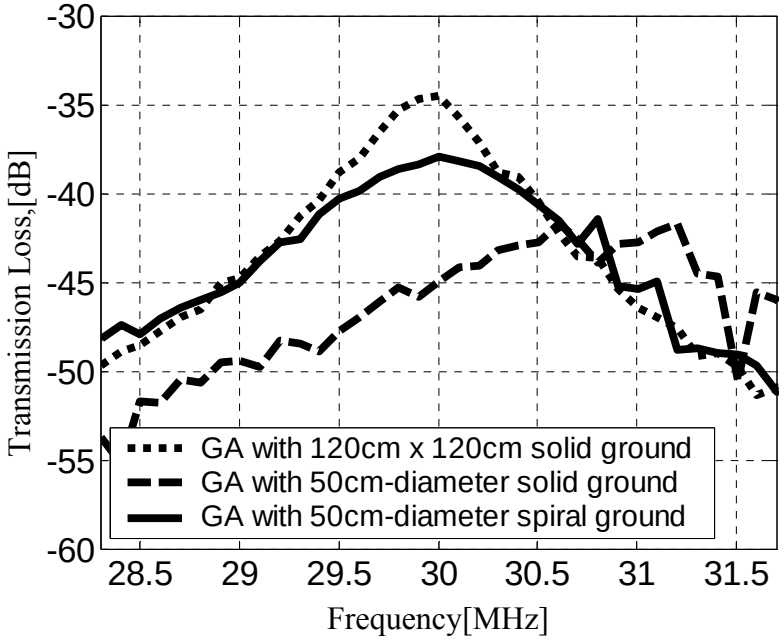

Figure 3.13: Measured transmission losses of three different ground planes versus frequency.

Figure 3.13 shows the outdoor transmission-loss tests of the small antenna with different ground planes. A commercial whip (from GLA Systems) is used as the receiver. For the transmitter, the small antennas with three different ground planes are used: a 120cm square solid ground plane, a 50cm octagonal-shaped solid ground plane without spirals, and the 50cm octagonal solid ground plane with spiral design, as shown in the inset. The test setup is similar to that for the quarter-wave monopole measurements. We observe that the transmission loss drops by about 10dB when the ground plane is changed from the 120cm to the 50cm solid ground plane at the intended operating frequency of 30 MHz. The operating frequency of the small antenna on the smaller ground plane shifts upwards, which is similar to the quarter-wave monopole. By using the spiral ground plane, a transmission loss improvement of 7dB over the same sized solid ground plane at

30 MHz can be achieved. The structure clearly resonates at the intended frequency of operation. There is about a 3dB difference between the 120cm ground plane and the miniaturized spiral ground plane.

3.5 SUMMARY

In this chapter, it was shown that, as the ground plane size is reduced, the mismatch loss is the main cause for the decrease in HF ground wave transmission performance. A spiral ground plane concept was proposed to reduce the mismatch loss. Prototypes of the spiral ground plane were designed and tested with a quarter-wave monopole and an electrically small antenna. The measured transmission losses of the spiral ground planes were 6 to 7dB better than those of the same sized ground planes at the intended operating frequency.

Chapter 4

A Tunable Electrically Small Antenna for Ground Wave Transmission

4.1 INTRODUCTION

Ground wave propagation along the Earth's surface in the HF and VHF region is very useful for extended-range, non-line-of-sight communications [36]. A major challenge of HF and low-VHF communication is the antenna size. Therefore it is desirable to develop electrically small antennas for such applications. In Chapter 2, the design of a top-loaded, inductively-coupled, electrically small antenna is introduced. The antenna has a kr of 0.2. A genetic algorithm was used to optimize the design for maximum ground wave transmission. The antenna showed a transmission loss within 1dB of a commercial whip in open field testing in spite of its small size. However, as with other electrically small antennas [12, 13], this antenna suffers from very narrow bandwidth. Because the bandwidth of an antenna in relation to its size is limited by the Wheeler-Chu limit [2, 6], it is not possible to improve the bandwidth significantly without sacrificing the efficiency of the antenna.

In this chapter, methods to change the resonant frequency of the GA antenna using a variable capacitor are investigated. Although it is impossible to increase the bandwidth of the antenna with this technique, the GA antenna can achieve the frequency agility necessary to overcome various deployment variances and propagation effects, such as multi-path fading. Frequency tuning of antennas using varactor diodes and capacitors is a well known idea and has been applied to various microstrip patch antennas [40-42] and wire antennas [43]. Its utilization for electrically small antennas has also been reported in [44-46] for applications above 1GHz. Here, the focus is on HF/VHF ground wave transmission. In particular, the discussion focuses on the development of the

frequency-tuning capability to combat fading for fixed-point communication in complex multi-path environments, which can be especially detrimental to a narrow band antenna.

This chapter is organized as follows. In Section 4.2, the top-load, inductively-coupled small antenna at 39.7MHz is introduced and its operating principles explained. In Section 4.3, the tuning of the antenna via the insertion of a serially connect variable capacitor is presented. The various locations for the placement of the capacitor on the antenna are evaluated via simulation using the NEC. The tuning range and sensitivity are also investigated. In Section 4.4, the measured tuning performance of an experimental prototype is presented and compared to the simulation. Transmission loss tests are performed in the presence of multi-paths in both indoor and outdoor environments. The measured transmission loss of the tunable small antenna is compared with that of a commercial whip. Conclusions are given in Section 4.5.

4.2 TOP-LOADED, INDUCTIVELY-COUPLED ANTENNA WITH A VARIABLE CAPACITOR AT 39.7MHZ

Figure 4.1 shows a top-loaded, inductively-coupled, small antenna operating at 39.7MHz. The measured 3dB bandwidth of the antenna is 620KHz, or 1.6%, and is optimized for ground wave transmission. Figure 4.1(a) shows the antenna structure. The antenna consists of four parts: (i) a vertical antenna body, (ii) a spherical-helix top loading, (iii) a primary feed loop, and (iv) a secondary set of windings. The primary feed loop and the secondary windings comprise the inductively coupled feed. The purpose of the inductively coupled feed is to step up the input resistance [20]. It is located at the bottom part of the antenna body. The vertical antenna body is the main radiating part into the vertically polarized ground wave. The inverted spherical helix top-loading is used to achieve self resonance in a small space. Its dimensions are optimized to minimize any reduction in the ground wave coupling. Both a two-arm and a four-arm design were

presented in Chapter 2. The two-arm top-loading design is used in this chapter. The physical size of the antenna fits within a 22.75cm hemisphere, which corresponds to a *kr* of 0.19 at 39.7 MHz. The length of the vertical antenna body is 16.75cm. The secondary windings include one and a half turns. The areas of the primary feed loop and the secondary windings are both 9.9cm × 4.9cm. The distance between the primary feed loop and the secondary windings is 2.5cm. For the top loading structure, each arm includes two and half turns along the hemisphere, and the two arms are symmetrical. The height from the ground plane to the end of the top loading arms is 15.9cm. Figure 4.1(b) is a photo of the prototype antenna. The antenna is made with copper wires of 1.5mm radius. The curved gray rods in the photo are bent PVC rods used to support the top-loading structure.

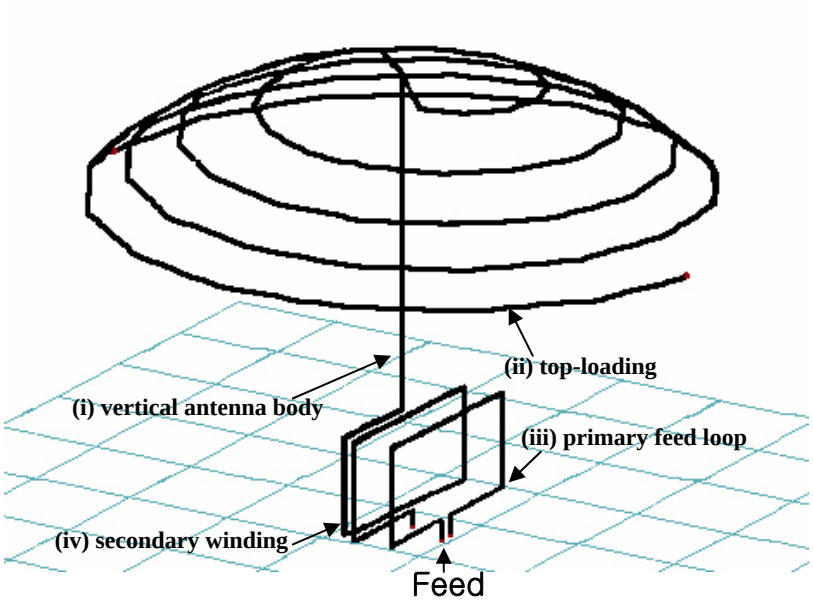

(a)

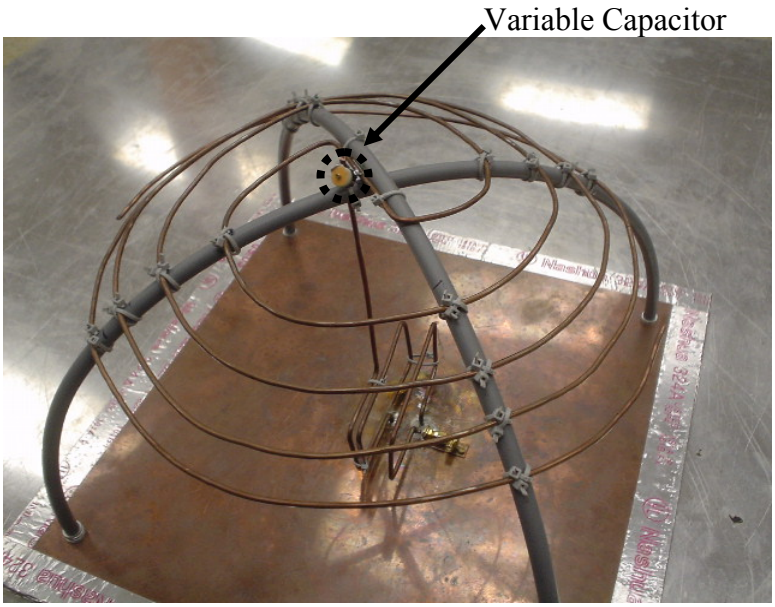

(b)

Figure 4.1: A GA antenna at 39.7MHz.
(a) Four divisions of the GA antenna.
(b) A prototype of the GA antenna with a variable capacitor.

4.3 FREQUENCY TUNING

In this section, lumped-element tuning is investigated for the electrically small antenna. Since a shunt connection is difficult to realize in the antenna, a serial lumped-element connection is considered. First, simulation of the effect of variable capacitance and inductance on the antenna operating frequency is performed with NEC. The simulation results show that an inductor reduces the resonant frequency, whereas a capacitor raises the frequency. However, it is difficult to find inductors with sufficiently large inductances to operate at HF/VHF frequencies due to parasitic capacitances. For this reason, capacitive tuning is chosen.

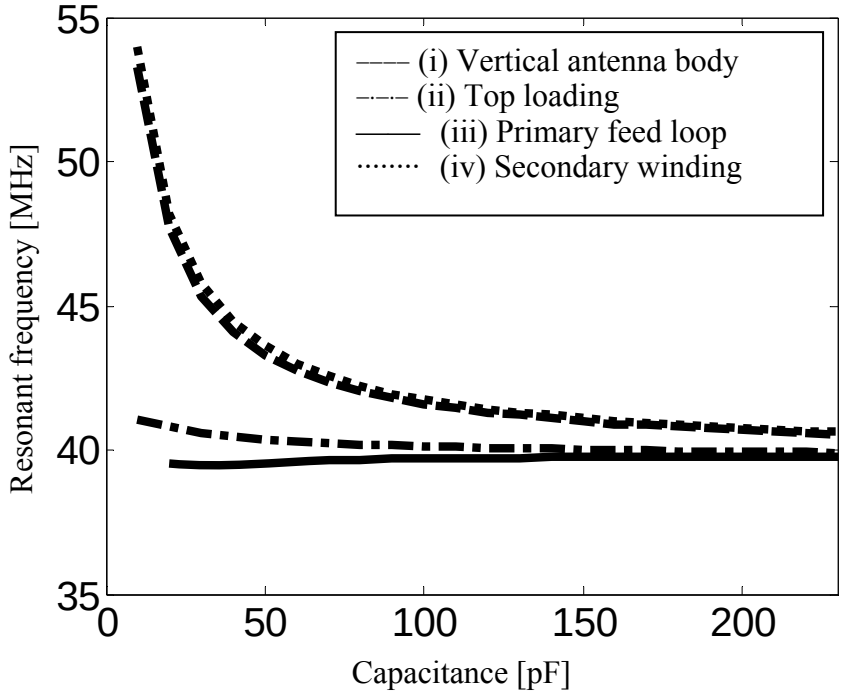

Figure 4.2: Tuning range at different loading position on the antenna.

The effect of the variable capacitor location on the antenna tuning is investigated. Figure 4.2 shows the simulated results of the resonant frequency variation versus the capacitance value with the capacitor placed in four different sections: (i) the vertical antenna body, (ii) the top loading, (iii) the primary feed loop, and (iv) the secondary winding. Although several different positions are tested within each section, the variations in performance due to different positions within each section are fairly small. The graph shows that the tunable frequency range is dependent on which section the capacitor is located. The tunable range when the capacitor is placed along (i) the vertical antenna body or (iv) the secondary winding is similar and ranges from 40.5MHz to 54MHz as the capacitance value is changed from 230pF to 10pF. On the other hand, the tunable range when the capacitor is placed along (ii) the top loading or (iii) the feed loop is very narrow. This result correlates well with the observation that the currents are strong in sections (i) and (iv) and weak in sections (ii) and (iii). Therefore, it is concluded that large tuning range is achieved by placing the capacitor at a location on the antenna where the current is strong. We can also see that small capacitance change leads to large frequency change at the high frequency end of the tuning range in sections (i) and (iv).

Based on the result of the simulation study, the topmost point of the vertical antenna body is chosen as the position for introducing the variable capacitor in the prototype, as shown in Figure 4.1(c). It is one of the optimal positions from the simulation study, and it is easier from the construction viewpoint, because the top loading and the antenna body are built separately and soldered together during final assembly. A mechanically tunable variable capacitor with a tuning range from 10pF to 230pF is used.

4.4 SIMULATED AND MEASURED RESULTS

4.4.1 Return loss

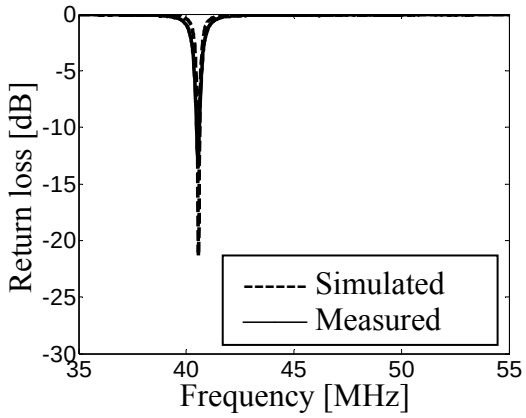

(a)

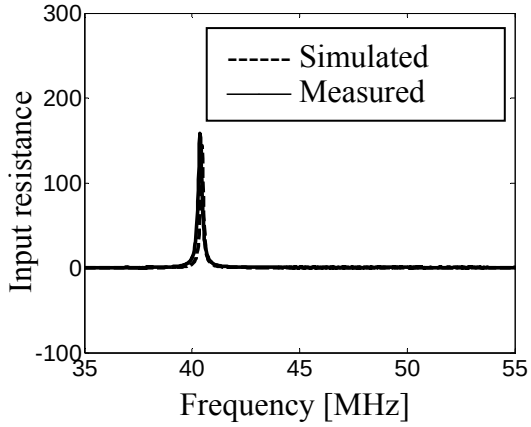

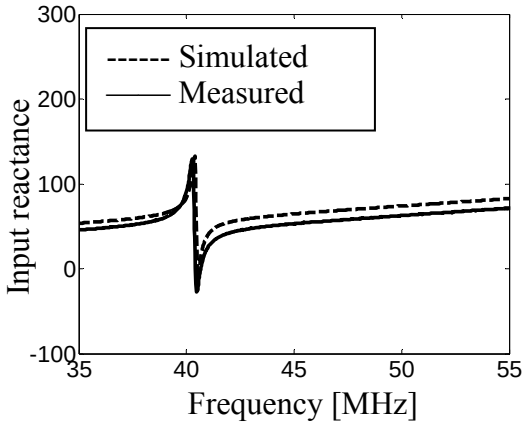

(b)

Figure 4.3: Simulation vs. measurement with a 230pF load.
(a) Return loss.
(b) Input impedance.

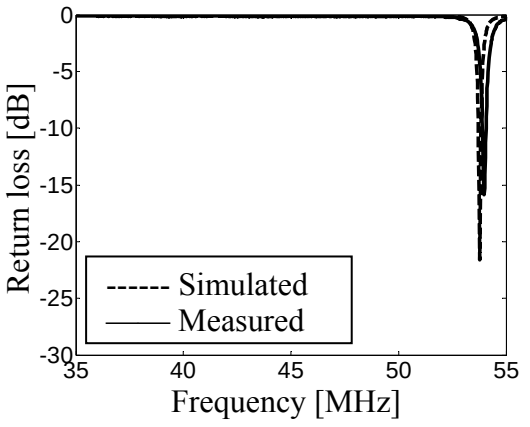

(a)

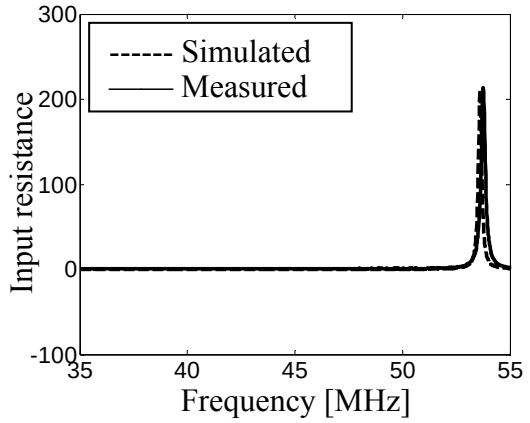

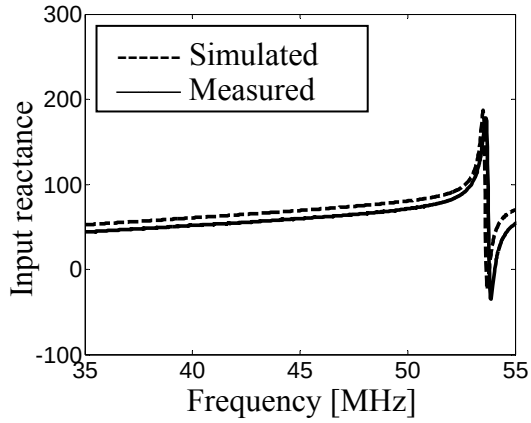

(b)

Figure 4.4: Simulation vs. measurement with a 10pF load.
(a) Return loss.
(b) Input impedance.

Figure 4.3 is a comparison between simulation and measurement with a 230pF load. Figure 4.3(a) shows the return loss (with respect to a 50Ω reference), and Figure 4.3(b) is the input impedance data. The measured resonant frequency is 40.55MHz, which is shifted slightly upward (by 0.8MHz) compared to that of the original antenna without the capacitor. The measured result agrees well with the simulated resonant frequency of 40.56MHz.

Similar comparison tests with the capacitor set at 10pF, the other end of the tuning range, are reported in Figure 4.4. This time, the measured antenna resonant frequency is shifted to 54.02MHz, and the simulated one is at 53.78MHz. The simulation and measured results differ by about 0.24MHz. The larger discrepancy between the simulated and measured results for the 10pF load is due to the higher tuning sensitivity at the upper frequency end. As observed earlier in Figure 4.2, a small difference in the capacitance value leads to a large difference in the resonant frequency at the high frequency end of the tuning range. The simulated and measured input impedances with the 10pF capacitance value are also shown in Figure 4.4(b). The impedance matching and the bandwidth of the antenna remain fairly stable throughout the tuning range. The measured 3dB bandwidth at 40.55MHz is 520KHz (1.3%) and that at 54.02MHz is 560KHz (1.0%).

4.4.2 Efficiency

The antenna efficiency is simulated by NEC and measured using the Wheeler cap method. For the latter, the procedure is slightly more complicated than the usual process, since the antenna does not behave like a simple RLC circuit at resonance. The procedure entails using the equivalent circuit model in Figure 2.7, determining the circuit parameters from the measured input impedance data, and backing out the efficiency from the extracted radiation resistance and loss resistance. This procedure was introduced

previously in Chapter 2. It is assumed that R(ω) in the circuit models is the radiation plus the loss resistance of the antenna. A Taylor expansion is used to model its frequency dependence. An optimizer is used to extract all the lumped-element values from the measurement data about the resonant frequency (for both the with-cap and without-cap cases). After the parameter extraction, the efficiency is computed based on the resistance R(ω).

The antenna efficiencies for three cases are simulated and measured. The Wheeler cap used in the measurement is a rectangular conducting box of dimensions 51cm by 54cm by 54cm. Figure 4.5(a) shows the efficiency of the antenna without any capacitive loads. Figure 4.5(b) shows the efficiency of the antenna with the 230pF load. Figure 4.5(c) shows the efficiency of the antenna with the 10pF load. The results indicate that the antenna efficiency stays relatively stable within the tuning range and that the capacitive load does not degrade the efficiency of the unloaded antenna significantly. The simulated and measured efficiencies range between 50% and 66%.

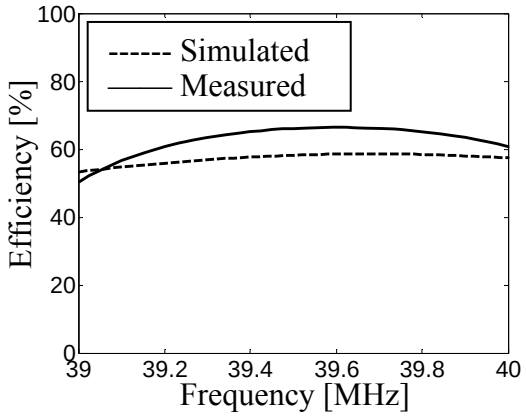

(a)

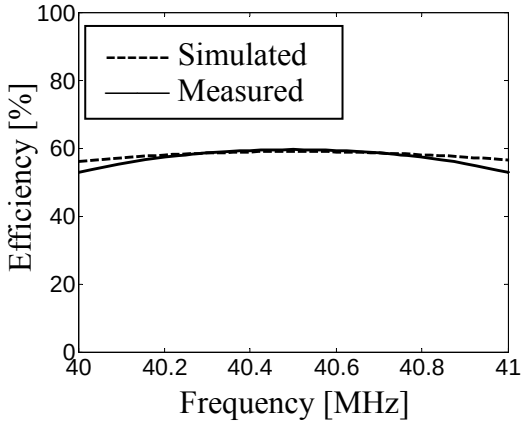

(b)

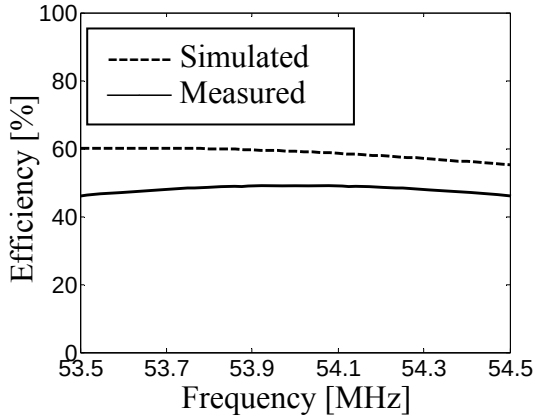

(c)

Figure 4.5: Simulated and measured efficiencies.
(a) Efficiency without a capacitor.
(b) Efficiency with a 230pF load.
(c) Efficiency with a 10pF load.

4.4.3 Transmission loss test for non-line-of-sight scenarios

Next, transmission loss measurements are carried out indoors and outdoors in the presence of multi-path fading. A vector network analyzer is used to measure the transmission (i.e., S_{21}) data. Commercial whips (from GLA Systems) and the tunable small antenna are used. The resonant frequencies of the whips are tuned to 43MHz. The commercial whips are calibrated against a quarter-wavelength copper tubing monopole (outer diameter: 1.2cm, inner diameter: 0.8cm), and their realized gains are about 0.5dB below that of the copper tubing monopole at 43MHz.

Figure 4.6 represents the indoor measurement result collected in a building. The geometry of the test area is shown in Figure 4.6(a). Both the transmitter and the receiver are located in the hallway of the building in a non-line-of-sight configuration. Figure 4.6(b) shows the measured transmission losses. First, two identical whips are used for the transmitter and the receiver. The solid line is the result of this whip-to-whip test. We can see that deep fades (more than 10dB) occur at 45.2MHz and 49.6MHz. Even though the whips are tuned to 43MHz, they are fairly broadband and the overall transmission loss is dominated by the channel. The dashed curve shows the small-antenna-to-whip result. In this case, the small antenna is tuned to 42.2MHz. Because the small antenna is very narrow band, the transmission loss is now dominated by the antenna itself. Away from its operating frequency, the transmission loss falls off quickly. The peak value reached at 42.2MHz is approximately 2dB below the whip-to-whip result. Next, the resonant frequency of the small antenna is tuned to other operating frequencies, and the transmission losses at those frequencies are measured. The results for 12 different frequencies are shown as green dots in Figure 4.6(b). They show that the small-antenna-to-whip data are within 1~2dB of the whip-to-whip results. Note that the small-antenna-to-whip data appear to be even better than the whip-to-whip reference at higher

frequencies. This is due to the fact that the matching characteristic of the whip begins to come into play at frequencies too far removed from the frequency at which it is tuned.

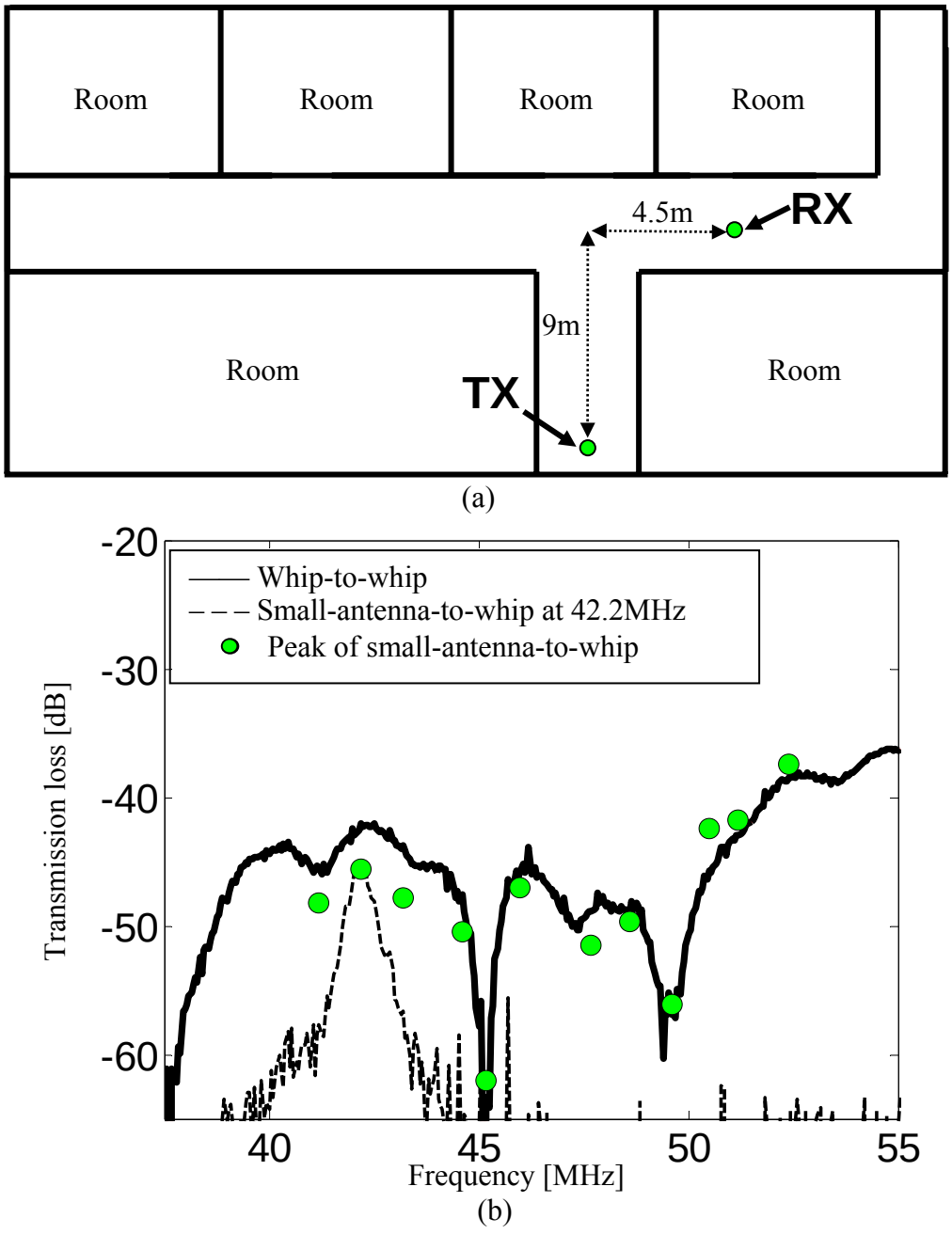

Figure 4.6: Indoor transmission loss results.
(a) Indoor geometry.
(b) Transmission loss vs. frequency of the small-antenna-to-whip link.

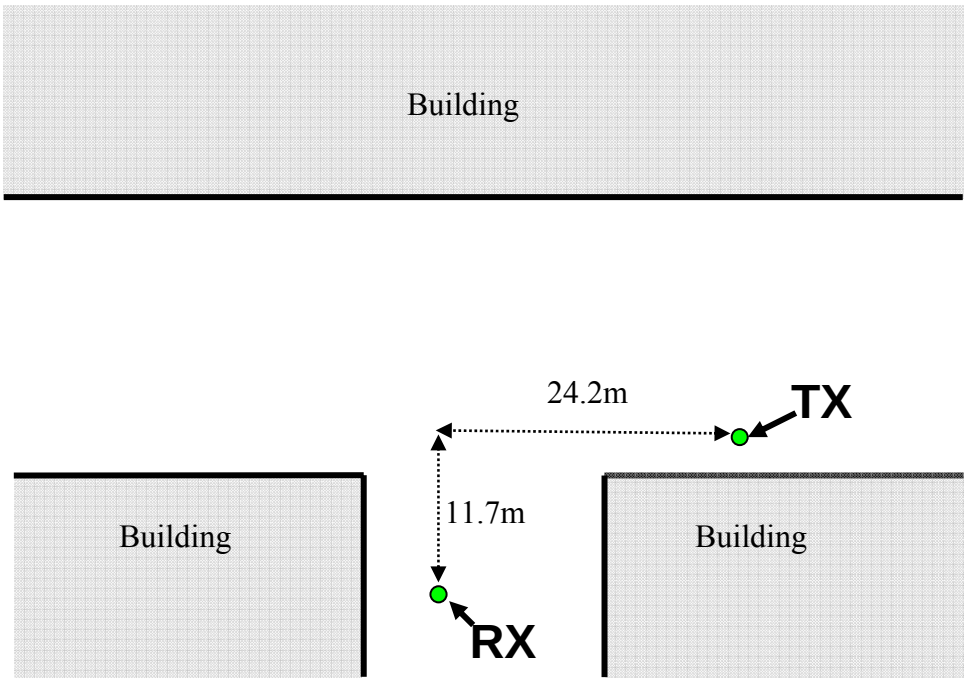
Building
24.2m
TX
11.7m
Building
Building
RX

(a)

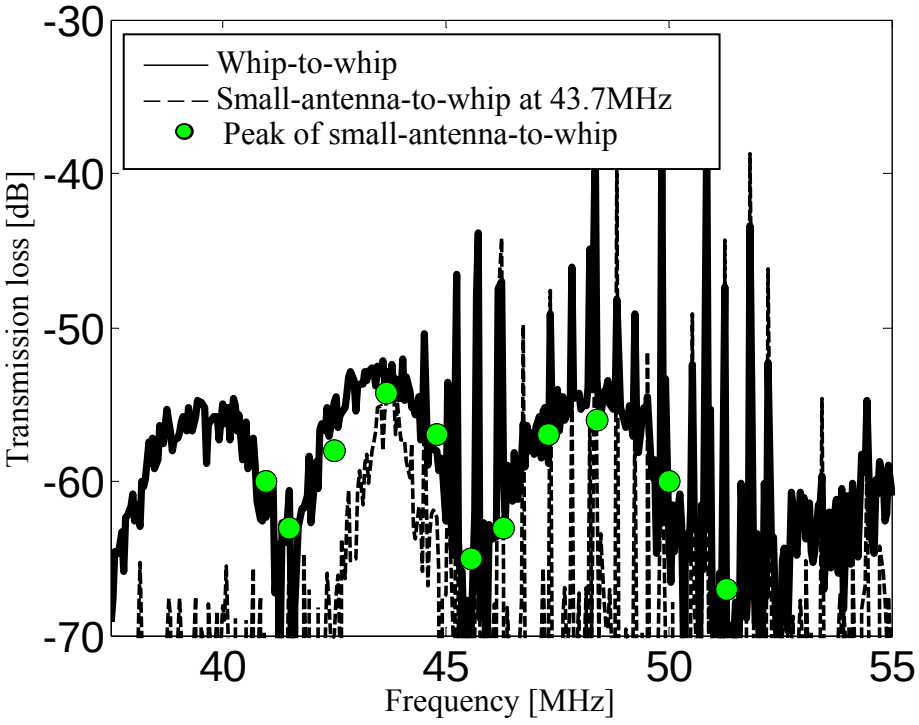
Whip-to-whip
Small-antenna-to-whip at 43.7MHz
Peak of small-antenna-to-whip
Transmission loss [dB]
-30
-40
-50
-60
-70
40
45
50
55
Frequency [MHz]

(b)

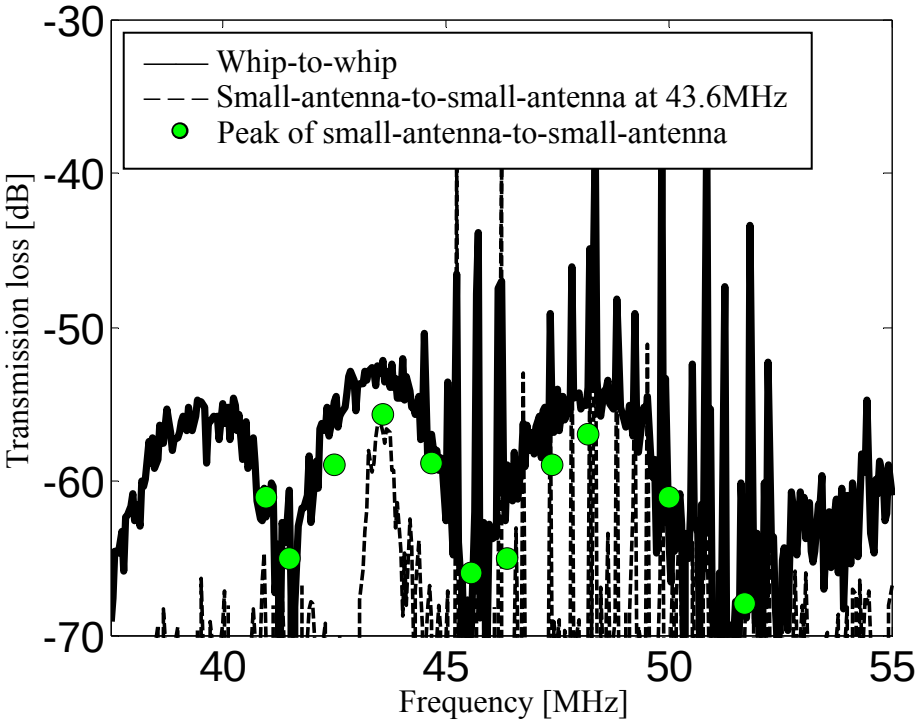

(c)

Figure 4.7: Outdoor transmission loss results.
(a) Outdoor geometry.
(b) Transmission loss vs. frequency of the small-antenna-to-whip link.
(c) Transmission loss vs. frequency of the small-antenna-to-small-antenna link.

A similar transmission loss test is performed outdoors, again under a non-line-of-sight configuration. Figure 4.7(a) shows the geometry of the test area and the position of the transmitting and receiving antennas outside the building. The results are shown in Figure 4.7(b). During the data collection, there was considerable RF interference from other sources, and it shows up as spikes in the traces. Other than that, the results are consistent with the indoor results. The peaks in the small-antenna-to-whip measurements nearly match that of the whip-to-whip data. Figure 4.7(c) shows the measured results

with two tunable small antennas at both ends of the link. The data show a slightly worse transmission loss in comparison to the small-antenna-to-whip link.

Measurements in other, more realistic non-line-of-sight environments have been carried out, and the data are consistent with those shown here. The frequency fade duration in the propagation environment dictates the tuning range required in the antenna design. The use of a varactor element to achieve electronic tuning has also been tested. Other than a slightly narrower tuning range due to the varactor values, the results are very similar to those reported in this chapter.

4.5 SUMMARY

A frequency-tuning capability has been developed to provide frequency agility to a narrow-band, electrically small antenna. A variable capacitance was connected serially at the strong current location on the antenna to provide good tuning performance. Measured results on a prototype showed good agreement with the simulation results. Transmission loss tests were carried out in several non-line-of-sight environments. The measured transmission loss of the tunable small antenna came within 1 to 2 dB of that of a commercial whip across the tested frequency range. In non-line-of-sight communications, it is often not desirable to operate the link at a single fixed frequency due to multipath fading or RF interference. This is particularly problematic for small antennas, which are intrinsically very narrow band. By combining the frequency tuning capability of the small antenna with a frequency agile radio system, it becomes feasible to operate at frequencies where the channel characteristics are most favorable.

Chapter 5

Design of a Thin, Efficient, Electrically Small Antenna Using Multiple Foldings

5.1 INTRODUCTION

It is well known that the radiation resistance of an electrically small antenna drops precipitously as the size of the antenna is decreased. As a result, the loss resistance becomes a predominant portion of the total input resistance, and the efficiency of the antenna suffers. Therefore, in the design of electrically small antennas, it is important to effectively boost up the radiation resistance. Previously, an inductively coupled feed (ICF) concept was proposed to step up the input resistance in electrically small antennas [20]. Several antennas have been subsequently reported based on the ICF [21, 47].

Another useful approach to increase the input resistance is the use of the folding concept [19, 13]. In this chapter, the achievable efficiencies of electrically small antennas based on the ICF are compared to the multiply folded design. It is shown that the folding concept can theoretically outperform the ICF. Then the design of an electrically small, thin monopole antenna using multiple foldings is presented. The design has a height of 9cm and operates at 150MHz. The resulting efficiency of the antenna is significantly higher than that of the corresponding ICF design.

5.2 EFFICIENCY LIMIT

Let us first compare the theoretical efficiencies of the ICF design and the multiply folded design. The radiation resistance of an electrically small, resonant monopole scales quadratically as a function of kr:

$$R_{rad} = C_1 (kr)^2 \qquad \text{Eq. 5.1}$$

By assuming that the radiation resistance of a quarter-wave-length monopole is 36Ω, C_1 is found to be 14.1Ω. The loss resistance is given by

$$R_{loss} = \frac{L_{eff}}{2\pi a \sigma \delta} \qquad \text{Eq. 5.2}$$

where σ is the conductivity of copper, L_{eff} is the effective length (λ/8 for a quarter-wavelength monopole), and δ is the skin depth. The ICF acts as a transformer to achieve improved impedance matching. However, it steps up both the radiation resistance and the loss resistance by the same ratio. Thus, the efficiency of the antenna is not altered by the use of the ICF and is given by

$$Efficiency(ICF) = \frac{R_{rad}}{R_{loss} + R_{rad}} = \frac{C_1 (kr)^2}{R_{loss} + C_1 (kr)^2} \qquad \text{Eq. 5.3}$$

Figure 5.1 shows the resulting efficiency curves based on Eq. 5.3 at 150MHz and 400MHz. The antenna is assumed to be made of 18-gauge copper wire. Also plotted for reference is the efficiency of the 400MHz planar ICF antenna reported in [20]. It is observed that the efficiency of the ICF degrades drastically for *kr* less than 0.4.

Next, the efficiency of the multiply folded design is considered. When *N* multiple folded arms are used and equal induced currents are excited on all the arms, the radiation resistance scales approximately as N^2, since the amount of radiation power is proportional to the square of the current [19]. To reach $N^2 R_{rad} = 50\Omega$ for good matching, the required number of folds is

$$N = \sqrt{\frac{50}{(kr)^2 C_1}} \qquad \text{Eq. 5.4}$$

The loss resistance, at the same time, is increased by a factor of N due to the multiple arms. The resulting achievable efficiency is then given as

$$Efficiency(\ foldings) = \frac{N^2 R_{rad}}{N R_{loss} + N^2 R_{rad}} = \frac{50}{R_{loss}\sqrt{\frac{50}{(kr)^2 C_1}} + 50} \qquad \text{Eq. 5.5}$$

Also plotted in Figure 5.1 is the efficiency curves based on Eq. 5.5 at 150MHz and 400MHz. It is observed that the efficiency of the multiply folded design is always higher than that of the ICF design in the VHF/UHF frequency range. It remains above 90% for an antenna size as small as kr=0.05.

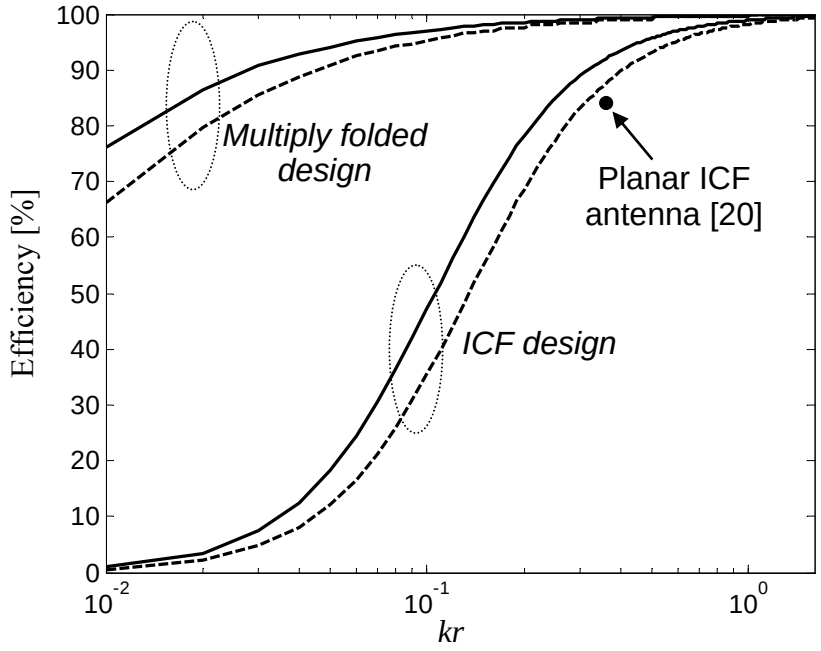

Figure 5.1: Theoretical efficiencies of antennas using the ICF design and the multiply folded design versus size at two different frequencies.
(—): 400MHz, (·····): 150MHz, (•) Efficiency of the ICF antenna reported in [20].

5.3 ANTENNA DESIGN

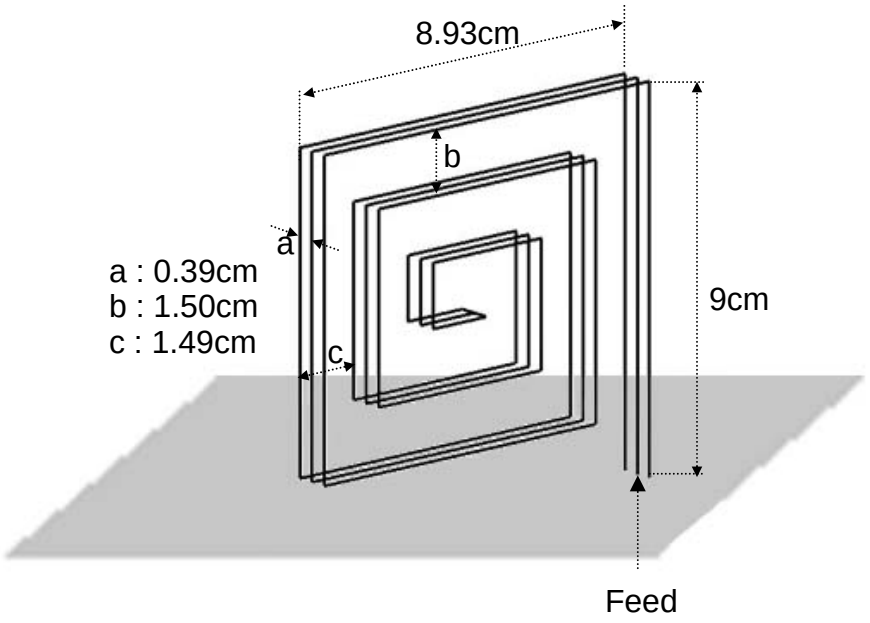

Figure 5.2: Optimized design of a thin, electrically small, multiply folded antenna.

Based on the analysis in Section 5.2, a thin, folded antenna that outperforms the planar ICF antenna in [20] in terms of efficiency is generated. A multiply folded monopole design wound in a rectangular spiral shape is considered (see Figure 5.2). The antenna is designed to operate at 150MHz for applications in VHF radio. The height and the width of the antenna are confined to a maximum dimension of 9cm, and 18-gauge copper wire is used in the design. Each antenna arm comprises a planar rectangular spiral, and the arms are stacked and connected at the end to make the folding geometry. A genetic algorithm is used in conjunction with NEC to optimize the antenna dimensions within the confined size, including the width and the number of turns of the spiral, the number of arms, and the distance between the arms. The cost function is chosen to be the realized gain. It is found that three arms are sufficient to achieve good matching to 50Ω.

The number of turns of each spiral is three. The spacing between the arms (shown as in Figure 5.2) is 0.39cm. The height of the antenna is 9cm, and the width is 8.93cm. The corresponding *kr* is 0.3156. The vertical distance between each segment in the spiral (shown as b in Figure 5.2) is 1.50cm, and the horizontal distance (shown as c in Figure 5.2) is 1.49cm. The coaxial feed is connected to the middle arm.

5.4 SIMULATED AND MEASURED RESULTS

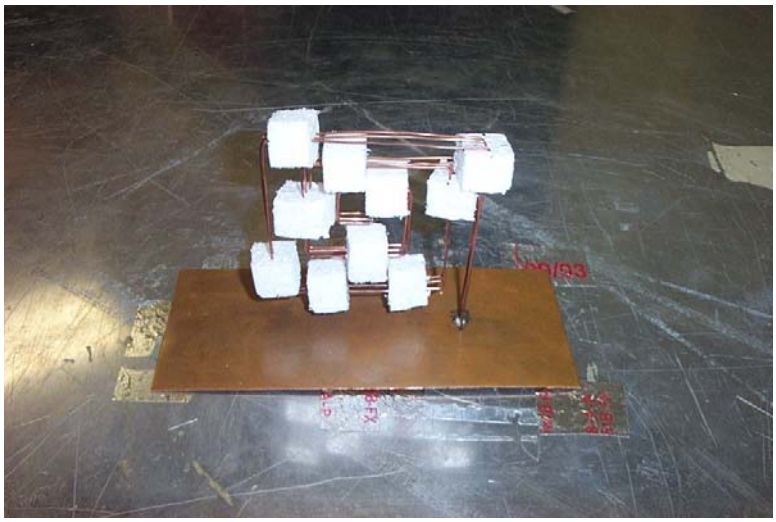

Figure 5.3: A prototype of the antenna.

Based on the simulation result, a prototype of the antenna is built and measured. Styrofoam, shown as white blocks in Figure 5.3, is used to support the antenna structure. A large ground plane (120cm × 120cm) is used in the measurement.

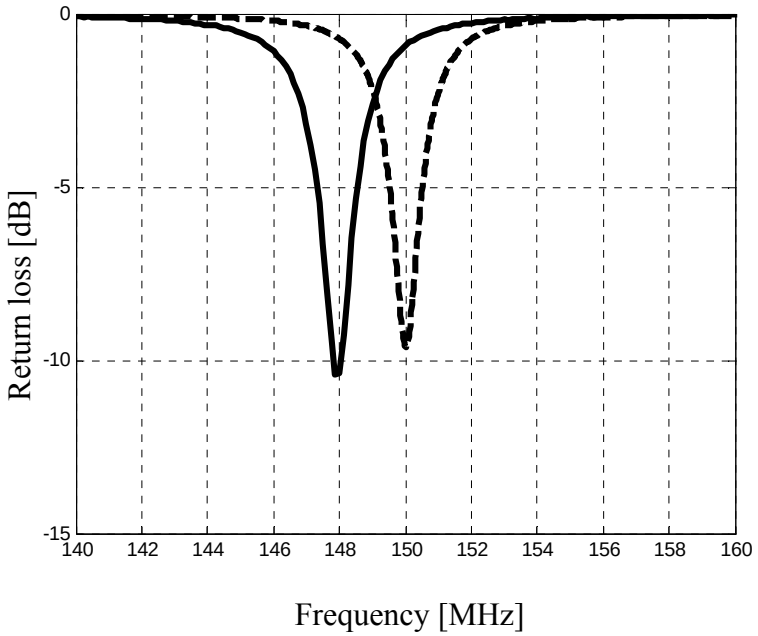

Figure 5.4: Simulated and measured return loss.

(---): Simulation, (—): Measurement.

The simulated return loss of the antenna shows a resonant dip of -9.6dB at 150MHz. The simulated radiation resistance and the loss resistance are 21.82Ω and 3.47Ω, respectively. As a result, the simulated efficiency is 86.3% at 150MHz. Contrary to the earlier analysis where the currents are assumed equal, the current on the center arm of this antenna is not equal to those on the two outside arms. This is not surprising since the structure does not have symmetry with respect to all three arms. The measured return loss of the antenna has a minimum of -10.4dB at 147.9MHz. The measured resonant frequency is 1.4% lower than the simulated one, due likely to inaccuracy in the construction. The efficiency is measured using the Wheeler cap method [4]. The measured radiation resistance and the loss resistance are 22.11Ω and 4.76Ω, respectively. The measured efficiency is 82.3% at 147.9MHz, which agrees fairly well with the simulated one. Figure 5.5 shows the comparison of the measured vs. simulated results

(for easier comparison, the measured VSWR and efficiency are shifted up by 1.4% in the figure). The simulated 3dB-bandwidth is 1.07%, whereas the measured 3dB-bandwidth is 1.31%.

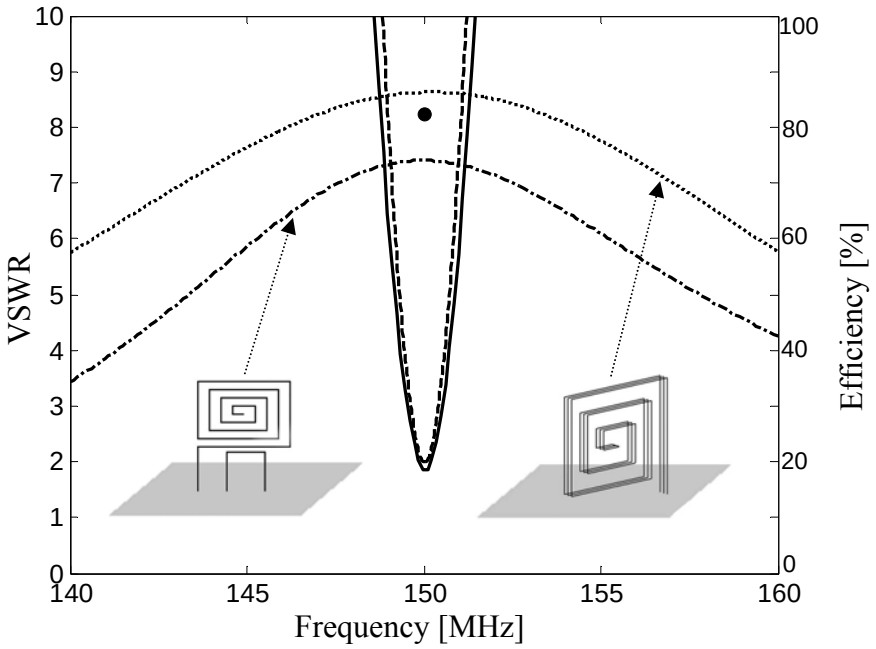

Figure 5.5: VSWR and efficiency versus frequency for the multiply folded antenna at 150MHz. (---): Simulated VSWR, (—): Measured VSWR, (·····): Simulated efficiency, (●): Measured efficiency, (-·--·): Simulated efficiency of an optimized ICF antenna at 150MHz.

Finally, a planar ICF antenna [20] is designed and optimized at 150MHz using18-gauge copper wire for a direct comparison with the new folded design. The resulting efficiency (simulated using NEC) is plotted as the dashed-dot line in Figure 5.5. The maximum efficiency is 74.0%, which is much lower than that of the multiply folded antenna.

5.5 SUMMARY

In this chapter, a thin, electrically small, multiply folded antenna has been designed, built and measured. Measurements matched well with the simulation results. The efficiency of the antenna is better than that of the previously reported ICF antenna. This three-layered thin design is fairly easy to fabricate and is a good candidate for an electrically-small, highly efficient antenna in VHF applications.

Chapter 6

Optimization of the Folded Conical and Spherical Helix Small Antenna

6.1 INTRODUCTION

A folded conical helix (FLEX) antenna, shown in Figure 1.13, was proposed earlier by Dobbins and Rogers for achieving a highly efficient antenna with good bandwidth performance with an electrically small antenna size [12]. The antenna had a *kr* of 0.7 and operated at 111MHz. In that antenna, a single folding in each of the 16 wound arms was used to step up the input resistance. The antenna showed a broad bandwidth (29.0%) and a high efficiency with an 18AWG (0.5mm, $2\times10^{-4}\lambda$) wire radius. More recently, Best [13] described a folded spherical helix antenna (Figure 1.15) that also demonstrated excellent results with a geometry that efficiently filled a spherical volume. The antenna operated at 300MHz, and the size of *kr* was 0.38, and multi-folding was used to achieve self-resonance. The antenna showed high efficiency (98.6%) and excellent bandwidth (3.1%) for its size; however, we cannot compare the bandwidth and efficiency directly with those of the FLEX because the electrical sizes and wire radii are different.

In this chapter, the effect of geometry on the performance of an electrically small antenna is assessed. In Section 6.2, the effect of geometry (apex-down, apex-up) on the performance of the folded conical helix structure is evaluated. Optimizations of the folded conical helix structure are performed by using the GA and NEC, where both shapes are included in the same population, to generate optimized designs under either the optimum efficiency or optimum bandwidth criterion. In Section 6.3, the geometry is generalized, and the folded helix structures, including both the apex-down folded conical helix and the spherical helix designs in the same population, are re-optimized. All optimizations are performed for an antenna size *kr* of 0.2.

6.2 ASSESSMENT OF THE FOLDED CONICAL HELIX STRUCTURE

(a) (b)

Figure 6.1: The folded conical helix structure.
(a) Apex-down geometry. (b) Apex-up geometry.

For the optimization of the folded conical helix structure, both the apex-down geometry (Figure 6.1(a)) and the apex-up geometry (Figure 6.1(b)) are considered in the GA population within the same *kr* hemisphere. Multi-arm folding is used to step up the input impedance, and the antenna feed is connected to the end of one of the arms. The antenna shape could be chosen as either apex-down or apex-up by the GA. The GA optimization parameters also included the flare angle. The angle for the apex-up cone is allowed to vary from 10 to 70 degrees, and for the apex-down cone the angle could vary from 10 to 45 degrees. The number of turns and the number of folding arms are also allowed to vary by the GA. The wire radius is fixed at 0.5mm. The optimization is carried out separately for different antenna sizes at *kr*=0.2, 0.3, 0.4 and 0.5. Figure 6.2 shows the possible shapes in the population, which are either apex-down or apex-up. Note that all shapes have symmetry among all arms. Therefore, the currents of each arm are balanced.

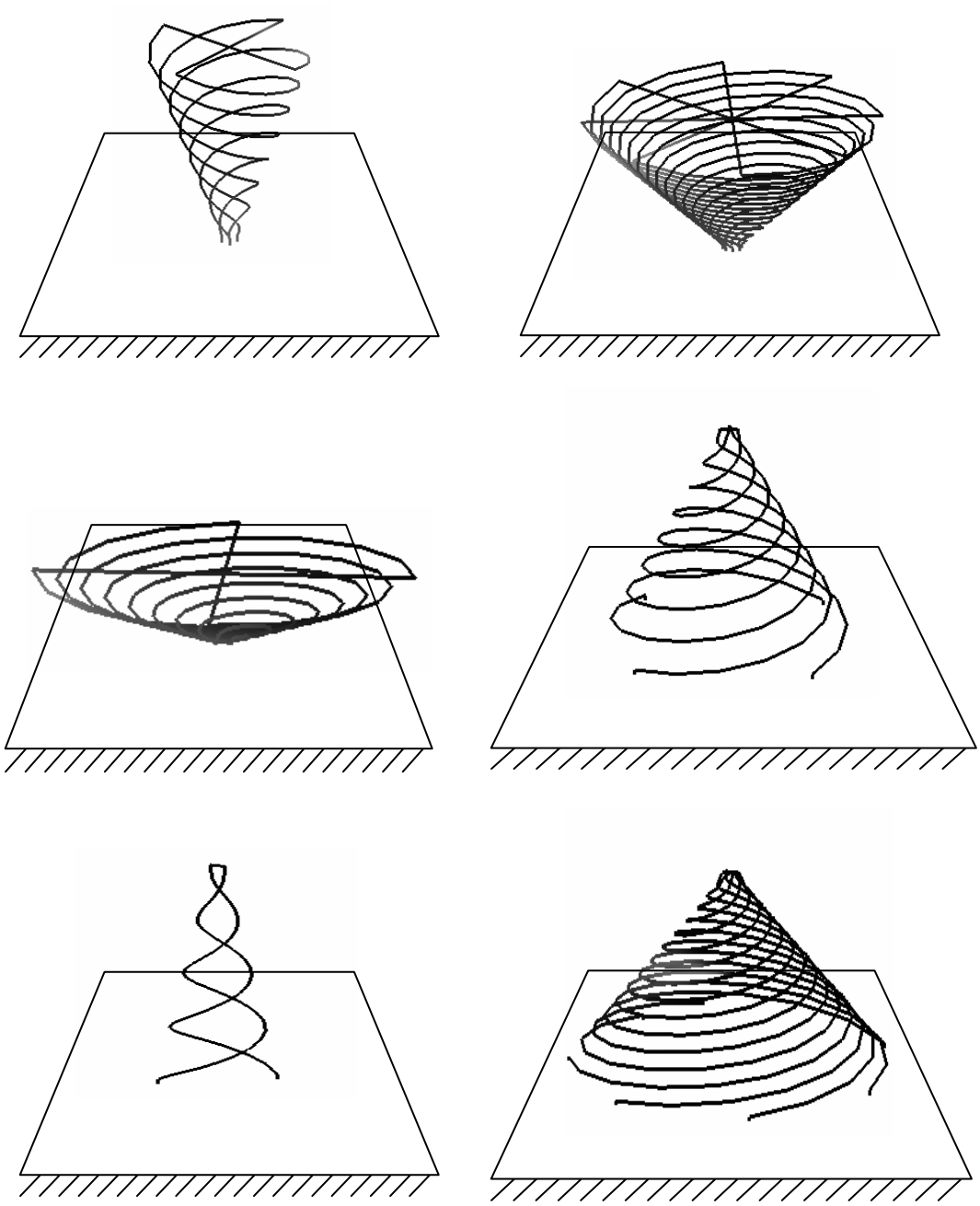

Figure 6.2: Possible shapes of the folded conical helix structures in the population.

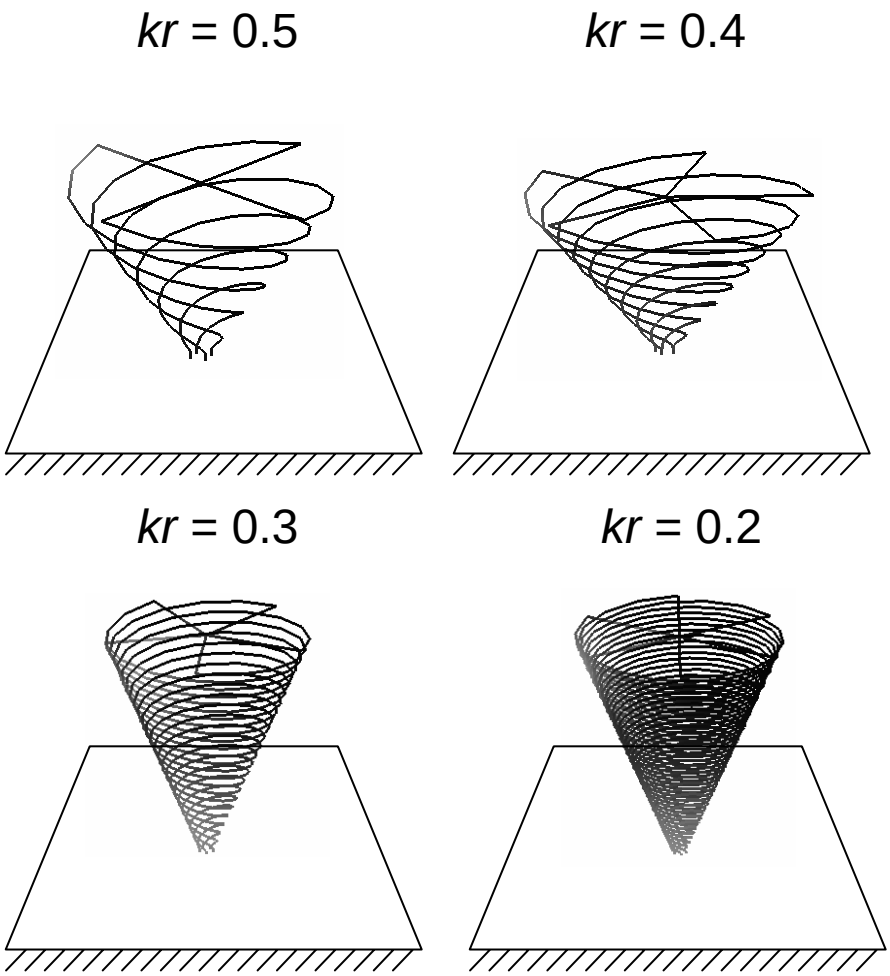

Figure 6.3: Efficiency-optimized samples of the folded conical helix.

kr	Antenna shape	Flare angle	# of turns	# of arms	Efficiency
0.5	apex-down	35	1.5	4	97.4%
0.4	apex-down	40	1.75	5	95.9%
0.3	apex-down	22	4.88	5	92.8%
0.2	apex-down	22	7.44	6	85.0%

Table 6.1: Efficiency optimization results of the folded conical helix.

Efficiency and bandwidth are studied separately in the GA optimization while satisfying the 50Ω matching requirement at 30MHz. The results show that the apex-down design is preferred over the apex-up design for the efficiency optimization at all sizes considered, as shown in Figure 6.3 and Table 6.1. As expected, the number of turns and the number of arms increase as the size becomes smaller. The maximum efficiency decreases as the size decreases. We believe the apex-down design provides more capacitance between the antenna and ground, which is from the top-loading effect. This effect makes the total electrical length of the antenna shorter and reduces the loss resistance, which in turn increases the efficiency.

Next, Figure 6.4 and Table 6.2 show the bandwidth optimization results. We again find that the number of turns and the number of arms increase as the size becomes smaller, whereas the minimum Q value increases as the size becomes smaller. Again, the apex-down shape is chosen for all sizes. The reason is that the top loading of the apex-down design helps increase the radiation resistance, which in turn reduces the required number of folds and reduces the wire density. As a result, self capacitance decreases, Q decreases, and therefore the bandwidth increases.

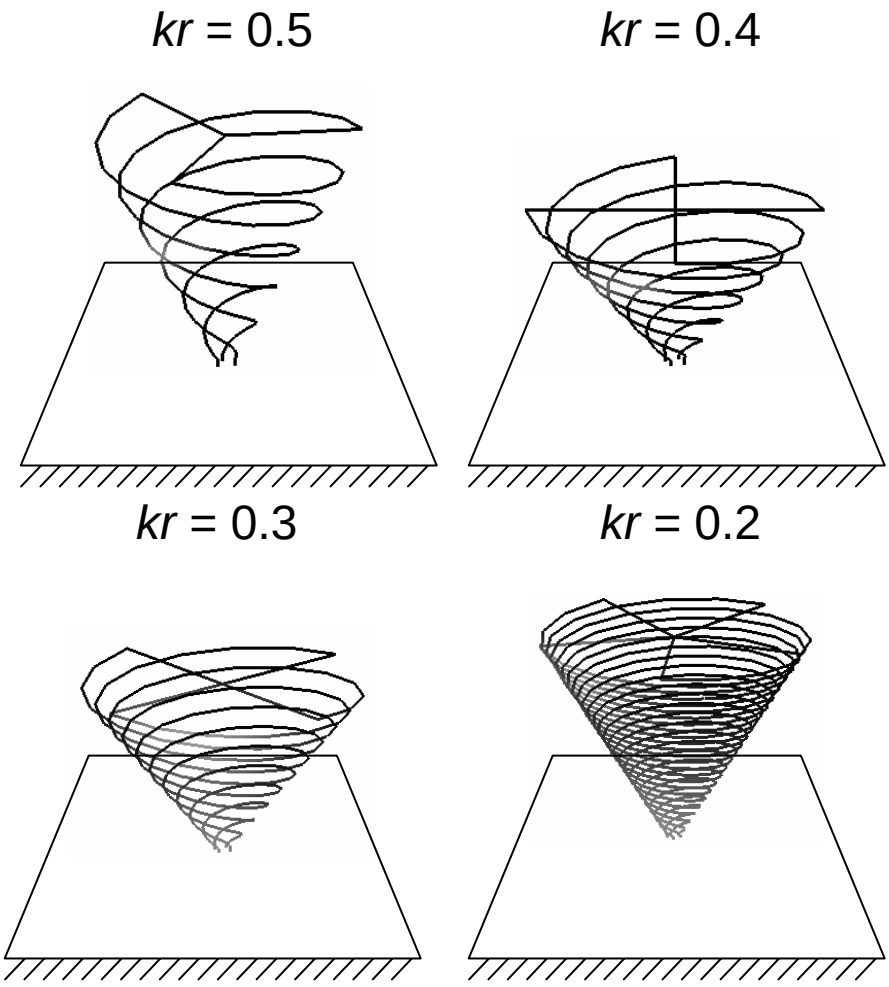

Figure 6.4: Bandwidth-optimized samples of the folded conical helix.

kr	Antenna shape	Flare angle	# of turns	# of arms	Q
0.5	apex-down	27	2	3	29.8
0.4	apex-down	40	1.75	4	51.7
0.3	apex-down	38	2.63	4	108.9
0.2	apex-down	31	5.06	5	288.3

Table 6.2: Bandwidth optimization results of the folded conical helix.

6.3 ASSESSMENT OF BOTH THE CONICAL AND SPHERICAL HELIX STRUCTURES

After the assessment in Section 6.2, it is realized that the spherical surface area is much wider than that of the conical surface area. Therefore, it is decided to generalize the geometry and re-optimize the folded shaped helix structure, including both the apex-down folded conical helix and the folded spherical helix designs in the same GA population. The optimization is performed at kr=0.2, and a frequency of 29.2MHz is chosen. The wire radius is fixed at 0.5mm. The design of the folded shaped helix is composed of an upper part and a lower part, as shown in Figure 6.5. The upper part can be a flat or spherical top, and the lower part can be a linear or quadratic envelope.

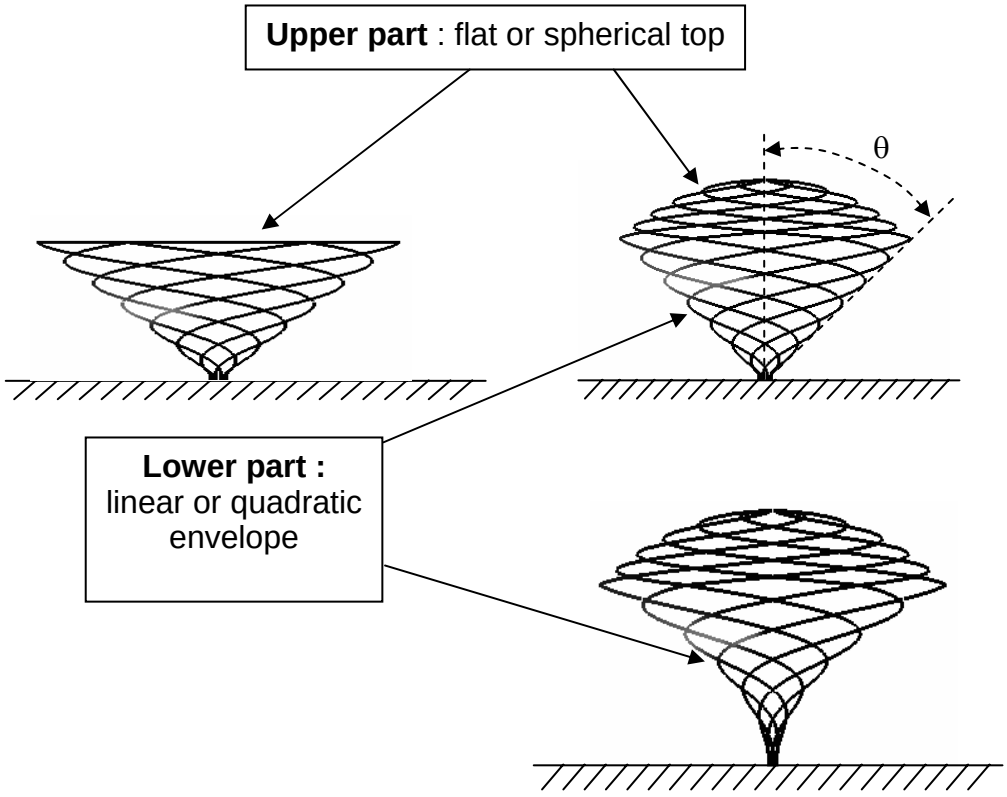

Figure 6.5: Design of the folded shaped helix.

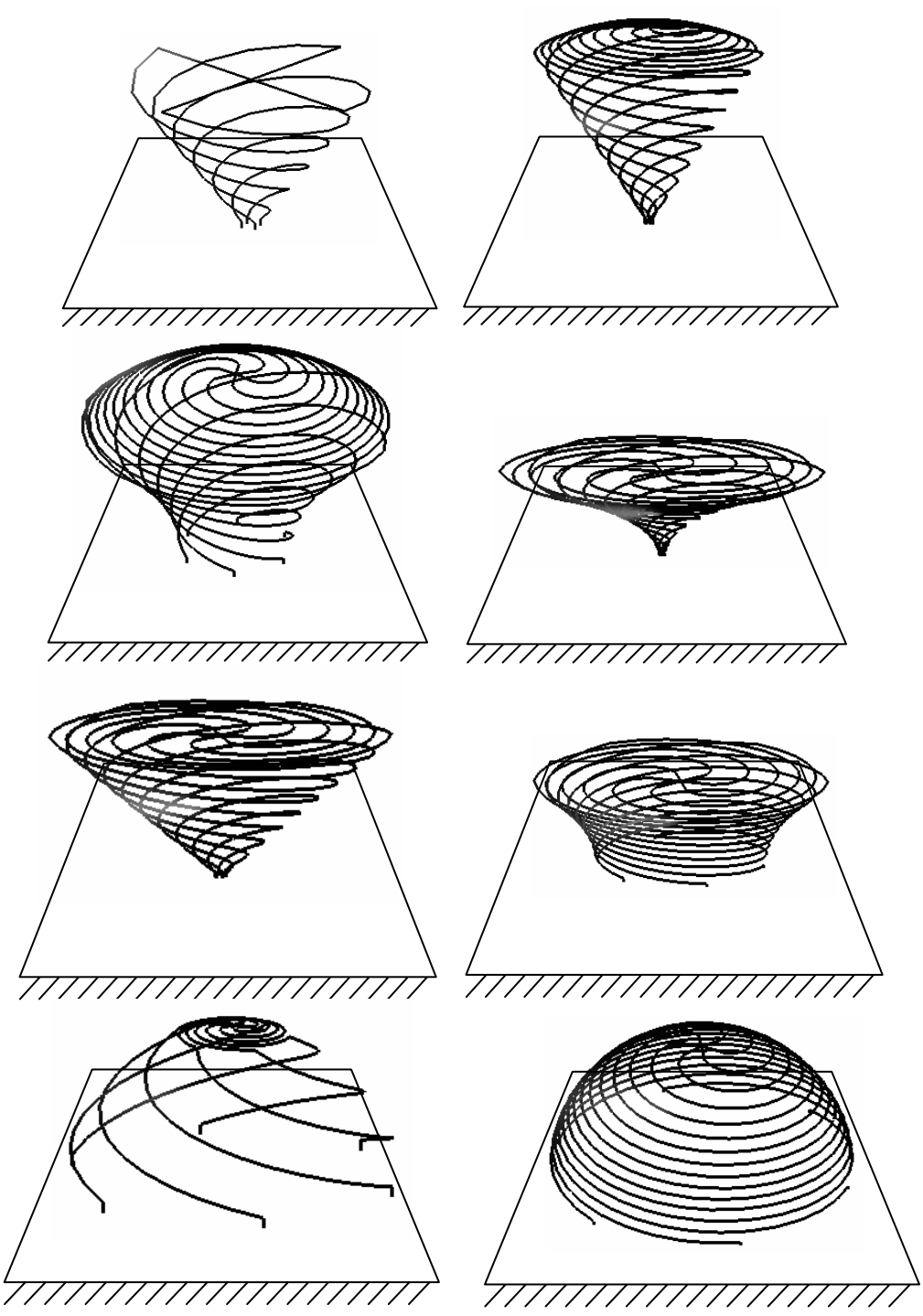

Figure 6.6: Possible shapes in the GA population of the folded shaped helix.

The circle radius made by the junction of each arm with the ground can be chosen to be as great as the radius of the hemisphere. The GA parameters include flare angle (shown as θ in Figure 6.5), number of arms, number of turns of the upper part, number of turns of the lower part, shape (flat or spherical) of the upper part, shape (linear or quadratic) of the lower part, and the radius made by the junction of each arm with the ground. Figure 6.6 shows the possible shapes of the GA optimization, from the apex-down folded conical helix to the folded spherical helix.

As described in Section 6.2, once the matching $(1-|\Gamma|^2)$ is satisfied, either the efficiency or 1/Q can be chosen as the objective function. Figure 6.7 and Table 6.3 give the results of the efficiency optimization, and Figure 6.8 and Table 6.4 give the results of the bandwidth optimization.

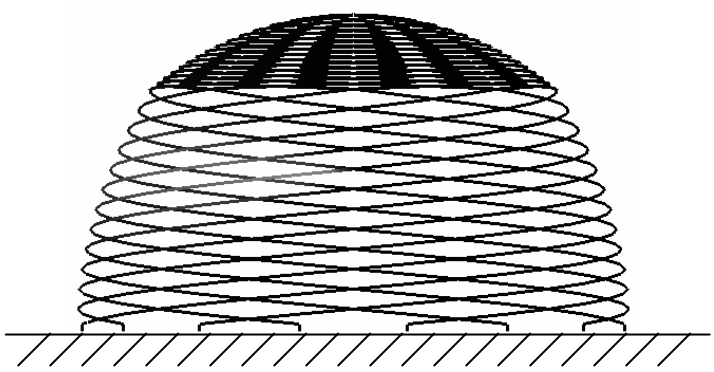

Figure 6.7: Efficiency-optimized samples of the folded shaped helix.

kr	Flare angle	# of turn of upper part	# of turn of lower part
0.2	40	1.75	1.5
Bottom radius	# of arm	Efficiency	Q
0.88*r*	8	87.5[%]	208.0

Table 6.3: Efficiency optimization results of the folded shaped helix.

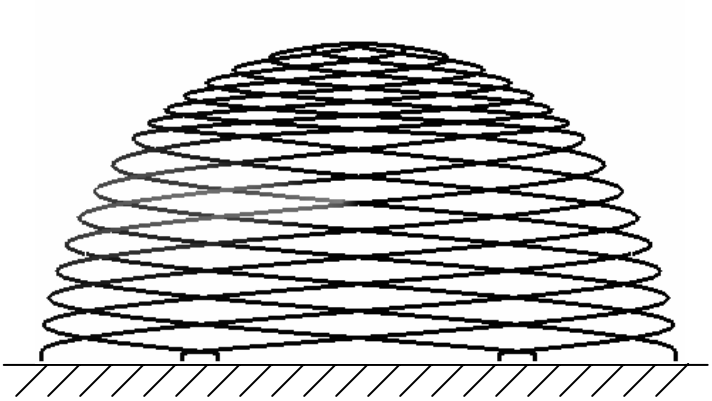

Figure 6.8: Bandwidth-optimized samples of the folded shaped helix.

kr	Flare angle	# of turn of upper part	# of turn of lower part
0.2	45	1.13	1.38
Bottom radius	# of arm	Efficiency	Q
r	6	82.8[%]	187.8

Table 6.4: Bandwidth optimization results of the folded shaped helix.

In the results of both the efficiency and bandwidth optimizations, the GA chose the spherical helix design, and the GA preferred a spherical helix with a dense upper part to make the top-loading effect strong, and strong currents were placed on the sparse lower part for both efficiency and bandwidth optimization. Moreover, the GA preferred a wider surface area for the lower part to reduce the wire density related to the Q value.

	Efficiency optimized	BW optimized	Efficiency optimized	BW optimized
	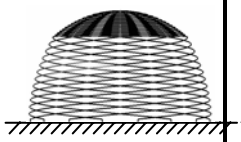	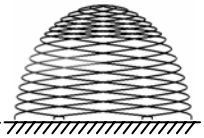	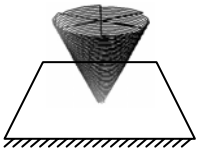	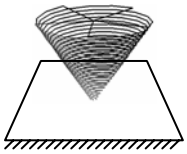
Frequency	29.2[MHz]	29.2[MHz]	30[MHz]	30[MHz]
Efficiency	87.5[%]	82.8[%]	85.0[%]	80.0[%]
Q	208	188	347	288

Table 6.5: Comparison between the dense-top folded spherical helix antennas and the folded conical helix antennas.

In Table 6.5, the dense-top folded spherical helix antennas shown in Figure 6.7 and Figure 6.8 are compared with the optimized folded conical helix antennas described in Section 6.2. The size (kr=0.2) and the wire radius (18 AWG wire) are kept the same in all antenna designs. The maximum efficiency of the dense-top folded shaped helix antennas in the efficiency optimization is 87.5%, and the Q in the bandwidth optimization is 187.8. In contrast, the maximum efficiency of the folded conical helix antenna is 85%, and the Q in the bandwidth optimization is 288.3. It is evident that the performance of the dense-top spherical helix is better than that of the conical helix.

Next, the dense-top folded spherical helix antennas are compared with the uniform spherical helix antenna in Table 6.6. All dimensions except the wire radius of the folded uniform spherical helix design are quoted from [48]. The result in efficiency is 79.8%, and the Q is 197.1. We can observe that the performance of the dense-top, spherical helix is better than that of the uniform spherical helix.

	Efficiency optimized	BW optimized	Uniform Spherical helix[x]
	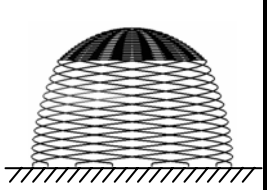	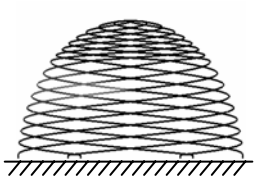	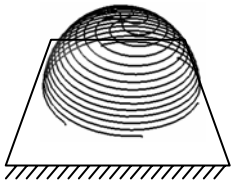
Frequency	29.2[MHz]	29.2[MHz]	29.2[MHz]
Efficiency	87.5[%]	82.8[%]	79.8[%]
Q	208	188	197

Table 6.6 Comparison between the dense-top, folded spherical helix antennas and the uniform folded spherical helix antenna.

6.4 SUMMARY

The effect of geometry on the performance of folded conical and spherical helix antennas were assessed using the GA. In Section 6.2, the conical helix was considered, and the apex-down and apex-up folded conical helix antennas were optimized for efficiency and bandwidth using the GA for several antenna sizes. The apex-down geometry was preferred over the apex-up in both efficiency and bandwidth because of the top-loading effects. In Section 6.3, a more general optimization that included the spherical helix design was performed for efficiency and bandwidth for kr=0.2. A spherical helix-like structure was chosen for its better performance. The upper part of the design was denser to induce top loading. The efficiency and the bandwidth of the dense-top folded spherical helix antennas were superior to those of the folded conical helix antennas and to those of the uniform folded spherical helix antenna.

Chapter 7

Design of a Closely Spaced, Folded Yagi Antenna

7.1 INTRODUCTION

The traditional Yagi antenna is an elegant design that achieves good gain in a very simple structure. The antenna comprises a driven element and parasitic elements, the latter of which include a reflector and one or more directors. The spacing between the elements is typically on the order of 0.15 to 0.4λ [19, 26]. In some applications, it is desirable to decrease the inter-element spacing in order to reduce the overall size of the structure. For example, for the excitation of HF skywaves with wavelengths on the order of tens of meters, a high-gain antenna with its radiation directed toward the zenith and yet having low height is desirable for easy deployment. Other potential applications include HF ground wave antennas and RFID antennas.

Much work has been done to reduce the spacing between a radiating element and a ground plane to achieve uni-directional radiation. For example, an electromagnetic bandgap (EBG) surface can be used as a perfect magnetic conductor to obtain a 0° reflection phase [49, 50]. However, the EBG surface is complicated and difficult to fabricate. Best [51] reported that, for a horizontal dipole placed very close to a perfect electric conductor (PEC), the oppositely flowing image current in the PEC leads to a low radiation resistance, which in turn increases the mismatch loss and decreases the efficiency of the antenna. To overcome the mismatch loss, Best proposed a folded dipole structure. Although the bandwidth of the resulting system is decreased significantly as compared to that of a dipole placed a quarter-wavelength away from the PEC plane, it is well matched to 50Ω and has high efficiency. More recently, Altshuler et al. [52-54]

considered a monopole array in which the spacing between the elements is reduced to achieve super directivity.

In this chapter, a new Yagi antenna structure whose elements are very closely spaced is proposed. The folding concept is incorporated into the design to make the antenna self-resonant at 50Ω. The NEC is used to simulate the antenna. The dimensions of the antenna are then optimized by a genetic algorithm for a close driver-reflector and director-driver spacing of 0.02 wavelength. For verification, a 1GHz prototype design is built, and the measured result is compared with the simulated result. An 8MHz optimized design is then evaluated over a lossy ground for potential applications in HF skywave transmission. The antenna performance is compared with that of conventional antennas in the same environment.

7.2 DESIGN OF THE COMPACT YAGI ANTENNA

The effect of the spacing between the reflector and the driver on the performance of a conventional Yagi antenna was first investigated. The length of the reflector is 0.49λ and that of the driver is 0.4781λ [26]. Each element is a copper wire with a radius of 0.0017λ (which corresponds to an 18-gauge wire at 1 GHz). The results were computed by NEC. Figure 7.1(a) shows that the radiation resistance of the antenna drops quickly as the element spacing is decreased, while the loss resistance stays about the same. Consequently, the efficiency and the matching factor ($1-|\Gamma|^2$) of the antenna drop quickly, as shown in Figure 7.1(b). Figure 7.1(c) shows the resulting directivity, gain, and realized gain of the antenna. For example, at a 0.02λ spacing the radiation resistance is 0.57Ω, and the loss resistance is 0.37Ω. These values lead to an efficiency of 60.7% and a matching factor of 7%. The directivity, gain, and realized gain are 7.2dB, 5.0dB, and -6.5dB, respectively. This phenomenon is similar to the case when the dipole is closely located over a PEC ground plane [51].

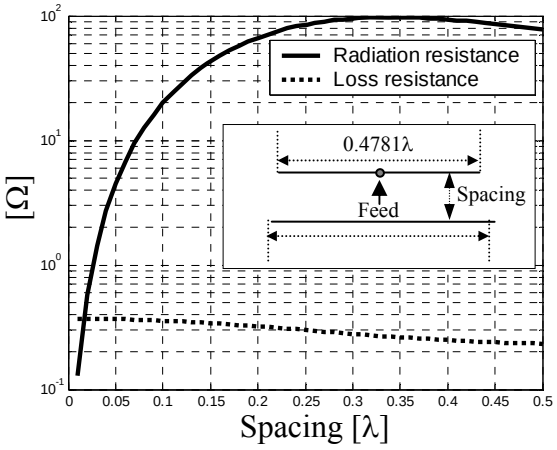

(a)

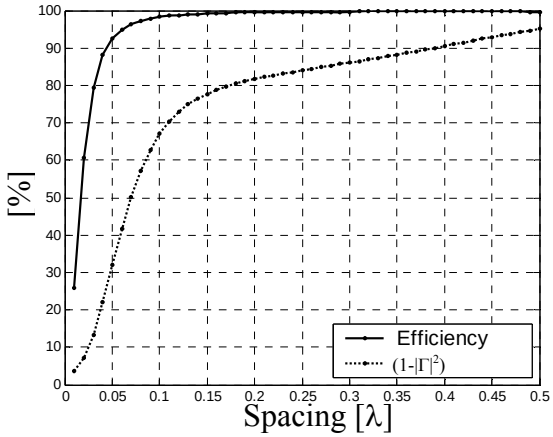

(b)

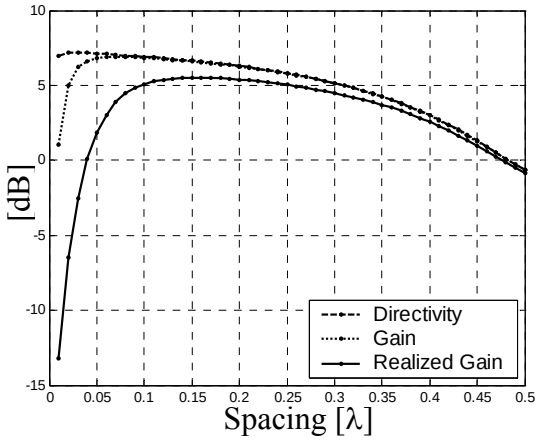

(c)

Figure 7.1: Spacing effect on a 2-element Yagi antenna.
(a) Radiation resistance and loss resistance.
(b) Efficiency.
(c) Directivity, gain, and realized gain.

To overcome the mismatching and the efficiency problem for close spacing, a new Yagi structure is suggested. A 3-element structure with one director is considered for simplicity. Figure 7.2 shows the design of the proposed Yagi antenna, which is designed to operate at 1GHz. The copper wire has a radius of 0.5mm (0.0017λ). The folding technique [19, 51] is used to boost the reduced input resistance. The reflector, driver, and director are all folded twice; thus, each element is composed of three straight arms. In the NEC simulation, it was confirmed that two folds are sufficient to match the antenna to 50Ω. If the number of folds is further increased, the input resistance overshoots 50Ω.

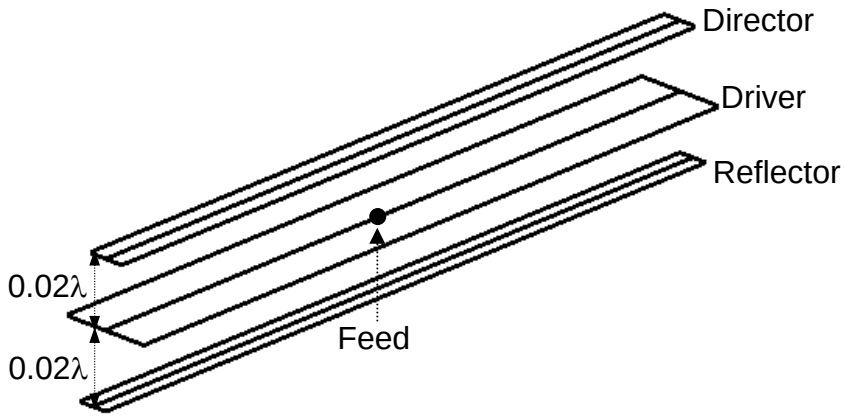

Figure 7.2: Design for a closely spaced, folded dipole Yagi antenna.

The spacing between the reflector and the driver and the spacing between the driver and the director are both fixed at 0.6cm (0.02λ). The length of the director, driver, and reflector elements and the spacing between the folded arms are optimized by a GA. In the GA optimization, the realized gain in the director direction is chosen as the objective function. The resulting lengths of the reflector, the driver, and the director are 14.446cm (0.4815λ), 13.856cm (0.4619λ), and 13.828cm (0.4609λ), respectively, and

the spacing between each arm of the reflector, the driver, and the director are 0.300cm (0.0100λ), 0.900cm (0.0300λ), and 0.375cm (0.0125λ), respectively.

7.3 VERIFICATION OF THE SIMULATED AND MEASURED RESULTS

Figure 7.3(a) shows the simulated return loss of the antenna with respect to a 50Ω characteristic impedance. The resulting 3dB fractional bandwidth is 1.9%. Figure 7.3(b) shows the input impedance of the antenna. The resulting radiation resistance is 46.5Ω, the loss resistance is 3.3Ω at the 1GHz resonant frequency, and the efficiency is 93.4% at resonance. The directivity, gain, and realized gain of the optimized antenna toward the director direction are found to be 7.44dB, 7.14dB, and 7.12dB, respectively. The front-to-back ratio is 5.98dB.

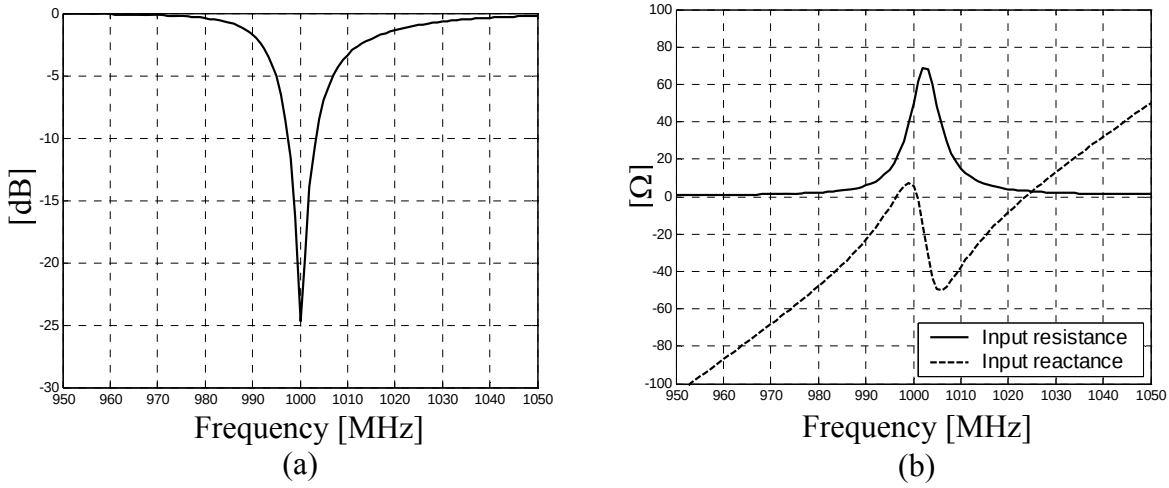

Figure 7.3: Return loss and input impedance of the Yagi antenna.
(a)Return loss.
(b) Input impedance.

The design was verified by measurements. To avoid any balun issues, a monopole version of the Yagi antenna was fabricated as shown in Figure 7.4 and measured (with a

large ground plane of size of 0.92m × 3.00m). The dimensions of the monopole Yagi are the same as those of the dipole version except that the lengths of the arms are cut in half and the antenna is mounted vertically on the ground plane. Figure 7.5(a)-(c) show the simulated and the measured return loss and the input impedance of the monopole Yagi. The simulated return loss has a minimum of -14dB at 1GHz, whereas the measured result has a minimum of -19dB at 980.2MHz. This 2% shift in the resonant frequency is likely due to fabrication tolerance. As expected, the bandwidth of the monopole Yagi antenna is narrow. The simulated and the measured 3dB bandwidth of the monopole Yagi are 1.3% and 1.7%, respectively. Figure 7.6 shows the simulated and measured realized gains of the monopole Yagi versus a quarter-wave monopole. The maximum realized gain of the monopole Yagi is 10.08 dB in the measurement and 9.91dB in the simulation. Therefore, agreement between the measurement and simulation is good. The result is about 3dB higher than that of dipole version of the Yagi due to the factor-of-two directivity increase from the presence of the ground plane. The measured front-to-back ratio is 6.49dB, which also shows good agreement with the simulation.

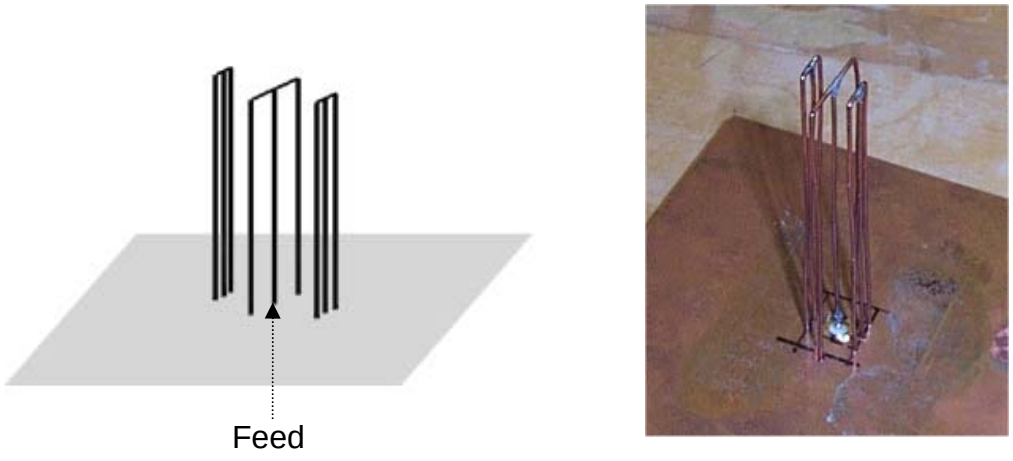

Figure 7.4: A monopole version of the Yagi antenna.

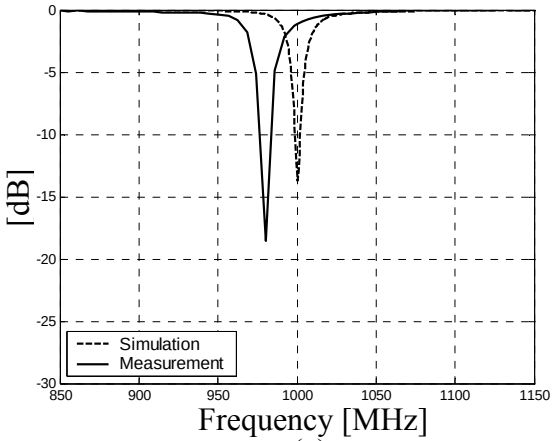

(a)

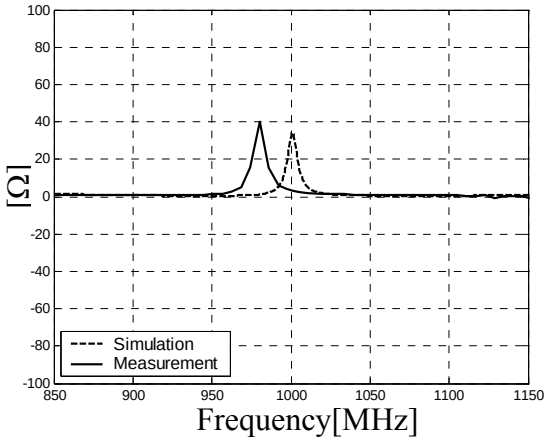

(b)

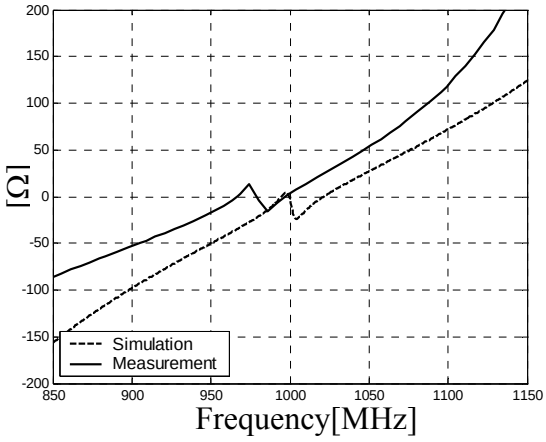

(c)

Figure 7.5: Return loss and input impedance of the monopole Yagi antenna. Return loss. (b) Input resistance. (c) Input reactance.

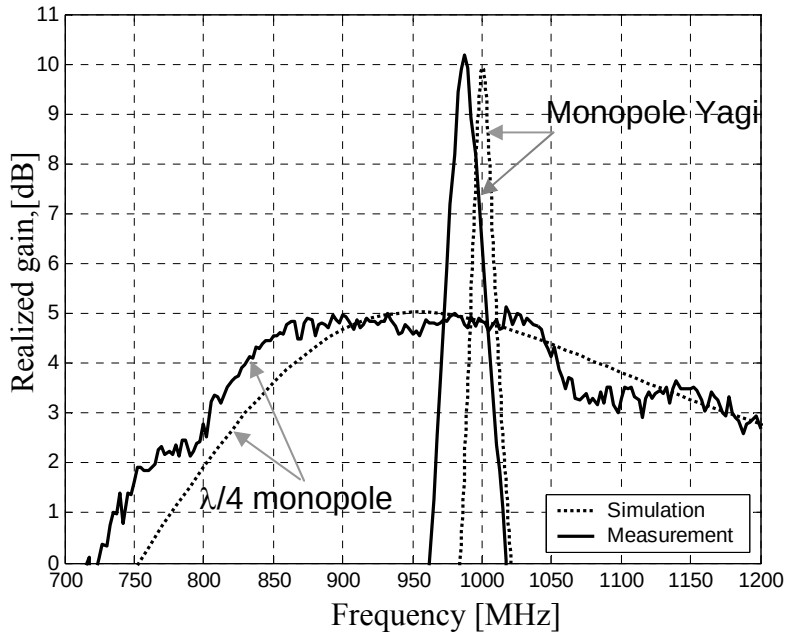

Figure 7.6: Simulated and measured realized gains of the monopole Yagi and a quarter-wave monopole.

7.4 EVALUATION OF THE COMPACT YAGI ANTENNA

After the verification of the design at 1GHz, the antenna structure is re-optimized to operate at 8MHz to evaluate the antenna for HF skywave transmission. The spacing between the reflector and the driver and the spacing between the driver and the director are kept at 0.02λ (0.75m). The wire radius is chosen to be 2.5mm ($6.67\times10^{-5}\lambda$), which is electrically thinner than that of the 1GHz design. The antenna is assumed to be in free space. The resulting optimized lengths of the reflector, the driver, and the director are 18.234m (0.4863λ), 17.848m (0.4759λ), and 17.777m (0.4741λ), respectively, and the spacing between the arms of the reflector, the driver, and the director are 37.500cm (0.0100λ), 38.672cm (0.0103λ), and 11.719cm (0.0031λ), respectively.

Figure 7.7 shows the power gain patterns of the compact Yagi antenna in the elevation plane. The term 0° corresponds to the director direction in the graphs. Figure 7.7(a) is the pattern in free space. The front-to-back ratio is 7.16dB, the efficiency is 86.7%, and the return loss at 8MHz is -21.7dB. The resulting directivity, gain, and realized gain in the director direction are 7.42dB, 6.80dB, and 6.77dB, respectively. Figure 7.7(b) is the pattern when this design (optimized for free space) is placed over a lossy ground at the reflector height of 0.02λ. Wet soil parameters ($\varepsilon_r = 10$, $\sigma = 0.01$S/m) are used for the ground. The Sommerfeld integral option of the NEC is used in the simulation. The return loss at 8MHz is found to be -3.0dB. The resulting directivity, gain, and realized gain toward the director direction are 6.55dB, 6.37dB, and 3.39dB, respectively. It is observed that, since the antenna in free space has a high front-to-back ratio, when the antenna is placed over the lossy ground, its directivity is not strongly affected. The 3.4 dB decrease in the realized gain comes mainly from the input impedance mismatch.

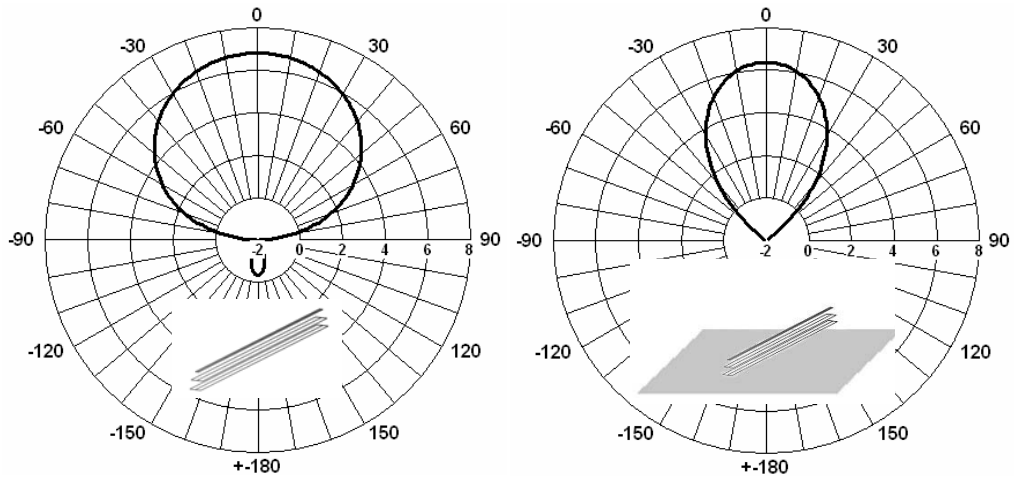

(a) (b)

Figure 7.7: Power gain pattern of the folded Yagi antenna in the elevation plane [dB].
(a) In free space.
(b) Over the ground at the height=0.02λ.

Next, the performance of the compact Yagi antenna is compared with other wire antennas over the ground. Three antennas, including a resonant horizontal loop, a resonant horizontal dipole, and a Shirley dipole [55], as shown in Figure 7.8(a), are simulated. All the antennas are located at a height of 0.02λ over the ground. Again, the same wet soil parameters are used for the ground in all cases. Figure 7.8(b) shows the realized gains of the four different antennas toward the zenith direction. Based on the simulation, the resulting realized gains of the horizontal loop, the horizontal dipole, and the Shirley dipole are found to be -6.90dB, -5.50dB, and -6.37dB, respectively. They are more than 9 dB worse than that of the compact Yagi antenna. Therefore, the presented Yagi design can potentially provide high gain for HF skywave transmission.

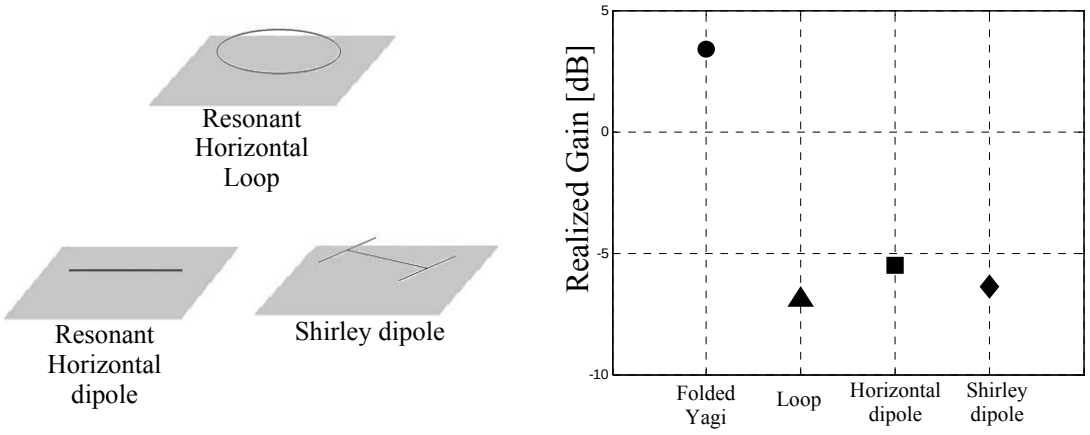

(a) (b)

Figure 7.8: Comparison of the folded Yagi antenna with several conventional antennas over the ground at the height of 0.02λ.
(a) Several conventional antennas.
(b) Realized gain.

7.5 SUMMARY

In this chapter, a closely spaced, folded Yagi antenna design was proposed for HF transmission. First, it was shown that the Yagi antenna suffers from small radiation resistance when the spacing between the driver and the reflector is close (less than 0.05λ). To increase the radiation resistance, a folded structure was used. A 3-element Yagi in free space was designed by the genetic algorithm to optimize its dimensions. The results showed that the antenna has a high realized gain despite the fact that the spacing between the elements is only 0.02λ. Measurements were performed on a 1GHz monopole version of the design to verify the simulation results. An 8-MHz design is then evaluated to assess its performance over a lossy ground. The realized gain of the antenna in the director direction is 6.77dB in free space and 3.39dB over wet ground. These values are about 9dB better than those of conventional wire antennas.

Chapter 8

A Printable Yagi Antenna with Closely Spaced Elements

8.1 INTRODUCTION

In Chapter 7, a Yagi antenna with closely spaced elements for HF skywave applications was introduced. The optimized design has good realized gain performance despite an inter-element spacing of only 0.02λ. There has also been other recent work on arrays with closely spaced driven elements [56, 57].

In this chapter, a planar realization of the closely spaced Yagi antenna is investigated. The concept of multiple folding on the driver element is used to step up the radiation resistance. The antenna dimensions are first optimized using a GA in conjunction with NEC based on a wire implementation of the antenna. The wire version of the optimized antenna is then transferred into a printed version on PET film. Prototype structures are constructed and measured. The resulting structure is simple, and it is potentially useful as a high-gain printed antenna in such application as RFID.

8.2 ANTENNA DESIGN

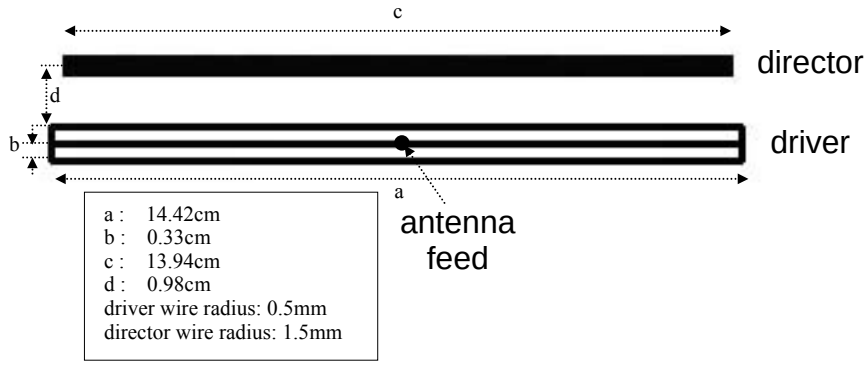

Figure 8.1: Optimized planar dipole Yagi antenna shape and its dimensions based on a wire implementation and its simulation results using NEC.

A planar wire version of a two-element, closely spaced, dipole Yagi antenna is first investigated. Because the radiation resistance drops drastically when the driven element and the parasitic element are located close to each other, multiple folding is used in the driver to step up the radiation resistance to 50Ω. Here, two folds are considered because sufficient step-up can be achieved for element spacing as small as 0.02λ [3]. The feed is located in the center of the middle arm of the driver.

A driver plus a director case is studied. Figure 8.1 shows the antenna design. GA is used to optimize its dimensions for maximum realized gain toward the director (upward direction in the figure). The operating frequency is set at 1GHz. The GA optimization parameters include the length of the driver and the director, the spacing between the arms in the driver, the spacing between the driver and the director, and the wire radius of the director. The wire radius of the driver is fixed at 0.5mm (18 AWG), and copper wire is assumed. The optimized spacing between the center arm of the driver and the director is 1.31cm (0.0437λ), the director length is 13.94cm (0.4647λ), and the length of three driver arms is 14.42cm (0.4807λ). Indeed, the GA chose a slightly shorter director length than the driver. The phase of the current in the center of the director is approximately anti-phase with respect to the currents on the three arms of the driver. Moreover, the current on the director is approximately equal to the sum of the currents on the three arms of the driver. Therefore, this antenna operates much like the standard Yagi with a driver and a director. The wire radius of the director was chosen to be 1.5mm (9AWG) by the GA. Because the strongest current on the antenna is on the director, the thicker director element helps reduce conductor loss and increase the efficiency of the antenna.

Figure 8.2 shows the simulated return loss of the antenna with respect to a 50 Ω characteristic impedance. The minimum return loss is -22.1dB at 1GHz. The radiation and loss resistances are respectively 55.6Ω and 2.71Ω at 1GHz. The resulting antenna efficiency is 95.4%. The 3dB fractional bandwidth of the antenna is 1.54%. Figure 8.3 show the simulated power gain patterns of the antenna in the E-plane and the H-plane. 0° corresponds to the director direction in the graphs. The front-to-back ratio is 7.59dB. The resulting simulated realized gain of this driver-plus-director Yagi antenna is 7.18dB. the driver-plus-reflector structure have also been explored in detail. The optimized structure shows almost the same performance except that it has a slightly lower realized gain (less than 0.5 dB) than that of the driver-plus-director case above.

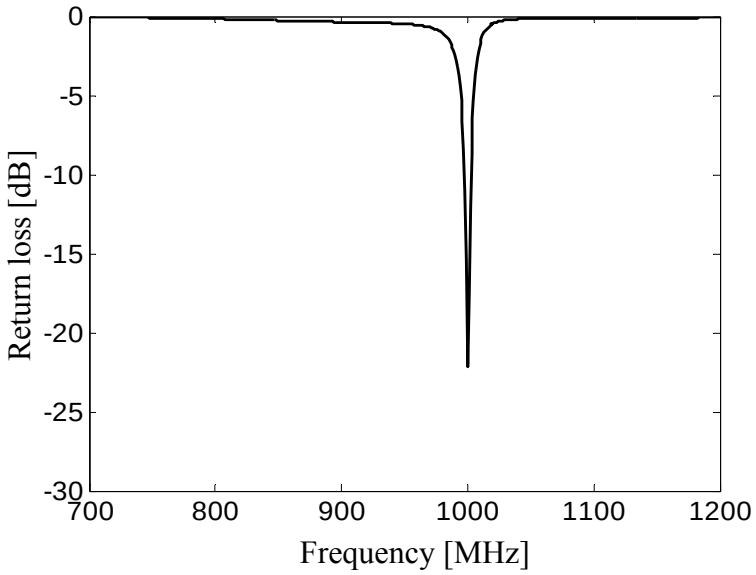

Figure 8.2: Simulated return loss of Optimized planar dipole Yagi antenna.

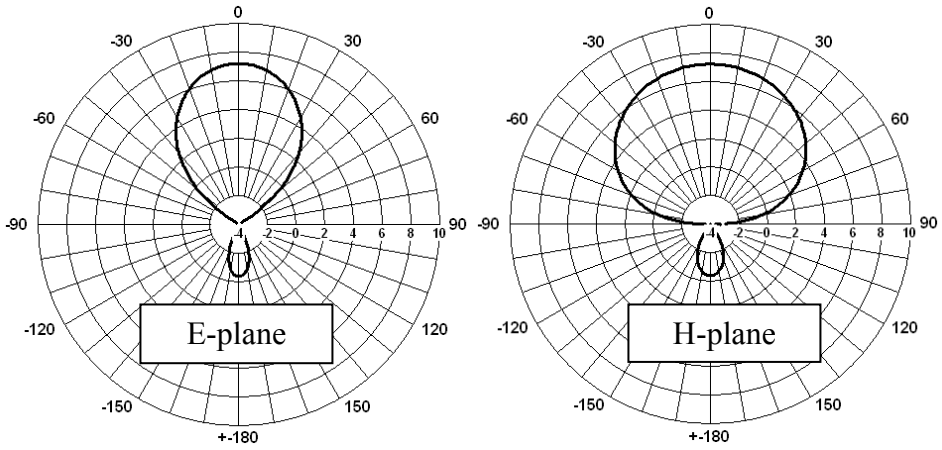

Figure 8.3: Power gain patterns in the E- and H-plane [dB].
(a) E-plane.
(b) H-plane.

8.3 MEASURED RESULTS

To make the antenna purely planar, the wire version of the antenna is next transferred into a printed version. The strip width in the printed version is chosen to be four times the wire radius, based on the equivalent radius rule in [58]. A prototype of the strip version is built as shown in Figure 8.4. In the construction, copper strips of 2mm width for the driver and 6mm width for the director are attached to a 50μm PET film. To avoid any balun issues, a monopole version of the antenna is fabricated and measured. The length of the monopole is exactly half of the dipole version and the antenna is mounted vertically on a large ground plane (1.2m×1.2m). The measured return loss of the strip antenna on PET is shown in Figure 8.5. The minimum return loss is –17.3dB at 987.5MHz. The resonant frequency is shifted down by about 1.3% due to the PET film. The measured 3dB fractional bandwidth is 2.75%.

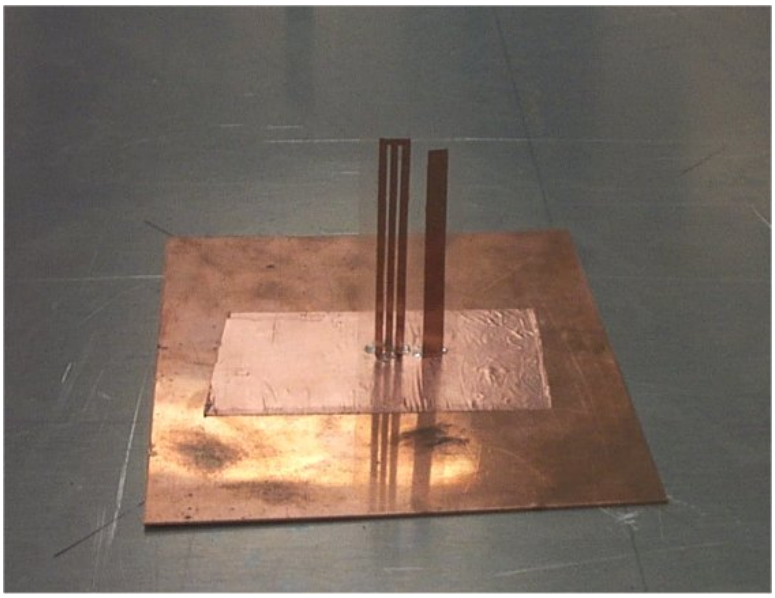

Figure 8.4: Fabricated prototype of the planar monopole Yagi on 50μm PET film

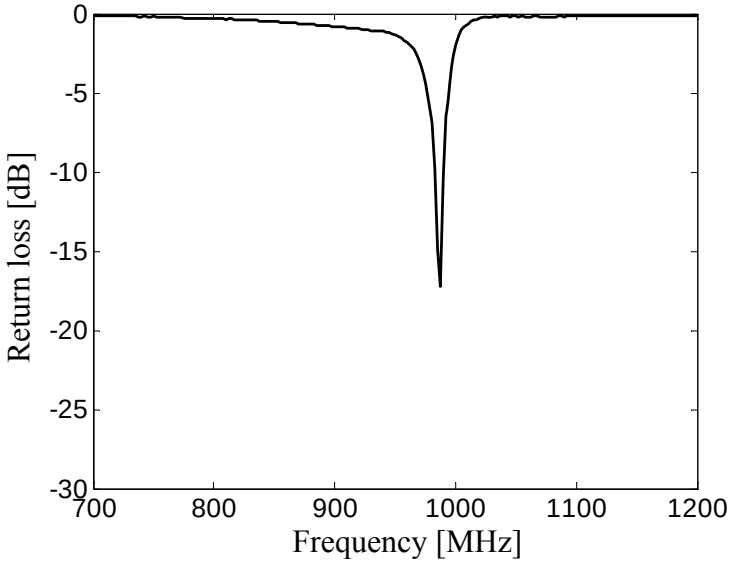

Figure 8.5: Measured return loss of the planar monopole Yagi.

Next, the efficiency of the antenna is measured using the Wheeler cap method [4]. The measured radiation resistance is 56.9Ω. Combined with the measured loss resistance of 8.62Ω, the measured efficiency is found to be 86.8%. It is believed that the PET film in the structure contributes to the broader bandwidth and lower efficiency of this structure in comparison to the simulation in free space. The realized gain toward the direction of the fabricated antenna is also measured and the result is compared with that of a quarter-wave monopole, as shown in Figure 8.6. Since there is a factor-of-two directivity increase due to the ground plane, the result of the monopole version is about 3dB higher than that of the dipole version. The maximum realized gain of the strip antenna is 9.56dB at its operating frequency, which is more than 4dB higher than that of the quarter-wave monopole. The measured front-to-back ratio of the strip antenna is more than 10dB. The measured results match fairly well with the simulation, despite the fact that the simulation results were generated for the wire version.

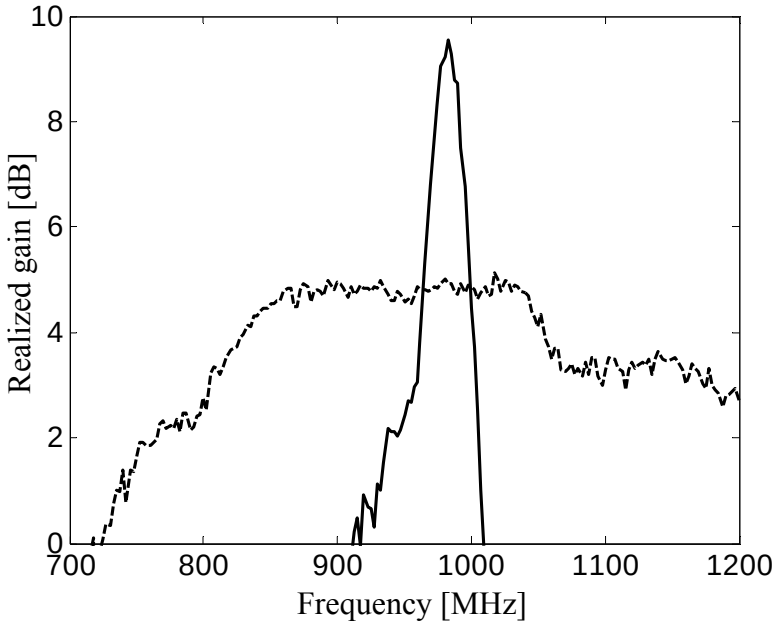

Figure 8.6: Measured realized gains.
(—) Planar monopole Yagi.
(---) A quarter-wave monopole.

8.4 SUMMARY

In this chapter, a two-element, planar Yagi antenna with closely spaced elements has been described. Multiple folding in the driver was used to boost the low radiation resistance due to the close spacing between the elements. The antenna dimensions were optimized using a genetic algorithm and NEC at 1GHz. A prototype planar monopole Yagi was built and measured on 50μm PET film. The measurement results agreed well with the simulation results. The maximum realized gain of the monopole Yagi was measured to be 9.56dB. This planar Yagi antenna is potentially useful as a high-gain printed antenna in such application as RFID. The extension of the concept to more than two elements is currently been investigated.

Chapter 9

Design of an Electrically Small Yagi Antenna

9.1 INTRODUCTION

Werner *et al*. recently reported on a miniaturized three-element, dipole Yagi antenna optimized using particle-swarm optimization [59]. In the optimized design, the length is reduced to 0.27λ, and the spacing is 0.11λ between the reflector and the driver. O'Donnell and Yaghjian reported on a two-element, super-directive, parasitic array using electrically small monopole antennas [60]. The height of the antenna is only 0.073λ, while the total volume of the antenna is 0.18λ×0.073λ×0.073λ. Because the size of the parasitic element is identical to that of the driven element, lumped element loads are used to tune the antenna. In Chapter 7, a Yagi antenna with closely spaced elements for HF skywave applications is also introduced. Whereas the elements are full-sized, it is shown that the spacing between the elements can be reduced to as small as 0.02λ by using the folding concept.

In this chapter, a two-element, electrically small, closely spaced Yagi antenna is proposed. The design of the antenna elements is based on the electrically small antenna element that was introduced in Chapter 5. The basic antenna shape is a rectangular spiral with multiple folds. A director element is then added to form the two-element Yagi. The antenna dimensions are optimized by using the GA and NEC. The tradeoff between the element height and the spacing between the elements is studied. A prototype antenna is built and measured at 450MHz. The total volume of the monopole Yagi is 0.065λ × 0.095λ × 0.095λ, and the measured realized gain is 8.81dB.

9.2 ANTENNA DESIGN

Figure 9.1 shows the basic design concept in a monopole form. The antenna feed is located at the bottom of the middle arm in the driver. To make the driver element electrically small, the wire is wound into a rectangular spiral shape. Multiple folded arms in the driver are used to step up the radiation resistance, which drops precipitously due to both the small antenna size and the close inter-element spacing between the driver and the parasitic element, as shown in Chapter 7. For the two-element Yagi structure, a driver-plus-director configuration is chosen, as described in Chapter 8. From simulation results, multiple folds in the director element do not improve the antenna performance, and only a thick, single arm is used for the director. Because the strongest current on the antenna is in the director, the thicker director reduces the conductor loss and improves the efficiency of the antenna.

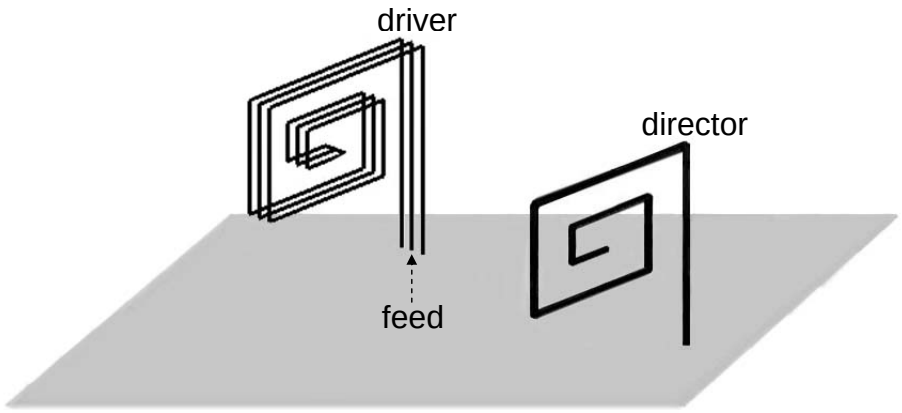

Figure 9.1: Design concept of an electrically small, two-element, closely spaced Yagi antenna.

The graphs of Figure 9.2 show the tradeoff between element height and inter-element spacing. The antenna element height is represented by *kh*, where *k* is the wave number and *h* is the driver height. The inter-element spacing is measured from the center of the driver to the center of the director. Sixteen different GA optimizations are performed for four different inter-element spacings (0.03λ, 0.06λ, 0.09λ, 0.12λ) and four different antenna heights (*kh*= 0.3, 0.45, 0.6, 0.75) at 450MHz. A wire radius of 0.5mm (18 AWG) is chosen for the driver, and copper wires are assumed.

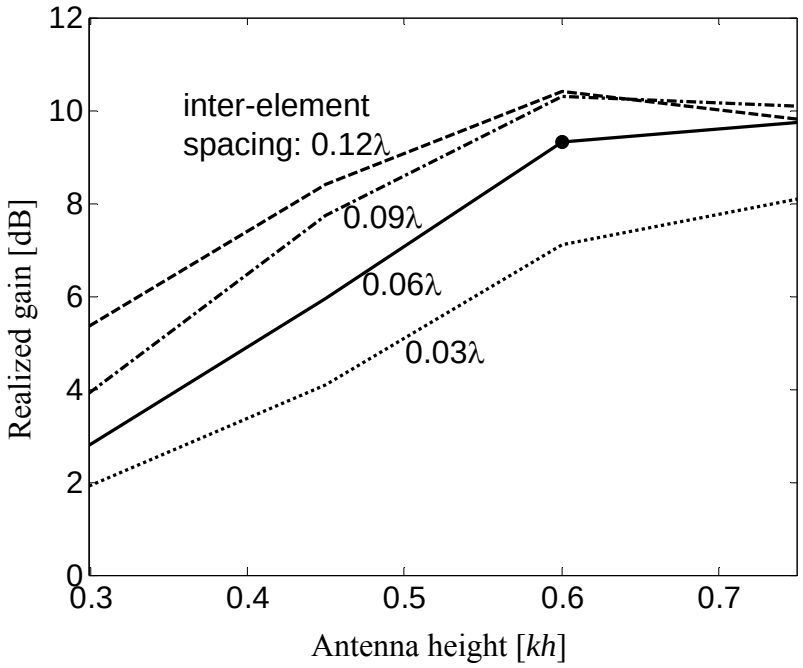

Figure 9.2: Optimized realized gain vs. antenna height *kh* at different inter-element spacing between the driver and the director.

Once the antenna height and the inter-element spacing are given, the GA chooses the number of folds in the driver, the number of turns of the spiral, the width of the spiral (the maximum of which is the antenna height), the distance from the ground to the bottom of the spiral, the height of the director, and the wire radius of the director. The number of turns and the spiral width of the director are kept the same as those of the driver, and the spacing between each arm in the driver is fixed at 3mm. The realized gain toward the director direction is selected as the objective function in the GA.

Figure 9.2 shows that the achievable realized gain drops as either the height or the inter-element spacing is reduced. It was found that the reduction in antenna height is more detrimental to the realized gain than the inter-element spacing. For example, a 2.56dB reduction in the realized gain results when the inter-element spacing is reduced from 0.12λ to 0.06λ at kh=0.3. On the other hand, a 6.54dB reduction in the realized gain results when the antenna height is reduced from kh=0.6 to 0.3 at an inter-element spacing of 0.06λ.

The optimized design for kh=0.6 and an inter-element spacing of 0.06λ (marked with a black dot in Figure 9.2) is chosen for a detailed examination. The maximum realized gain of this antenna is above 9dB, and the antenna height is less than 40% of that of a quarter-wave monopole. The optimized antenna design and its dimensions are shown in Figure 9.3. Only a single-turn spiral and three arms are needed in the driver element. The driver height is 6.37cm (0.095λ), and the director height is slightly smaller at 6.12cm (0.092λ). The wire radius for the director is 1.3mm (10AWG). The minimum simulated return loss of the antenna is -14.41dB at 450MHz. This loss value is accomplished without any matching networks. The simulated efficiency of the antenna is 90.3%. The maximum simulated directivity, gain, and realized gain toward the director direction are 9.94dB, 9.50dB, and 9.33dB, respectively. The front-to-back ratio is 7.93dB.

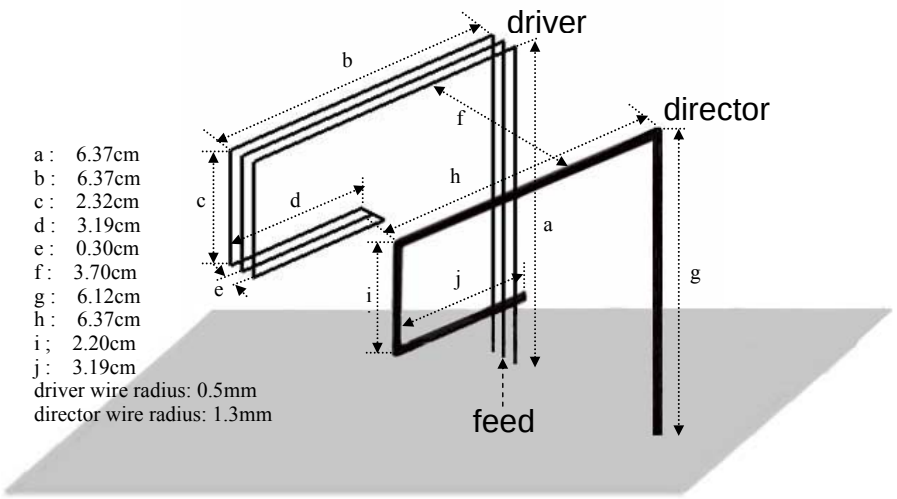

Figure 9.3: Optimized antenna shape and its dimensions for *kh*=0.6 and spacing=0.06λ.

9.3 MEASURED RESULTS

A prototype of the antenna design in Figure 9.3 was fabricated and measured. The photo of the antenna is shown in Figure 9.4. The antenna is built on a small ground plane, and the measurement is performed after mounting the antenna on a large 120cm×120cm conducting ground. The return loss of the antenna is measured and compared with the simulation results in Figure 9.5. The minimal measured return loss of the antenna is -17.12dB at 448MHz, and the 3dB bandwidth is 2.58%. The efficiency of the antenna, measured by using the Wheeler cap method [4], is found to be 88.6%. The measured realized gain toward the director direction is shown as the solid curve in Figure 9.6. Its maximum is 8.81dB, which is about 4dB higher than that of a quarter-wave monopole (shown as the dashed curve). The realized gain in the backward direction is shown as the dotted curve in the figure. The resulting front-to-back ratio is 8.30dB. The measured results show good agreement with the simulation results.

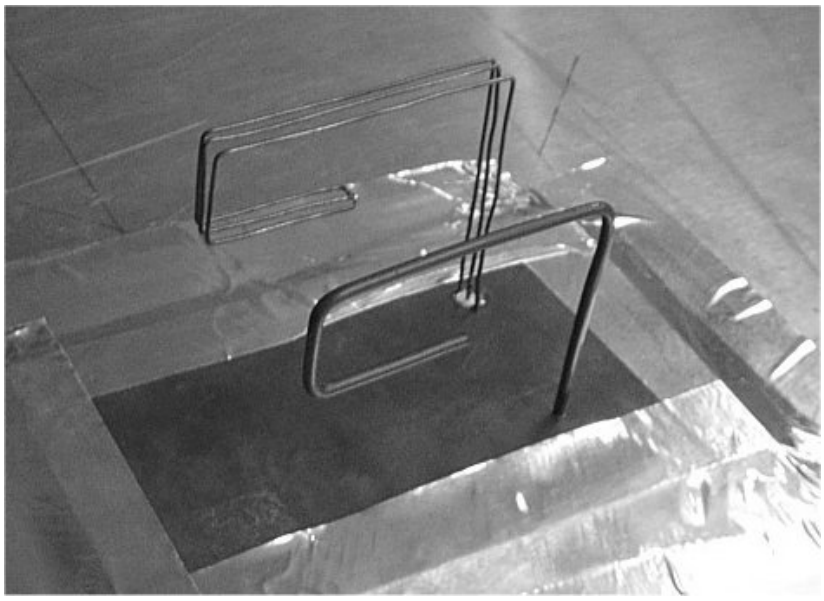

Figure 9.4: Photo of the antenna prototype.

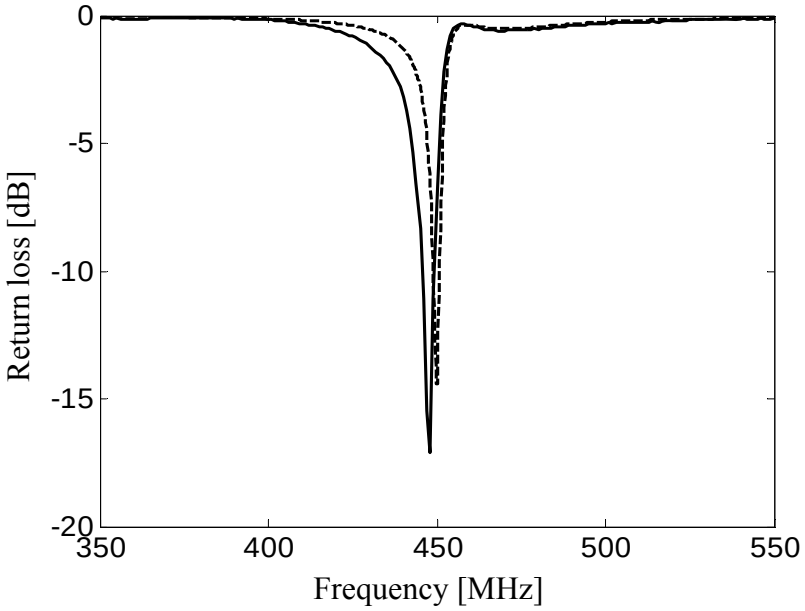

Figure 9.5: Return loss of the small Yagi antenna.

(----): simulated, (—): measured.

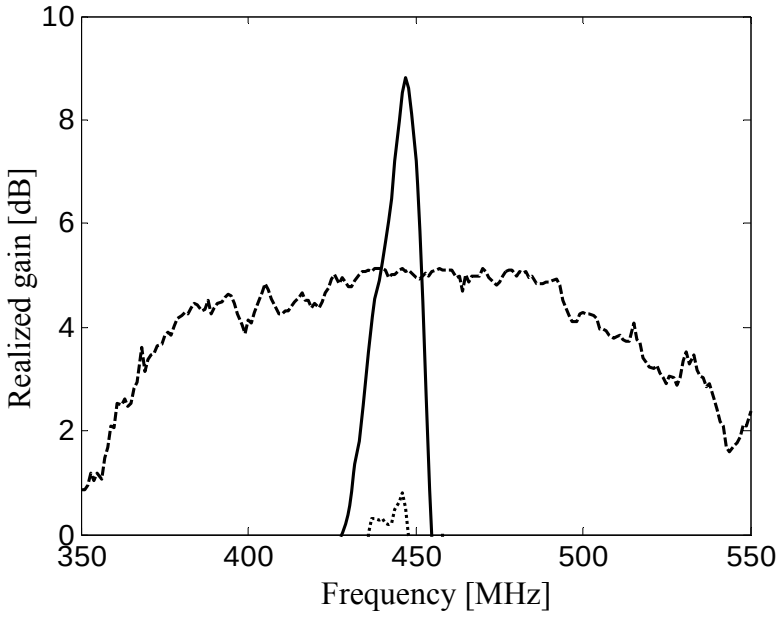

Figure 9.6: Realized gain of the small Yagi antenna and a quarter-wave monopole. (—): Small Yagi in the forward direction. (---): A quarter-wave monopole. (·····): Small Yagi in the backward direction.

9.4 SUMMARY

An electrically small, two-element, closely spaced Yagi antenna was designed. A genetic algorithm and the NEC were used for the antenna optimization. Multiple folded arms were used on the driver element to step up the low radiation resistance due to the close inter-element spacing and the small element size. A prototype of the antenna was built and measured. The height of the designed antenna is 0.095λ, and the inter-element spacing between the driver and the director is 0.06λ. The measurement results showed good agreement with the results of simulation. Despite its small size, the maximum realized gain of the antenna was measured to be 8.81dB.

Chapter 10

Conclusions

This dissertation has introduced several small antennas for non-line-of-sight HF/VHF communication; assessed new design methodologies for electrically small antennas, including radiation-resistant step-up techniques; and presented the geometry effects on small antennas and compact-sized high-gain antennas based on the Yagi structure.

Chapter 2 described a new antenna design (the GA antenna) in a monopole shape for maximizing the HF ground wave (30MHz). Spiral-shaped multi-arms were used for top loading. A vertical antenna body was used for antenna radiation with linear polarization, and the inductively coupled feed was used to step up the input resistance. The measured efficiency based on an equivalent circuit model matched fairly well with that of the simulation. Whereas the physical antenna size was only 1/8 of a quarter-wavelength monopole, the measured transmission loss in an outdoor test showed that the transmission loss of the GA antenna was within 1dB of the commercial whip.

Chapter 3 presented an electrically small ground plane with a quarter-wave monopole and the GA antenna. As the ground-plane size was reduced, the transmission loss dropped drastically because of the loss from mismatching. A spiral ground plane was introduced to compensate for the mismatching problem. A prototype of the spiral ground planes was constructed, and its measurements showed that the transmission loss difference between the spiral ground plane and the three-times-larger solid ground plane was within 1dB of that in a quarter-wave monopole. Moreover, it was 6 to 7dB better than that of the same-sized ground plane with the GA antenna.

Chapter 4 introduced the tunable GA antenna, the purpose of which was to overcome the narrow bandwidth of the small antenna. A variable capacitor was used to tune the resonant frequency of the GA antenna. The position test of the variable capacitor was performed with NEC simulation. The transmission loss of the tunable antenna was measured indoors and outdoors. The results showed that the measured transmission loss of the tunable small antenna came within 1 to 2 dB of that of a commercial whip across the tested frequency range. The GA antenna was able to operate at a favorable frequency where multi-path channel fading occurs.

In Chapter 5, the inductive coupled feed was compared with the multiple folds as input resistance step-up techniques. It was found that the multiple folds helped increase efficiency, whereas the inductively coupled feed did not. On the basis of the comparison results, a thin, electrically small, multiply folded antenna was designed. The simulation results the new design matched well with the measured results. The efficiency of this antenna proved to be better than that of the inductively coupled feed antenna.

Chapter 6 gave an assessment of the geometry effect in the performance of the small antennas. First, folded conical helix structures were investigated. The apex-down structure showed superior performance in both efficiency and bandwidth. Next, folded shaped helix structures, including an apex-down folded conical helix and a folded spherical helix, were optimized for the same GA population. The efficiency and the bandwidth of the dense-top folded spherical helix design were better than those of the folded conical helix and the uniform folded spherical helix.

Chapter 7 showed a closely spaced, folded Yagi antenna for HF sky wave transmission. In a typical Yagi antenna, when the spacing between the driven elements and the parasitic elements becomes smaller, the radiation resistance drops precipitously, which causes mismatching loss and low efficiency. Multiple folds in each element were

used to boost the radiation resistance. The resulting element spacing was only 0.02λ. The antenna was validated with a 1GHz monopole version, and an 8MHz design was then evaluated to assess its performance over a lossy ground. The realized gain in the zenith direction of the closely spaced, folded Yagi antenna was 9bB better than those of other, conventional HF sky wave antennas.

In Chapter 8, the closely spaced, folded Yagi antenna achieved a planar realization for potential applications such as use as an RFID antenna. Two elements with a driver and a director were investigated. A prototype planar monopole Yagi was designed on 50μm PET film, and its measured maximum realized gain was 9.56dB.

Chapter 9 presented an electrically small, two-element, closely spaced Yagi antenna. The size of each element of the closely spaced Yagi structure was reduced by combining the thin, electrically small, multiply folded design concept that was described in Chapter 5. A two-element monopole version of the Yagi was then considered. The maximum height of the antenna was 0.095λ and the inter-element spacing between the driver and the director was 0.06λ. The measured maximum realized gain of this antenna was 8.81dB despite its very small size.

This dissertation has shown that the design of small antennas represents a critical issue in wireless communication. Based on the promising results described this dissertation, I believe that research on small antennas should continue. Promising topics for future research include the following: miniaturized antennas for wireless communication, the design of high-gain antennas for HF/VHF communications and radio frequency identification (RFID) applications, and the use of meta-materials to enhance the performance of antennas. Each of those topics is discussed in the following paragraphs.

Miniaturized Antennas for Wireless Communication: Small antennas will become essential in next-generation wireless communications. The miniaturization of antennas, however, has an impact on antenna efficiency and bandwidth, the two critical parameters in high-data-rate, low-power-consumption devices. To contribute significantly to the technology of antenna miniaturization, I would like to research advanced antenna designs, particularly those of printable antennas, wire antennas, and high-gain antennas, by combining computational electromagnetics with evolutionary-based optimization algorithms. Moreover, I would like to design miniaturized antennas for multiple-input multiple-output (MIMO) communication systems. Multiple antennas have recently been investigated for methods to increase channel capacity and service quality in mobile communication systems; however, size reduction of the MIMO antennas is preferable. I would also like to design miniaturized antennas with polarization and pattern diversity in a small volume for mobile handset terminals in MIMO systems. I am looking forward to exploring this topic with other faculty members in the communications area.

Design of Miniaturized High-Gain Antennas for HF/VHF Communications and RFID Applications: The use of the multi-element Yagi extension to achieve more gain should be explored. With the combination of the miniaturization technique, the high-gain antenna can be usefully applied to lateral wave excitation in forests in HF/VHF communications. In addition, with its host of new applications, RFID is almost ubiquitous, and in fact it has become one of the most important of the new technologies. I plan to conduct more research on the miniaturization of RFID tags and reader antennas. High-gain, reconfigurable structures with two-element dipoles will also be investigated.

Use of Meta-Materials to Enhance Performance of Small Antenna: Meta-materials, which have properties not commonly found in nature, are artificially engineered substances. They are the focus of one of the most fascinating areas of research

into methods for overcoming the natural characteristics of antenna performance. Some of meta-materials currently receiving attention are electromagnetic band gap (EBG), double-negative meta-materials (DNG), the epsilon-negative meta-materials (ENG), and mu-negative meta-materials (MNG). In the continuation of my previous research, I would like to improve the performance of small antennas by incorporating meta-materials into their designs.

Bibliography

[1] J. S. Belrose, W. L. Hatton, , C. A. Mckerrow, and R. S. Thain, "The engineering of communication systems for low radio frequencies," *Proc. IRE*, vol. 47, pp. 661-680, 1959.

[2] H. A. Wheeler, "Fundamental limitations of small antennas," *Proc. IRE*, vol. 35, pp. 1479-1484, 1947.

[3] H. A. Wheeler, "Small antennas," *IEEE Trans. Antennas Propagat.*, vol. 23, pp. 462-469, 1975.

[4] H. A. Wheeler, "The radiansphere around a small antenna', *Proc. IRE*, vol. 47, pp. 1325-1331, 1959.

[5] R.C. Hansen, "Fundamental limitations in antennas," *Proc. IEEE*, vol.69, pp170-182, 1981.

[6] L.J. Chu, "Physical limitations of omni-directional antennas," *J. Appl. Phys*., vol.10, pp. 1163-1175, 1948.

[7] R.F. Harrington, "Effect of antenna size on gain, bandwidth and efficiency," *J. Research*, 64D, pp.1-12, 1960.

[8] W. L. Weeks, *Antenna Engineering*, McGraw-Hill, New York, 1968.

[9] J. S. McLean, "A Re-Examination of the fundamental limits on the radiation Q of electrically small antennas,' *IEEE Trans. Antennas Propagat.*, vol. 44, pp. 672-676, 1996.

[10] G. Goubau and F. Schwering, "Multi-element monopole antennas," *Proc. Workshop on Electrically Small Antennas ECOM-ARO*, Fort Monmouth, NJ, pp. 63-67, 1976.

[11] H. D. Foltz, J. S. McLean, and G. Crook, "Disk-Loaded Monopoles with Parallel Strip Elements,' *IEEE Trans. Antennas Propagat.*, vol. 46, pp.1894-1896, 1998.

[12] J. A. Dobbins and R. L. Rogers, "Folded Conical Helix Antenna," *IEEE Trans. Antennas Propagat.*, vol. 49, pp. 1777-1781, 2001.

[13] S. R. Best, "The radiation properties of electrically small folded spherical helix antennas", *IEEE Trans. Antennas Propagat.*, vol. 52, pp. 953-960, 2004.

[14] K. Fujimoto, A. Henderson, K. Hirasawa, and J. R. James, *Small Antennas*, Research Studies Press, England; John Wiley and Sons, New York, 1987.

[15] T.L. Simpson "The theory of top-loaded antennas: Integral equations for the currents," *IEEE Trans. Antennas Propagat.*, vol. 19, pp. 186-190, 1971.

[16] H. R. Bhojwani and L. W. Zelby, "Spiral top-loaded antenna: Characterisation and design," *IEEE Trans. Antennas Propagat.*, vol. 21, pp. 293-298, 1973.

[17] R. C. Johnson, *Antenna Engineering Handbook*, 3rd ed., McGraw-Hill Book Co., New York, 1993.

[18] A. Safaai-Jazi and J. C. Cardoso, "Radiation characteristics of a spherical helix antenna" *Proc. Inst. Elect. Eng. Microwave Antennas Propagat.,* vol. 143, pp. 7-12, 1996.

[19] C. A. Balanis, *Antenna Theory: Analysis and Design*, 2nd ed., New York: Wiley, 1997.

[20] H. Choo and H. Ling, "Design of electrically small planar antennas using inductively coupled feed," *IEE Electron. Lett.* vol. 39, pp. 1563 – 1565, 2003.

[21] S. Lim, H. Choo, R. L. Rogers, and H. Ling, "Electrically small antenna for maximizing transmission into HF ground waves," *IEE Electron. Lett.,* vol. 40, pp. 1388 –1389, 2004.

[22] S. Lim, R. L. Rogers, and H. Ling, "Design of electrically small ground plane for minimizing transmission loss," *IEE Electron. Lett.,* vol. 41, pp. 993-994, 2005.

[23] S. Lim, R. L. Rogers, and H. Ling, "A tunable electrically small antenna for ground wave transmission," *IEEE Trans. Antennas Propagat.*, vol. 54, pp. 417-421, 2005.

[24] S. Lim and H. Ling, "Design of a thin, efficient, electrically small antenna using multiple foldings," *IEE Electron. Lett.*, vol. 42, pp. 895-896, 2006.

[25] S. Lim and H. Ling, "Optimization of the folded conical helix small antenna using a genetic algorithm," *URSI Nat. Radio Sci. Meet. Dig.*, pp. 427, 2006.

[26] W. L. Stutzman and G. A. Thiele, *Antenna Theory and Design*, 2nd ed., New York: Wiley, 1998.

[27] S. Lim and H. Ling, "Design of a closely spaced, folded Yagi antenna," *IEEE Antennas Wireless Propag. Lett.*, vol. 5, pp. 302-305, 2006.

[28] S. Lim and H. Ling, "Design of a planar, closely spaced Yagi antenna," submitted to *Microwave Optic. Tech. Lett.*, Feb., 2007.

[29] S. Lim and H. Ling, "Design of an electrically small, closely spaced Yagi antenna," accepted in *IEE Electron. Lett.*, Dec., 2006.

[30] E. E. Altshuler, "Electrically small self-resonant wire antennas optimized using a genetic algorithm," *IEEE Trans. Antennas Propagat.*, vol. 50, pp. 297-300, 2002.

[31] H. Choo and H. Ling, "Design of electrically small wire antennas using genetic algorithm taking into consideration of bandwidth and efficiency," *IEEE Antennas Propagat. Soc. Int. Symp. Dig.*, pp. 330 – 333, June 2002.

[32] H. T.Hui, K. Y. Chan, and E. K. N. Yung, "The low-profile hemispherical helical antenna with circular polarization radiation over a wide angular range," *IEEE Trans. Antennas Propagat.*, vol. 51, pp. 1415-1418, 2003.

[33] E. Newman, P. Hohley, and C. H. Walter, "Two methods for the measurement of antenna efficiency," *IEEE Trans. Antennas Propagat.*, vol.23, pp. 457-461, 1975.

[34] J. C. Lagarias, J. A. Reeds, M. H. Wright, and P. E. Wright, "Convergence Properties of the Nelder-Mead Simplex Method in Low Dimensions," *SIAM Journal of Optimization*, vol.9, pp. 112-147, 1998.

[35] R. L. Rogers, D. P. Buhl, H. Choo, and H. Ling, "Size reduction of a folded conical helix antenna," *IEEE Antennas Propagat. Soc. Int. Symp. Dig.*, pp. 34-37 June 2002.

[36] R. L. Freeman, *Telecommunications transmission handbook*, 4th ed. Wiley, 1998.

[37] J. Mclean, M. Leuvano, H. Foltz, "Reduced-size, folded ground plane for use with low-profile, broadband monopole antennas," *Radio and Wireless Conference*, pp. 239 –242, Aug. 1999.

[38] S. Collins, Y. M. Antar, "Antenna size reduction using Yagi-Uda loops and shorted circular patches," *IEEE Trans. Antennas Propagat.*, vol. 52, pp. 855-864, 2004.

[39] M. Weiner, "Monopole element at the center of a circular ground plane whose radius is small or comparable to a wavelength," *IEEE Trans. Antennas Propagat.,* vol. 35, pp.488-495, 1987.

[40] D. Schaubert, F. Farrar, A. Sindoris and S. Hayes, "Microstrip antennas with frequency agility and polarization diversity," *IEEE Trans. Antennas Propagat.*, vol. 29, pp. 118-123, 1981.

[41] R. B. Waterhouse and N. V. Shuley, "Scan performance of infinite arrays of microstrip patch elements loaded with varactor diodes," *IEEE Trans. Antennas Propagat.*, vol. 41, pp. 1273-1280, 1981.

[42] P. K. Panayi, M. O. Al-Nuaimi and I. P. Ivrissimtzis, “Tuning techniques for planar inverted-F antenna,” *IEE Electron. Letters*, vol. 37, pp. 1003-1004, 2001.

[43] D. Lamensdorf, “Capacitively tuned dipole,” *IEE Electron. Letters*, vol. 9, pp. 445-446, 1973.

[44] J. M. Carrere, R. Staraj and G. Kossiavas, “Small frequency agile antennas,” *IEE Electron. Lett.*, vol. 37, pp. 728-729, 2001.

[45] P. R. Urwin-Wright, G. S. Hilton, I. J. Craddock and P. N. Fletcher, “A reconfigurable electrically-small antenna operating in the 'DC' mode,” *IEEE Vehicular Technology Conference*, vol. 2, pp. 857-861, 2003.

[46] P. Hallbjörner, “Electrically small unbalanced four-arm wire antenna,” *IEEE Trans. Antennas Propagat.*, vol. 52, pp. 1424-1428, 2004.

[47] H.-W. Son and C.-S. Pyo, “Design of RFID tag antennas using an inductively coupled feed,” *IEE Electron. Lett.*, vol. 41, pp. 994-996, 2005.

[48] S. R. Best and J. M. (Best and McGinthy 2005)McGinthy, “A comparison of electrically small HF antennas,” *IEEE Antennas Propagat. Soc. Int. Symp. Dig.*, pp. 37-40, July 2005.

[49] D. Sievenpiper, L. Zhang, R. Broas, N. Alexópolous, and E. Yablonovitch, “High-impedance electromagnetic surfaces with a forbidden frequency band,” *IEEE Trans. Microwave Theory Tech.*, vol. 47, pp. 2059-2074, 1999.

[50] F. Yang and Y. Rahmat-Samii, “Bent monopole antennas on EBG ground plane with reconfigurable radiation patterns,” *in Proc. IEEE Antennas Propagat. Society Int. Symp*, pp. 1819-1822, June 2004.

[51] S. R. Best, “Improving the performance properties of a dipole element closely spaced to a PEC ground plane,” *IEEE Antennas Wireless Propag. Lett.*, vol. 3, pp. 359-363, 2004.

[52] E. E. Altshuler, T. H. O'Donnell, A. D. Yaghjian, and S. R. Best, “A monopole superdirective array,” *IEEE Trans. Antennas Propag.*, vol. 53, pp. 2653-2661, 2005.

[53] S. R. Best, E. E. Altshuler, A. D. Yaghjian, J. M. McGinthy and T. H. O’Donnell, “An efficient impedance matched 2-element superdirective array,” *in Proc. URSI National Radio Science Meeting*, pp.462, July 2005.

[54] A. D. Yaghjian, T. H. O’Donnell, E. E. Altshuler, and S. R. Best, “Electrically small superdirective linear arrays,” *in Proc. URSI National Radio Science Meeting*, pp. 67, July 2005.

[55] D. M. Fiedler and E. J. Farmer, *Near Vertical Incidence Skywave Communication*, 2nd ed., Sacramento, CA: Worldradio Books, 2000.

[56] E. E. Altshuler, T. H. O'Donnell, A. D. Yaghjian, and S. R. Best, "A monopole superdirective array," *IEEE Trans. Antennas Propagat.*, vol. 53, pp. 2653-2661, 2005.

[57] T. I. Lee and Y. E. Wang, "Parallel information channels in closely coupled dipole pairs," preprint to *IEEE Trans. Antennas Propagat*.

[58] R. S. Elliott, *Antenna Theory and Design*, Prentice Hall, 1981.

[59] Z. Bayraktar, P. L. Werner, , and D. H. Werner, "The design of miniature three-element stochastic Yagi-Uda arrays using particle swarm optimization," *IEEE Antennas Wireless Propagat. Lett.*, vol. 5, pp. 22-26, 2006

[60] T. H. O'Donnell and A. D. Yaghjian, "Electrically small superdirective arrays using parasitic elements," *Proc. Antennas Propagat. Soc. Int. Symp.*, pp. 3111-3114, July 2006.

[61] R. C. Hansen, *Electrically small superdirective, and superconducting antennas*, 1st ed. Wiley, 2006.

Vita

Sungkyun Lim was born in Seoul, Republic of Korea, on Jan 27, 1975, the son of Seunghyuk Lim and Youngsook Soh. After completing his work at Dankook High School, Seoul, Korea, in 1993, he entered Hanyang University in Seoul, Korea. He received the degree of bachelor of science in both Electrical and Computer Engineering and Mathematics in 1999. In August 2002, he attended the graduate school at The University of Texas, where he received the degree of master of science in Electrical and Computer Engineering in August of 2004. He was subsequently admitted as a candidate in his doctoral program at the University of Texas at Austin in May 2005.

Permanent address: 4600 Seton Center Pkwy #422, Austin, TX 78759-5255

This dissertation was typed by the author.